Design and Synthesis of Self-Assembled Polymeric Nanoparticles for Cancer Drug Delivery

by

Jennifer Logie

A thesis submitted in conformity with the requirements
for the degree of Doctor of Philosophy

Chemical Engineering and Applied Chemistry
Institute of Biomaterials and Biomedical Engineering
University of Toronto

© Copyright by Jennifer Logie 2017

Design and Synthesis of Self-Assembled Polymeric Nanoparticles for Cancer Drug Delivery

Jennifer Logie

Doctor of Philosophy

Chemical Engineering and Applied Chemistry
Institute of Biomaterials and Biomedical Engineering
University of Toronto

2017

Abstract

Current chemotherapeutics are plagued by poor solubility and selectivity, requiring toxic excipients in formulations and causing a number of dose limiting side effects. Nanoparticle delivery has emerged as a strategy to more effectively deliver chemotherapeutics to the tumour site. Specifically, polymeric micelles enable the solubilization of hydrophobic small molecule drugs within the core and mitigate the necessity of excipients. Notwithstanding the significant progress made in polymeric micelle delivery, translation is limited by poor stability and low drug loading. In this work, a rational design approach is used to chemically modify poly(D,L-lactide-co-2-methyl-2-carboxytrimethylene carbonate)-graft-poly(ethylene glycol) (P(LA-co-TMCC)-g-PEG) in order to overcome these limitations and effectively deliver drug to tumours.

The PEG density of the polymer system was optimized to enhance the stability of our polymeric micelles. Higher PEG densities permitted the lyophilization of micelles and enhanced the serum stability of the system. To increase the drug loading of our system, we facilitated specific intermolecular interactions within the micelle core. For drugs that form colloidal aggregates, such as pentyl-PABC doxazolidine, polymers were used to stabilize the colloidal core against aggregation and protein adsorption. For more challenging molecules, where self-assembly cannot

be controlled, such as docetaxel, we modified the polymeric backbone with a peptide from the binding site of the drug to achieve loadings five times higher than those achieved in conventional micelle systems. This novel docetaxel nanoparticle was assessed in vivo in an orthotopic mouse model of breast cancer, where it showed a wider therapeutic index than the conventional ethanolic polysorbate 80 formulation. The improved tolerability of this formulation enabled higher dosing regimens and led to heightened efficacy and survival in this mouse model. Combined, these studies validated P(LA-co-TMCC)-g-PEG nanoparticles as an effective delivery vehicle for two chemotherapeutics, and presents approaches amenable to the delivery of many other clinically relevant hydrophobic drugs or drug combinations.

Acknowledgments

I would first like to thank my supervisor and mentor, Molly Shoichet, who taught me so many things, but most importantly gave me the confidence to break my own glass ceiling and pursue a PhD. I am incredibly grateful for the opportunity to work in your lab.

To my collaborators, without whom I could not have done most of this work: Ahmed Aman, Rima Al-awar, Ben Barthel, Tad Koch, Ryan Hansen, Peter Poon and Armand Keating. I would also like to thank my committee members, Tim Bender and Warren Chan, who challenged me but were also incredibly supportive and reliable throughout my five years here.

I got to work with the most amazing group of individuals in the Shoichet lab- people who were so willing to be teachers and therapists and friends whenever I needed them. In particular, (but in no particular order): my first mentor in the lab, Shawn, whose enthusiasm was truly contagious and whose kindness to others I will forever try to emulate. Chris, Roger and Mike, who were not only killer postdocs but killer friends. My "gurls"- Kat, Steph, Jackie, Sam and Malgosia- who were always there to listen, but are also part of some of my favourite memories. The blood pact- Anup, Steph and Nick- I couldn't think of better people to have started and ended this journey with. The morning crew- Sam, Ahil, Chris, Jamie, Eric- which evolved over the years but always made waking up and coming in early easy. Thug Cluster, who could laugh with me when I needed it but were good enough friends to refocus me when I laughed for too long. Lastly, to OG, Ying Fang Chen, who doesn't receive enough praise but was the best lab mother a girl could ask for.

I would like to thank all of my family and friends who helped me achieve my goal of obtaining a PhD. To my Mom, who since I was a little girl encouraged me to follow my dreams and love learning. Even though she isn't here to see this, she has truly left an imprint on my heart forever. To my Dad, who is one of the best people I know, has provided me constant support and has never once doubted my abilities. His easy going nature and "don't worry Jenn" was just what I needed to hear when I was bogged down in research. To Liza, who has been an incredible mother when I needed one most, loves me unconditionally, and helps me keep my sanity when life gets crazy. My sisters, Colleen, Fanny and Amy, who are also some of my closest friends, were always there to keep me grounded and make me laugh uncontrollably. Finally, to my grandmothers, Thelma and Myra, who were way ahead of their time and always told me that I could be whatever I wanted to be, your attitudes have helped shape the person I am today.

Table of Contents

List of Figures and Tables

1 Introduction

Portions of this chapter are derived from the following manuscript:

McLaughlin, C.K., Logie, J. and Shoichet, M.S. (2013) Core and corona modifications for the design of polymeric micelle drug-delivery systems. *Israel Journal of Chemistry.* 53: 670-679.

Reprinted with permission from Wiley. C.K.M., J.L. and M.S.S. wrote and edited the manuscript. C.K.M. wrote sections on surface chemistry, multifunctional surfaces, and introduction (not included in this thesis). J.L. wrote sections on self-assembly and core chemical modifications.

1.1 Rationale

The effective diagnosis and treatment of human diseases using small molecule and macromolecular therapeutics continues to present significant challenges to the biomedical community. In part, this stems from the physical properties of individual drug candidates, which are typically hydrophobic and poorly water soluble. This necessitates the use of excipients to solubilize these compounds for delivery, which can often have their own associated toxicity. The poor selectivity of many small molecule therapeutics often results in dose limiting side effects when delivered systemically [1]. Alternative macromolecular therapeutics under development that use RNA, DNA and proteins, display good solubility in aqueous conditions but can suffer from degradation and short circulation times in vivo [2].

Nanoparticles have been studied as an alternative strategy to circumvent the broad distribution profile of small molecule therapeutics, protect sensitive biomacromolecules and deliver them more selectively to a required site of action [3]. A key feature of these composite nanoparticles is that they demonstrate ‘value added’ properties, which are greater than the sum of the individual parts. Moreover, such materials can now accurately interface with both small molecules and biological macromolecules in a manner that does not significantly disrupt their innate function [4]. Continuing efforts are now focused on developing these materials to meet the stringent requirements for benign in vivo circulation and improved pharmacokinetic properties.

P(LA-co-TMCC)-g-PEG is an amphiphilic copolymer designed to form monodisperse polymeric micelles that can be modified on the surface using click chemistry. The functionality of this polymer system provides opportunity for subsequent modifications in order to improve the

nanoparticle's drug loading and serum stability. These modifications would provide a robust particle platform for the delivery of chemotherapeutics to solid tumours.

1.1.1 Hypothesis and Objectives

The hypothesis governing the body of this work is:
Chemically designed poly (D,L-lactide- co-2-methyl-2-carboxytrimethylene carbonate)-graft-poly(ethylene glycol) will self-assemble to form stable nanoparticles with high drug loading and effectively deliver drug to tumours.

To test this hypothesis, this work was divided into four primary objectives:

1. **To increase polymeric nanoparticle serum stability.**
   In Chapter 2, I synthesized P(LA-co-TMCC) and varied the PEG density from 0.5 to 6 PEG/backbone. I established that higher PEG densities result in greater kinetic stability through both lyophilization and in serum conditions. Importantly, this was not at the cost of drug loading, which was maintained in all formulations relative to the backbone concentration.
2. **To encapsulate pentyl PABC-doxaz in a polymeric nanoparticle.**
   In Chapter 3, I investigate an alternative polymeric formulation strategy, which takes advantage of the colloidal properties of a subset of hydrophobic drugs. Here, I show the formation of stable colloidal nanoparticles of pentyl PABC-doxaz, a novel anthracycline derivative. By incorporating polymers during drug self-assembly, we form particles with unusually high loadings (> 50 wt%).
3. **To increase docetaxel loading in polymeric nanoparticles.**
   In Chapter 4, I modified our polymeric backbone to facilitate higher loading of DTX, a non-colloid forming small molecule. While less specific moieties, such as benzyl or DTX, significantly increased loading, the effect of incorporation of a peptide (taxol binding peptide) from the binding site of DTX was drastic (5-fold over unmodified polymers). Based on the maintained stability and toxicity of this formulation in vitro, the TBP-modified particle system was selected for further in vivo studies.
4. **To assess the in vivo efficacy of DTX loaded Fab 73J conjugated-nanoparticles in an orthotopic human xenograft tumour model in mice.**
   In Chapter 5, I compared the pharmacokinetics, biodistribution, maximum tolerated dose and efficacy of our novel nanoparticle (NP) DTX (with or without Fab 73J) to a

conventional, surfactant-based, free DTX formulation in orthotopic tumour bearing mice. We established that the incorporation of the Fab 73J targeting ligand had no benefit on the efficacy of the formulation. Nevertheless, the reduced toxicity of the NP DTX augmented the therapeutic window of the drug, allowing higher dosing regimens and better efficacy and survival.

1.2 Cancer Chemotherapeutics

Cancer is a devastating disease that represents the leading cause of death in Canada [5]. Despite its prevalence and substantial research investment, cancer remains a considerable clinical challenge due to the complexity and heterogeneity of the disease. In general, patients are treated with a combination of surgical intervention, radiation and chemotherapy upon diagnosis. The success of this treatment varies widely depending on the diagnosis, age and health of the patient. While significant progress has been made in diagnostics and surgical interventions over the past 20 years, chemotherapy has largely remained unchanged. The majority of clinically used drugs have poor selectivity, causing a wide range of dose-limiting systemic side effects. A further challenge is the solubility of these drugs, which are often bulky hydrophobic molecules and thus require excipients for intravenous delivery. Current formulations contain large volumes of toxic surfactants (e.g. cremophor EL, Pluronic F68, polysorbate 80), requiring pre-treatment of patients to prevent allergic reactions [6], [7].

While there are several types of chemotherapeutics, they generally target the fast growing cells by acting to inhibit a step in the cell division cascade. Unfortunately selecting a single cancer hallmark as a drug target can also negatively impact healthy cell types that rapidly divide. These drugs include alkylating agents (such as cisplatin), anti-tumour antibiotics (such as doxorubicin and the novel anthracycline Pentyl-PABC Doxaz), antimetabolites (such as gemcitabine), and mitotic inhibitors (such as vincristine and docetaxel). Of these, the taxane chemotherapeutics, a class of mitotic inhibitors, represent the most prescribed and arguably the most profitable oncology products ever developed. To circumvent some of the selectivity issues associated with conventional chemotherapeutics, targeted drug candidates have been explored. These drugs have a unique target that has no or limited presence in healthy cells, often a mutation or the overexpression of a gene specific to the cancer. Notable examples include tyrosine kinase

inhibitors, hormone therapies (such as the estrogen receptor antagonist fulvestrant), and immunotherapies.

Within this thesis, two chemotherapies were used in the development of novel drug delivery vehicles (Figure 1.1). Docetaxel was selected for its prevalence as a therapy in a range of cancers, and its compatibility with anti-HER2 immunotherapies. Pentyl PABC-Doxaz was selected for its colloid forming properties as a novel mechanism to achieve high-loading. Fab73J is a novel anti-HER2 fragment antigen binding developed by the Sidhu lab, which was explored as an alternative targeting ligand to the clinically used trastuzumab.

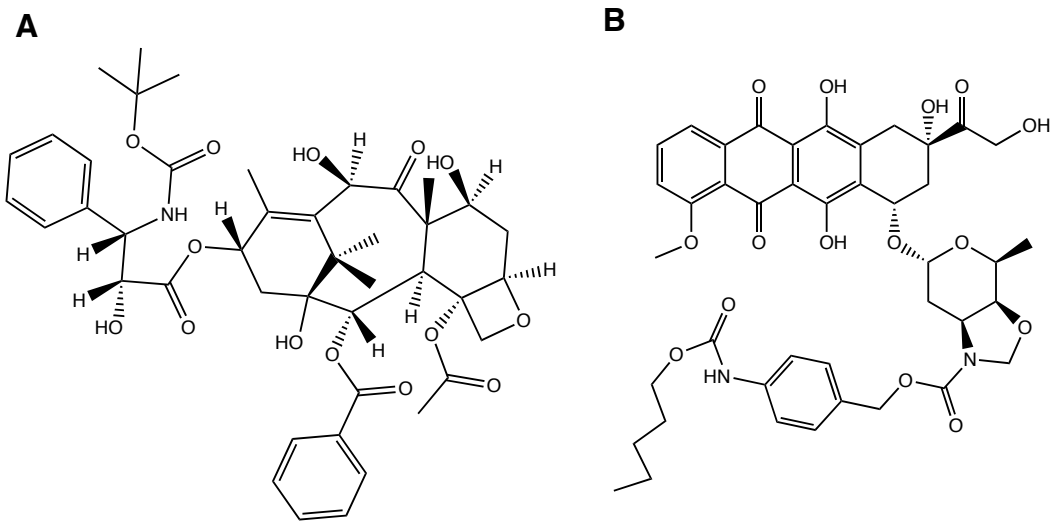

Figure 1.1: Small molecule chemotherapeutics. A) Docetaxel, and B) PPD.

1.2.1 Docetaxel

Taxanes, such as docetaxel, are clinically well-established chemotherapeutics used in patients with a wide range of cancers including breast, lung and pancreatic [8]. Docetaxel (marketed as Taxotere by Sanofi) became one of the most successful oncology products after its FDA approval in 2006, with a global market value of over $3 billion in 2010 [9]. Despite its success in the clinic, docetaxel has dose-limiting toxicity due to severe side effects such as neutropenia and thrombocytopenia associated with its lack of selectivity for cancer cells over healthy cells [8], [10]. Patients also suffer allergic reactions to the excipients, such as polysorbate 80, required to solubilize the drug for intravenous delivery [11]. Combined, the lack of selectivity and toxicity of excipients suggests a need for improved formulation strategies.

The mechanism of action of the taxanes is tubulin polymerization and microtubule stabilization, which blocks cell division and causes cell apoptosis [8]. Docetaxel is more potent than other taxanes (two times the potency of paclitaxel), due to an additional mechanism of action involving the inhibition of *BCL2* via phosphorylation [11], [12]. Intriguingly, the binding site of docetaxel on microtubules has been well characterized [13], and point mutations within the beta-tubulin have been implicated in docetaxel resistance [14]. The high affinity of docetaxel for this binding site provides an opportunity for a biomimetic drug formulation.

1.2.2 Pentyl PABC-Doxazolidine (PPD)

PPD is a novel anthracycline derivative developed by the Koch lab at the University of Colorado Boulder [15]. This drug was developed as a means to overcome the limitations of the clinically used doxorubicin. Specifically, doxorubicin treatment regimens are limited by cardiotoxicity and acquired resistance of tumours [16]. Modification of doxorubicin with a pentyl PABC linker forms a prodrug that is topoisomerase II independent and inhibits cell growth by cross-linking DNA [17]. This prodrug is cleaved specifically by carboxylesterase II, overexpressed in a number of cancers including liver cancer, non-small-cell lung cancer, and ovarian cancer. In a liver cancer mouse model, PPD shows growth inhibition compared to doxorubicin and significant reductions in cardiotoxicity [15].

Like docetaxel, delivery of PPD requires the use of excipients, which can limit dosing regimens due to severe tail vein damage and side effects such as lethargy. Pre-activation of the drug by carboxyesterases present in the mouse blood also limited PPD's use [15]. Encapsulation of PPD in a biocompatible vehicle could serve to both reduce excipient-associated toxicities and prevent premature activation of the drug.

1.2.3 Anti-HER2 Therapies

Recently, more targeted approaches to breast cancer treatment have been implemented. Human epidermal growth factor receptor 2 (HER2) belongs to the epidermal growth factor family of tyrosine kinase receptors [18]. This receptor is overexpressed in 20-30% of breast cancers, and acts by upregulating cell proliferation, cell survival and cell mobility [19], [20]. This is a result of the activation of intracellular signaling pathways due to HER2 homodimerization and heterodimerization with other receptors of the ErbB family [19]. Antibodies have been identified that bind to the extracellular domain of HER2 and inhibit cell division. Trastuzumab

(Herceptin®), developed by Genentech and approved by the FDA in 1998, is an antibody clinically used for HER2+ breast cancers either as a monotherapy or co-administered with chemotherapeutics, frequently from the taxane family [21]. Trastuzumab-drug conjugates, notably T-DM1, have had recent success due to their positive results in clinical trials [22], [23] and FDA approval [24], however the amount of drug delivered per antibody is low compared to the potential of targeted nanoparticle vehicles.

The mechanism of action for trastuzumab is not well understood, however several theories have been proposed [25]. Through interactions with HER2, trastuzumab may downregulate and inhibit tyrosine kinase pathways, leading to the inhibition of cell cycle progression [26]. Alternative theories suggest that it may facilitate the activation of antibody-dependent cellular cytotoxicity (ADCC) causing cell death [27], or that it eliminates HER2 receptor autophosphorylation averting other means of receptor activation [28]. Interestingly, work by the Sidhu lab has identified novel anti-HER2 ligands, including 73J, which bind to an alternative epitope of HER2 [29]. We recently showed that the 73J mAb is advantageous due to its fast disassociation from the HER2 receptor compared to trastuzumab, enabling increased intracellular trafficking [29]. This effect was augmented with conjugation of antibodies to nanoparticles, suggesting the potential of this novel anti-HER2 as a targeting ligand.

1.3 Nanoparticle Drug Delivery Vehicles

Many nanotechnologies have been used to tackle the problems of cancer. Their use as an anti-cancer technology spans from contrast agents for intraoperative imaging to detection methods for tumour-derived DNA and proteins. Most relevant to this research and one of the most studied uses of these nanotechnologies is the use of nanoparticles as drug delivery systems. Nanoparticles of various forms- including liposomes, semiconductors, metals, dendrimers, and polymeric micelles or particles - have been used as delivery vehicles to circumvent classical formulation challenges and to reduce the systemic toxicity of specific cargos [30]. Furthermore, targeting ligands can be conjugated onto nanoparticles to increase binding to specific cells and facilitate cargo internalization [31]-[33]. The means by which nanoparticles increase specificity can be grouped into two categories, passive and active, which are described herein. Additionally, the in vitro and in vivo evaluation of nanoparticles will be described.

1.3.1 Passive Targeting

Passive targeting exploits the enhanced permeability and retention (EPR) effect [34], which suggests that the vasculature around the tumours is leaky, allowing particles under 200 nm to pass into the tumour tissue [35]. As described in Figure 1.2, these particles are too large to pass through healthy vasculature. Furthermore, the tumour suffers from poor lymphatic drainage, meaning that particles will accumulate at the tumour site [36]. All clinically approved nanoparticle formulations of chemotherapeutics make use of passive targeting, notable examples including Abraxane, Marqibo, Genexol-PM and Doxil [37], [38]. Although specificity is increased, these formulations are still plagued by toxicity to surrounding healthy cells in the breast tumour microenvironment including endothelial cells, adipocytes and fibroblasts [39].

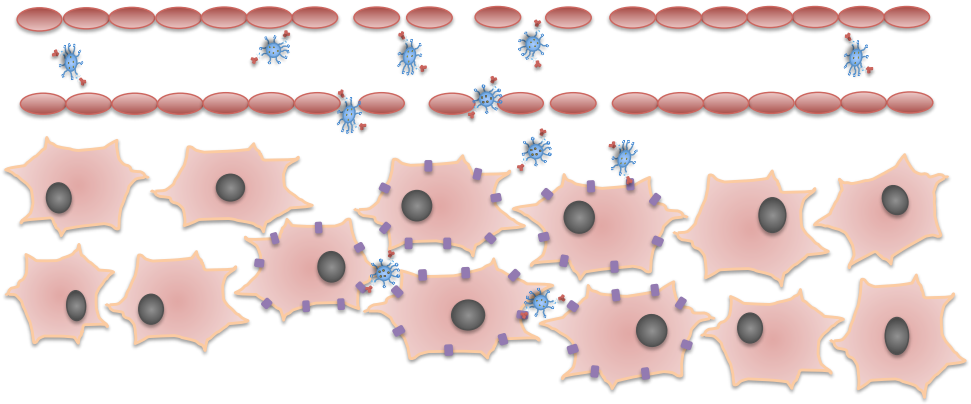

Figure 1.2: Enhanced permeability and retention effect in solid tumours leading to targeting of nanoparticles. Tumours possess disorganized blood vessel architecture causing gaps in the blood vessel wall that allows nanoscale materials into the tumour tissue. Active targeting can be achieved using antibody-modified nanoparticles that bind to overexpressed surface markers on the cancer cells.

There have been ongoing debates in the biomedical community about the validity of the EPR effect as a means of targeting the tumour site [40]-[44], especially after the failure of the Phase III clinical trial of NK-105 [45] and recent bankruptcy of BIND therapeutics. The heterogeneity of tumours has been implicated in the disappointing therapeutic efficacy of many nanoparticles in vivo [42], which has led to recent advancements in image-based methodologies to enable appropriate treatment design [46]-[48]. Another challenge that has plagued the nanoparticle community is non-specific distribution and insufficient accumulation of therapeutics [43], [49].

Despite the promise of nanoparticle delivery strategies, only a small percentage (< 2%) of the carrier accumulates at the tumour site [49], and the extent of tumour penetration suggests that cargo may only be delivered to the periphery of large tumours [41]. Re-imagining the role of the carrier could allow a shift to nanoparticle based drug delivery. Specifically, designing nanoparticles to overcome biological barriers (such as the mononuclear phagocyte system) [50] may overcome some of the current delivery challenges. In addition, taking advantage of the reduced toxicity of nano-formulations compared to current surfactant based formulations will allow more effective dosing regimens [43].

1.3.2 Active Targeting

Active targeting can be attained with the attachment of a moiety to the surface of the nanoparticle that serves to selectively target the cancer cells. Although unmodified nanoparticle carriers may display longer distribution times and passively enter specific areas (such as tumours via the EPR effect), cellular uptake is minimal without the inclusion of groups that will actively mediate entry via one of the endocytic pathways [51]. This is especially critical for cargo that cannot passively cross the cell membrane. In some cases, these targeting ligands also elicit a therapeutic activity themselves. These 'active' targeting groups are now being employed to help navigate through the various biological barriers en route to the intended site of action for a number of diseases [52].

A range of ligands are currently being explored for receptor-based targeting of therapeutics[53]. These include vitamins (e.g. folic acid), sugars (e.g. N-acetylgalactosamine, GalNAc), peptides (e.g. RGD), proteins (e.g. transferrin), aptamers (e.g. AS1411), antibodies (e.g. trastuzmab, huA33, brentuximab) and antibody fragments (e.g. trastuzmab Fab) [54]-[58]. The common feature amongst these ligands is that they can be used to selectively recognize receptors overexpressed on either cells or tissues specific for a particular disease-related molecular pathology. Cell-recognition of the targeting group-modified nanoparticles can enhance uptake into the cell with subsequent release of a therapeutic payload.

Antibodies are among the most common targeting ligands. A full immunoglobulin (IgG) antibody has two well-defined regions: the fragment antigen-binding region (Fab) and the fragment crystallizable region (Fc). The Fab region is responsible for binding to antigens while the Fc region modulates the immune cell activity. Using a full antibody, such as trastuzumab, as

the targeting ligand on a nanoparticle increases the immune response resulting in reduced circulation times [59]. As a targeting moiety, Fab fragments have the potential for higher binding capacity and cellular internalization rates as compared to full IgG antibodies, and may mitigate the immune response associated with antibody coated particles [59].

1.3.3 Evaluation of Nanomedicines

In order to evaluate the ability of novel nanomedicines to alleviate systemic side effects and enhance tumour efficacy, representative in vitro and in vivo models must be established. While in vitro assays provide important information about the toxicity of formulations against specific cell lines, the 2D cell culture conditions do not accurately model the complicated physical barriers of a tumour including multiple cell types, abnormal vasculature, hypoxic environments and changes in gene expression throughout [60]. For this reason, nanomedicines are evaluated using animal models of cancer before reaching the clinic.

There are several factors to be considered when selecting an in vivo model. Firstly, the consistency of the model is an important factor. While patient tumours are heterogeneous, choosing an animal model that has a poor tumour take rate, or variable tumour growth curves makes analysis extremely difficult. Secondly, orthotopic models should be used when possible to more accurately reflect the underlying pathophysiology of the patient tumour [61]. Namely, when tumours are grown in an organ environment consistent with that found in the patient, the vasculature and metastasis is also more consistent with patient disease [62]. Lastly, the gene expression profile of the cells used in the tumour model should accurately reflect native conditions, especially for relevant drug or ligand targets [63]. While no mouse model will perfectly reconstruct the patient's tumour, a well-designed experiment allows for better comparisons and evaluations to be made.

1.4 Polymeric Micelles

The studies presented here will focus attention on polymeric micelles and the recent strategies to bioengineer them for use as more efficient drug delivery systems. Specifically, this thesis will look at how chemical modifications of the core-forming polymer chains can be used to increase drug loading and in vivo stability. Moreover, we will also examine how functional groups can be

incorporated into the micelle corona for selective coupling to active targeting motifs using click-based reactions in a biorthogonal manner.

1.4.1 Self-Assembly

Polymeric micelles have been engineered in a number of ways for use as drug delivery platforms [64], [65]. Typically, these structures are comprised of amphiphilic polymers that self-assemble under specific conditions to yield micellar nanostructures that can be easily manipulated and handled in aqueous solutions [66]. Micelle properties can be tuned chemically to alter size, shape and composition [67]. Selective modification is a key facet to engineering polymeric micelles suitable for drug delivery applications where one needs to ultimately administer clinically relevant doses of a therapeutic to the disease site in a manner that limits toxic exposure. Some of the required features for a drug delivery system are biocompatibility (non-toxic), sustained stability under relevant in vivo conditions and selective delivery to diseased cells or tissue. These requisite features rely on specific physicochemical properties and can be implemented into the micelle design using recent advances in polymer and functional group chemistries [68].

As shown in Figure 1.3, micelle formation is dependent on the chemical nature of each hydrophilic (blue) and hydrophobic (grey) block, solvent composition and concentration [66]. In addition, the amphiphilic polymer can be comprised of either a linear or graft copolymer. Micellization is an entropically driven process based on an equilibrium between attractive and repulsive forces [69]. These forces are mainly hydrophobic in nature, with non-polar segments of the polymer backbone decreasing contact with water. Typical materials used in the hydrophobic block include polyesters (e.g. poly(lactic acid), poly(lactic-co-glycolic acid), poly(caprolactone)), polyimines (e.g. polyethyleneimine) and poly-amino acids (e.g. poly(aspartic acid)) [70]-[72]. These well-studied polymers are generally considered biocompatible, which makes them versatile components for drug delivery systems. Most amphiphilic polymers use PEG as their hydrophilic block. PEG has been approved by the FDA for clinical use and is used in a wide range of applications [73]. Alternative hydrophilic polymers to PEG include N-(2-hydroxypropyl)-methacrylamide (HPMA) and poly(acrylic acid) [65].

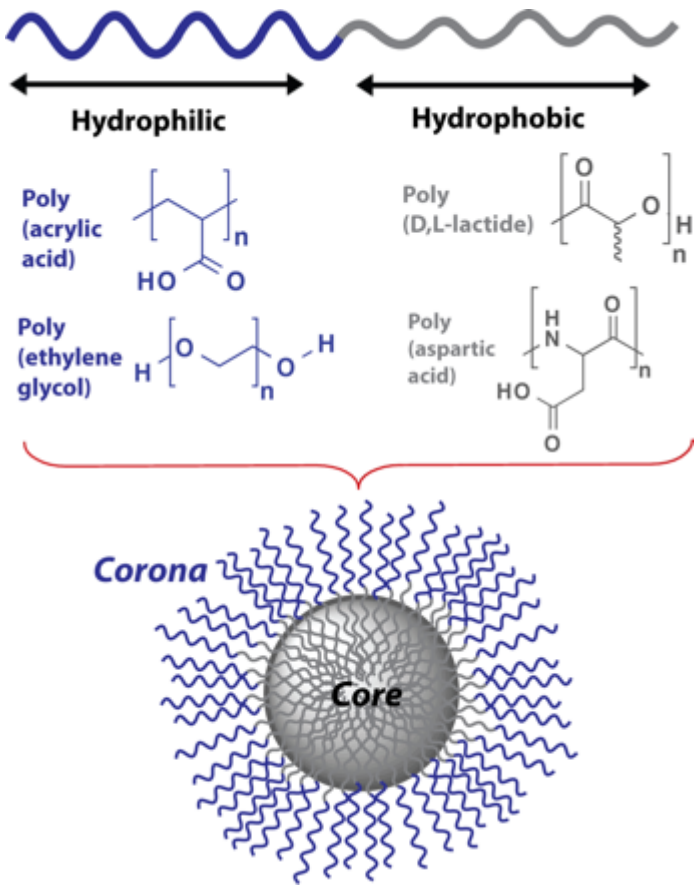

Figure 1.3: Amphiphilic polymers can be synthesized using a variety of chemistries and subsequently self-assembled into well-defined micelles. Each fully assembled micelle thus consists of a hydrophobic core and hydrophilic corona.

The micelles generated from these amphiphilic polymers are thus comprised of a hydrophobic interior ('core') and hydrophilic periphery ('corona'). The functional capacity for these nanosized structures stems from the unique properties inherent to these domains. The core can be used to selectively encapsulate hydrophobic drugs, while the hydrophilic corona ensures solubility and stability under the aqueous conditions required for in vivo administration. Overall, strategic chemical transformation of the core and/or corona can be used to better engineer drug loading, biodistribution and cellular targeting properties of polymeric micelle drug delivery systems.

1.4.2 Micelle Stability

Micelles are not static structures and changes in the environment, such as the presence of a hydrophobic drug, can dramatically change their characteristics. The thermodynamic stability is indicative of how the micelles form and reach equilibrium, while the kinetic stability describes the details of polymer exchange and micelle disassembly [74]. While the thermodynamic stability gives information about the critical micelle concentration (CMC), the kinetic stability is indicative of the rate of dissociation below the CMC, an important parameter for the use of micelles in vivo. Fast dissociation occurs when the dilution is below the CMC in the bloodstream and the nanoparticles immediately fall apart. If the dissociation is slow, a nanoparticle may stay intact long enough for it to reach its target within the body. Thus, the kinetic stability has significant implications for the efficacy of a polymeric micelle delivery system [74].

Efforts have been made to improve the long-term stability of micelles by cross-linking the core post-micellization. While this approach has shown some success, the drug loading of these micelles is generally low and crosslinking naturally reduces the mobility of the hydrophilic segments making the particles larger [75]. Thermodynamic modeling of drug loading in the micelle core has shown that it is limited by three parameters: the block copolymers size, the interaction parameter between the drug and the hydrophobic core, and the interfacial tension between the core and the corona [76].

1.5 Corona Modifications to Improve Stability and Targeting

The focus of this section is on polymer and micelle modification on the hydrophilic exterior, with concomitant installation of ligands that actively target receptors expressed on the cell surface of diseased cells [70]. The corona of the polymeric micelle directs its interactions and biological activity in vivo, making its design critical for effective delivery to the tumour.

1.5.1 Surface Chemistry

The surface of the micelle is a critical design parameter for polymeric micelles as it will ultimately determine the particle's fate in vivo. More specifically, the surface will dictate the interactions between the particle and the blood components (e.g. proteins, salt, cells) immediately upon intravenous injection, giving the particle a distinct "biological identity" [77]. This biological identity is what the cell encounters in vivo and may significantly change the

particle's transport and clearance. The majority of nanoparticles (including polymeric micelles) have an outer layer of polyethylene glycol (PEG) to increase their blood circulation time. PEG works by minimizing protein adsorption, and reducing uptake by the mononuclear phagocyte system (MPS) [78], [79]. Chan et al. showed, in an elegant study with gold nanoparticles, that an increased PEG density reduces protein adsorption and shifts to a serum-independent mechanism of macrophage uptake [77]. Interestingly, they showed in a later study that they could modify the protein corona fingerprint by changing the surface chemistry of the particles [80]. Increasing the serum half-life of particles by reducing uptake via immune cells is critical for accumulation at the tumour site.

The PEG density also significantly changes the distribution of particles. Work from Hanes et al. showed that densely coating particles with PEG reduces adhesive interactions with cells, allowing greater penetration through tissues including the brain [81], [82]. This could also have implications at the tumour site, where penetration through the tumour microenvironment allows better delivery of the cargo and can lead to a more efficacious response [41], [83], [84]. Polymeric micelles are easily amenable to dense PEGylation due to facile chemistry and flexibility with PEG molecular weights and branching. This hydrophilic corona is important not just for mitigating the immune response, as described above, but for circumventing premature release of cargo through interactions between the core with blood proteins [85]. By shielding the hydrophobic core, the partitioning of a drug from the core to the hydrophobic pockets of proteins is delayed.

1.5.2 Click Chemistry Conjugation Strategies

One of the primary challenges in designing micelle drug delivery systems is to accurately modify the corona with small molecules or biomolecules to create multi-functional surfaces. These can either be modified using physical adsorption or through covalent linkages, the latter of which is desirable to maintain orientation and attachment of ligands in vivo. Engineering the shell can also be done pre- or post-assembly of the amphiphilic polymers. This will depend mainly on the system being used, the functional group compatibility and whether polymer modification alters self-assembly. In general, the post-micelle modification strategy works well because the hydrophilic segments remain accessible at the aqueous interface and self-assembly is not hindered.

Tuning surface chemistry and controlling the degree of labelling both require the incorporation of functional groups that are capable of conjugating active targeting moieties. Coupling conditions are especially important for classes of biomacromolecules (i.e., proteins), which derive activity based on their specific topological folding. These molecules are sensitive to harsh conditions, and their structure can be destroyed by the most common organic solvents. Specifically, we focus here on functional groups that allow for both facile and orthogonal reactivity under aqueous coupling conditions where biomacromolecules should remain stable and optimally functional. As such, the use of biorthogonal chemistry is crucial to maintain activity for polymeric micelle delivery systems. Classical bioconjugation chemistry, which includes amidation reactions between amines and carboxyl groups, has been used extensively to modify the polymeric micelle shell [86], [87]. Other chemistries include the highly specific biotin/avidin and hydrazone formation[4]. While these approaches continue to find efficient use in micelle functionalization, they can be less selective and lead to cross-reactivity or byproduct formation.

In 2001, Sharpless and co-workers introduced the concept of the ‘click’ reaction, which generally refers to a reaction that is high yielding, produces few or no byproducts and contains functional groups that minimally cross-react (especially with other common biological functional groups) [88]. Two of the most popular reactions are based on existing chemistries: the Diels-Alder (DA) and Huisgen 1,3-dipolar cycloadditions. Although thiol-ene and thiol–yne reactions do meet a number of the main click criteria, conditions must be more tightly controlled to avoid cross-product formation. However, the thiol-maleimide reaction continues to be a common means to attach peptides or small molecules in a number of systems [89]. Click functional groups provide chemoselective coupling routes that can be performed under relatively benign conditions and are invaluable for introducing targeting ligands onto the polymeric micelle surface. A number of excellent reviews have compiled the specific reaction conditions used for the above mentioned coupling strategies and we focus here on two chemical conjugation strategies pertinent to this thesis [90]-[93].

1.5.2.1 Diels-Alder Cycloaddition

The Diels-Alder (DA) [4+2] cycloaddition reaction has gained support as an effective strategy for selective modification of various materials [94] and is well suited for surface functionalization of polymeric micelles. The DA reaction couples an electron-rich conjugated diene and electron-poor alkene (commonly referred to as a dienophile) to generate a stable

cyclohexene ring (Figure 1.4a) [95]. This reaction is generally selective, with maleimide and furan functional groups being two of the more common reactive precursors [95]. The reaction is also thermally reversible (retro-DA), but typically requires temperatures greater than 100 ºC. This cycloaddition has been demonstrated to proceed rapidly and in high yield under mild aqueous reaction conditions [94]. Additionally, no metal catalyst is required for the reaction to proceed, which makes this coupling strategy attractive for in vivo drug delivery system design.

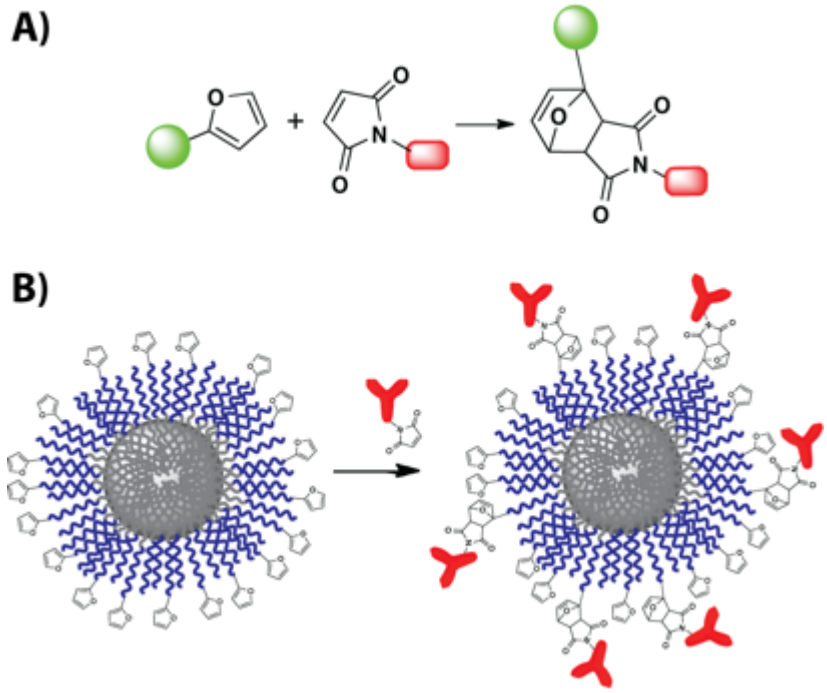

Figure 1.4: A) An example of the transition-metal free [4+2] DA cycloaddition between furan and maleimide functional groups. B) The high coupling efficiency of the DA reaction was used to selectively couple furan groups on the corona of a polymeric micelle with maleimide-modified antibodies [96].

An early example of polymeric micelles functionalized with DA cycloaddition chemistry incorporated a furan diene into the polymeric corona (Figure 1.4b) [96]. Coupling could be achieved between maleimide-modified antibodies (trastuzumab) and the furan functionalized PEG units on the micelle corona. Although the antibody conjugation for this post-micelle modification scheme proceeds efficiently (MES buffer, pH 5.5, 37 ºC), a large number of furans remain available for subsequent conjugation to small molecules. These immuno-polymeric micelles were shown to specifically target HER2-over-expressing cells. The selectivity and mild

coupling conditions for the DA cycloaddition make it an ideal reaction to engineer multi-functional polymeric micelle drug delivery systems,

1.5.2.2 Thiol-Maleimide Michael Addition

One of the most common reactions for biomolecule conjugation is the Michael addition between a free thiol and a maleimide group [97]. This chemistry works well in aqueous conditions at neutral pH and like the DA reaction does not produce any by-products. Importantly, this chemistry has orthogonal reactivity to biomacromolecules, such as proteins and peptides, allowing them to retain their functionality. The efficiency of the reaction makes it well suited for a variety of applications, including hydrogel synthesis, protein modification and nanoparticle conjugation. This chemistry forms the basis of several protein conjugates, such as the monoclonal antibody labelling with fluorescein shown in Figure 1.5 [29] and the two FDA-approved antibody-drug conjugates, brentuximab vedotin and trastuzumab emtansine [98].

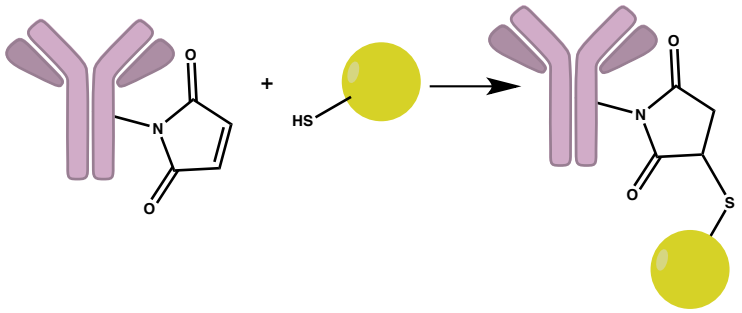

Figure 1.5: Michael addition between a maleimide modified monoclonal antibody and thiol conjugated fluorophore.

1.6 Core Modifications to Improve Drug Loading

Polymeric micelles are biocompatible and encapsulate hydrophobic chemotherapeutics within their core making them a promising drug delivery system [99]. However, drug delivery by polymeric micelles has been a challenging task due to poor stability and insufficient therapeutic loading. Many of these challenges stem from a lack of understanding of the dynamics of the micelle system and little characterization of the drug encapsulation mechanism [100]. Research on polymeric micelles for drug delivery has been focused on the characterization of the micelle itself and not necessarily on the interaction between the carrier and cargo. Specifically, polymers are developed that have a very low CMC, a narrow polydispersity index (PDI) and a uniform

spherical morphology upon micellization [74]. After polymer optimization, small hydrophobic drugs are encapsulated within the polymeric micelle for delivery to cells.

When a drug is introduced into the system it has a certain affinity for the core that dictates the magnitude of its incorporation. This is described by the Flory-Huggins interaction parameter, which evaluates the solubilization of a drug in the polymeric micelle,

$$\chi_{sc}=(\delta_s-\delta_c)^2 V_s /RT$$

where δ_s and δ_c are Scatchard-Hildebrand solubility parameters of the drug and core-forming polymer block respectively and V_s is the molar volume of the drug. A lower value indicates greater compatibility between the drug and the core. This parameter suggests that there is no universal polymer that can be used for every drug [101]. While hydrophobic interactions have shown moderate drug loading (~10% w/w), facilitating drug-polymer interactions based on the drug's chemical structure allows for higher drug loading and greater micelle stability. Ideally, delivery systems will have the high percent weight of drug while maintaining the pharmacokinetic profile of the micelle.

Introducing chemical functionalities into the core that can participate in non-covalent interactions with a drug is an alternative strategy to improve both the drug loading and kinetic stability of the micelle. A summary of these interactions is shown in Figure 1.6, and we will focus on some specific examples herein.

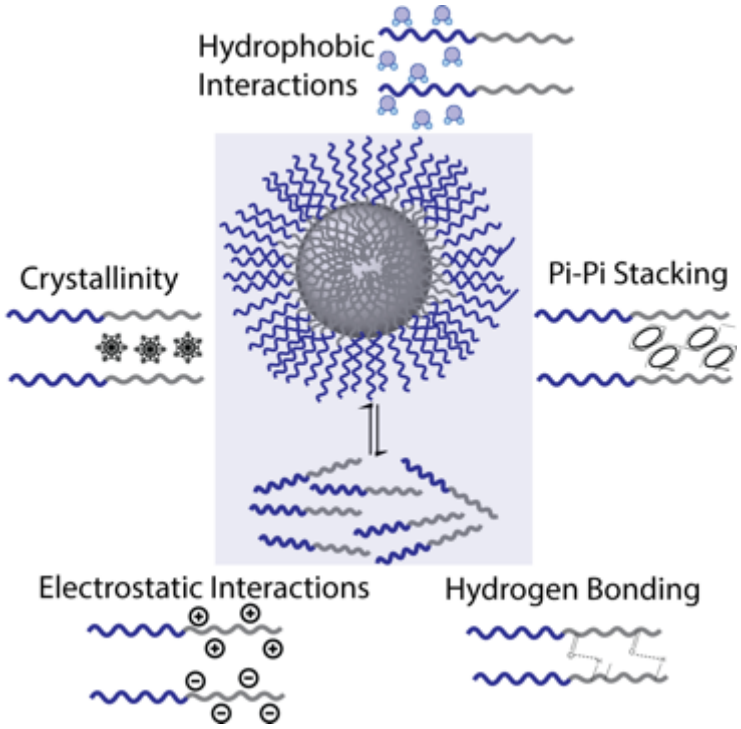

Figure 1.6: Schematic representation of various core interactions that can be incorporated to both stabilize micelles and increase drug loading.

1.6.1 Hydrophobic Interactions

Most of the interest in improving the affinity of the drug for the core is focused on hydrophobic interactions within the core of polymeric micelles. One of the fundamental ways to improve the drug loading is to increase the proportion of hydrophobic to hydrophilic polymer blocks [101]. While this modification increases the cargo space, it also causes a reduction in stability due to less shielding, causing the micelle to dissociate rapidly [102]. In order to evade a reduction in stability, higher drug loading can be achieved by increasing the hydrophobicity of the core without changing the ratio between the hydrophilic and hydrophobic blocks. This can be done by using alternative core-forming blocks or by chemically modifying polymers with hydrophobic functionalities.

Several groups have studied the differences in drug loading between poly(lactide) (PLA) and the more hydrophobic poly(ε-caprolactone) (PCL) cores with PEG coronas. Dormidontova et al. investigated the difference in loading of either doxorubicin or β-lapachone[102]. The core influenced the release kinetics of the drugs both experimentally and through modeling. The release rate of the drugs was significantly slower due to the increased hydrophobic PCL core, while the drug loading was significantly higher. A detailed explanation of this effect was recently described by Inoue et al., who showed using differential scanning calorimetry, wide angle x-ray

scattering and ultraviolet spectroscopy analyses the variations of interactions between these polymers and a hydrophobic drug, quercetin [103]. These techniques showed that interactions were limited to the hydrophobic core in PCL-PEG polymers, while the drug interacted with both the core and the corona in the more hydrophilic PLA-PEG formulation.

Hydrophobic effects can be further exploited by either post-functionalizing polymers or incorporating a modified monomer into their hydrophobic polymer block. Hedrick et al. used a PEG-poly(trimethylene carbonate) (PTMC) with several cholesteryl 2-(5-methyl-2-oxo-1,3-dioxane-5-carboxyloyloxy)ethyl carbamate groups incorporated in order to improve micelle formulations of paclitaxel. Polymers with incorporated cholesterol groups gave micelles with high paclitaxel loadings of around 15% and exceptional kinetic stability [104]. An alternative strategy to improve formulations of paclitaxel came from Hammond et al., who post-functionalized a poly(propargyl-L-glutamate) with six different hydrophobic side groups. They found that these modifications improved the drug loading, but more importantly had a dramatic impact on the particle stability in blood. Polar side chains led to higher CMC values, but also showed enhanced kinetic stability in the presence of serum proteins [105]. Together, these results suggest that post-functionalization can augment the drug loading and stability of polymeric micelles.

1.6.2 Core Crystallinity and Pi-Pi Stacking

While increasing the hydrophobicity of the core is a general strategy that will increase the loading of a wide range of hydrophobic drugs, recent strategies have focused on facilitating specific interactions between a drug and the core based on the chemical groups in the small molecule. One of the most explored interactions is pi-pi stacking to establish core crystallinity. The earliest example came from Kataoka et al., who conjugated doxorubicin to a polyaspartic acid-PEG to form the polymeric micelle *NK911* [106]. Although the conjugated doxorubicin showed no anti-tumour activity, free doxorubicin was entrapped within the hydrophobic core due to stacking interactions with the conjugated drug. These interactions give a gradual release of free drug over a 24 h period. Drug-drug stacking approaches have been applied to other polymers and drugs, including docetaxel [107], [108] and paclitaxel [109] with some success. The balance of conjugated drug to hydrophobic polymer is delicate and thus when taxanes are conjugated directly to polymers, the CMC increases causing rapid dissociation upon dilution [107].

In an effort to enable specific pi-pi stacking interactions, polymers with aromatic groups can be used. Hennink et al. have synthesized analogues of poly(2-hydroxypropyl) methacrylaminde (P(HPMA))-PEG with either benzoyl or naphthoyl groups to form polymeric micelles with the drugs paclitaxel and docetaxel [110]. Micelles formed showed very high drug loading (>30 wt%) and increased stability. Using solid state NMR spectroscopy, these improved features were attributed to pi-pi stacking between the aromatic rings on the drugs and those appended to the polymers. A similar strategy was used by Zhang et al. to improve doxorubicin loading in a PEG-polyamide amine micelle. Incorporating phenyl groups onto the hydrophobic segment of the copolymer enabled pi-pi stacking and increased drug loading up to 25 wt% [111]. Overall, the facilitation of more specific intermolecular interactions increases loading without jeopardizing the stability of the system.

1.6.3 Colloidal Drug Aggregation

We and others have observed that a subset of small molecule drugs self-assemble in aqueous media to form colloidal aggregates [112]-[116]. The intrinsic physicochemical properties of these drugs were considered a nuisance in early drug discovery due to artifactual results in biochemical and cell-based assays [117], [118]. Recent efforts to modify small molecules and facilitate self-assembly have proven to be a successful strategy for preparing nanoparticles with high loading that can be used in vivo [119]. Unlike the crystalline core of the particles described in the previous section, colloidal aggregation leads to the formation of amorphous liquid-liquid phase-separated particles that can be further stabilized with the addition of small volumes of surfactants or dye molecules [115], [120], [121]. Work by Couvreur et al. enabled the formation of an efficacious doxorubicin aggregate through the conjugation of a squalene tail. The squalenoyl doxorubicin assembled to form a 130 nm loop-train aggregate that was efficacious against a murine lung tumour model and prevented the cardiotoxicity typically associated with this drug [122]. A similar approach was used by Yan et al., who modified irinotecan with chlorambucil to make an amphiphilic drug conjugate [123].

While significant attention has been placed on the synthesis of self-assembling pro-drugs, few attempts have been made to use aggregates of drugs that innately self-assemble, potentially due to the lack of stability and predictability of these systems [113], [121]. In this thesis we investigate the use of polymers to stabilize these colloidal aggregates to form particles with high drug loading without chemical modification to the polymer or drug itself.

1.6.4 Electrostatic Interactions

Additional intermolecular interactions can increase the compatibility of a drug for the core as well as improve the core stability without covalent modifications that may influence the particle properties. Electrostatic interactions within the core can provide a sustained release profile of a specific drug and improve structural stability [124], [125]. By incorporating an opposing charge on the hydrophobic polymer, weak charges on small molecules are stabilized. Borsali et al. showed specific interactions between a poly([2-dialkylamino)ethyl methacrylate] core and several drugs with weak carboxylic acid groups, including ibuprofen and indomethacin [125]. ^{1}H NMR measurements confirmed acid-base interactions and improved loading capacities.

Acid functionalized polymers, such as poly(aspartic acid) or acid functionalized polycarbonates, are stabilized with the addition of cations during the micellization process to increase drug loadings and prevent burst releases [126]-[128]. Acid-functionalized polycarbonates have been used extensively in the Hedrick and Yang labs for the incorporation of amine-containing drugs through acid-base interactions [128]. Specifically, the anti-cancer drugs daunorubicin, tamoxifen, imatinib and doxorubicin, all of which contain amines, have been incorporated with drug loadings up to 35%. While the presence of the acids does increase the CMC due to a reduction in hydrophobicity, incorporating urea-containing polycarbonates to form mixed micelles provides enhanced stability within the core through hydrogen bonding[128].

Incorporating hydrogen bond donors and acceptors into the polymer can facilitate improved drug loading and stability, as has been shown through molecular dynamics simulation of cucurbitacin and polycaprolactone [129]. An increase in hydrogen bonds between the drug and the polymer decreases the Flory-Huggins interaction parameters, thereby increasing the drug solubility within the core. While this and other strategies have proven to be effective for improving drug loading over conventional micelle systems, the incorporation groups that can participate in more drug specific interactions may enable loadings above 20 wt%, allowing for lower polymer concentrations via intravenous injections.

1.7 P(LA-co-TMCC)-g-PEG graft copolymer

The polymer used in this research comprises a hydrophobic copolymer backbone and a hydrophilic graft that forms a unique co-polymer, poly(D,L-lactide-*co*- 2-methyl-2-carboxy-

trimethylene carbonate)-*graft*-poly(ethylene glycol)-furan or P(LA-co-TMCC)-g-PEG-furan. The components of this polymer are well known to the FDA and have been used for many years in medicine with composition-controlled degradation [130]. Due to its amphiphilicity, the polymer is able to self-assemble in water to form stable micelles (nanoparticles) that can encapsulate poorly soluble and systemically toxic chemotherapeutics such as docetaxel [131]. The structure of P(TMCC-co-LA)-g-PEG-furan is shown in Figure 1.7.

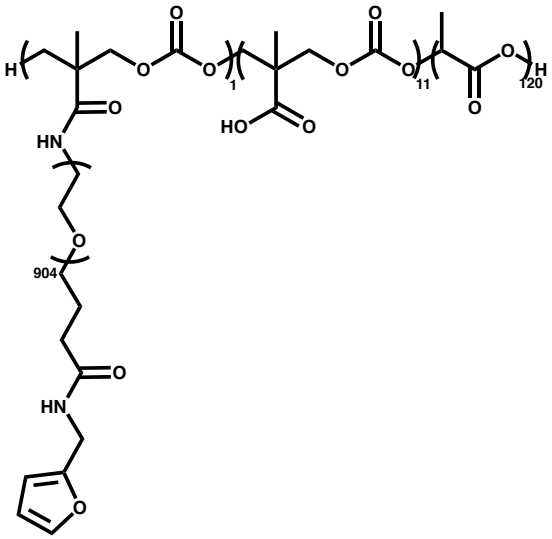

Figure 1.7: Structure of P(LA-co-TMCC)-g-PEG-furan, displayed with 1 PEG/backbone. This polymer is a random copolymer comprised of lactide (90%) and TMCC (10%).

The P(LA-*co*-TMCC) synthesis is catalyzed using a thiourea organocatalyst for the ring opening polymerization of *D,L*-lactide and TMCC-Bn with a pyrenebutanol initiator [132]. This catalyst was developed in the Hedrick lab for the preparation of polylactides with low polydispersity and avoids the use of toxic metal catalysts [133]. Reactivity ratios (r_{LA}=1.1, r_{TMCC}=0.072) predict that our copolymer will be statistical in nature, with enriched lactide repeats [132]. After deprotection of the benzyl ester of the TMCC, a carboxylic acid is produced. Furan-PEG-amine is conjugated onto the backbone using carbodiimide chemistry, producing a polymer with graft morphology.

This novel polymer offers many advantages over traditionally used polymers for micelles. The low CMC (0.26 μM) of this polymer suggests good thermodynamic stability and less susceptibility to dilution upon injection in vivo [132]. End group modification of the PEG with a furan allows for conjugation of biomolecules using DA click chemistry [55], [134], [135]. DA is advantageous as it can be done in aqueous conditions producing high yields and no byproducts

[136]. Previous work showed that maleimide-furan chemistry could be used to conjugate trastuzumab onto the surface of particles for targeted delivery to breast cancer cells. P(LA-co-TMCC)-g-PEG micelles loaded with DTX (4.2wt%) achieved greater tumour retention compared to the conventional ethanolic polysorbate 80 formulation [131]; however the efficacy of this system could not be assessed due to insufficient drug loading. The free carboxylic acids on the TMCC units allow for subsequent polymer modifications not possible with traditional linear polymers which do not bear functional groups along the chain, including modifications to increase the drug loading and stability over previous formulations.

2 PEG graft density controls polymeric nanomicelle stability

*This chapter was published in Chemistry of Materials.

Logie, J., Owen, S.C., McLaughlin, C.K., and Shoichet, M.S. (2014) PEG-graft density controls polymeric nanoparticle micelle stability. *Chemistry of Materials*. 26: 2847-2855.

Reprinted with permission from the American Chemical Society. J.L., S.C.O., C.K.M. and M.S.S. designed research; J.L. performed research and analyzed data; and J.L. and M.S.S. wrote and edited the manuscript.

2.1 Abstract

Polymeric nanoparticle micelles typically comprise amphiphilic block copolymers, having a hydrophobic core that is useful for chemotherapeutic encapsulation, and a hydrophilic corona for aqueous stability. Formulations often require the use of excipients to overcome poor particle stability, yet these excipients can be cytotoxic. In order to create a stable polymeric nanoparticle micelle without the use of excipients, we investigate a series of amphiphilic polymers where the hydrophobic core composition and molar mass is maintained and the hydrophilic corona is varied. With the graft copolymer, poly(D,L-lactide-*co*-2-methyl-2-carboxytrimethylenecarbonate)-*g*-poly(ethylene glycol) (P(LA-co-TMCC)-g-PEG), we demonstrate how PEG density can be tuned to improve the stability of the resulting self-assembled micelle. Increased PEG density leads to micelles that resist aggregation during lyophilization, allowing resuspension in aqueous media with narrow distribution. Furthermore, high PEG density micelles resist dissociation in serum protein containing media, with almost no dissociation seen in serum after 72 h. By changing the number of PEG chains per polymer backbone from 0.5 to 6, we observe increased stability of the nanoparticle micelles. All formulations are cytocompatible, as measured with MDA-MB-231 cells, and show no evidence for hemolysis, as measured with red blood cells. Importantly, PEG density does not impact drug loading within the nanoparticle micelle core, as demonstrated with the potent chemotherapeutic drug, docetaxel, confirming the role of the hydrophobic core for encapsulation. The surface properties of the polymeric nanoparticle micelles can thus be selectively modulated by variation

in PEG density, which in turn influences stability, obviates the need for excipients and provides key insights into the design of drug delivery platforms.

2.2 Introduction

Polymeric nanoparticle micelles have garnered significant attention over the past 20 years for targeted delivery of potent chemotherapeutics in cancer. Amphiphilic copolymers self-assemble in aqueous solution to have a hydrophobic core, in which hydrophobic small molecule drugs are encapsulated, and a hydrophilic corona, which provides stability in aqueous solutions. Given that chemotherapeutics are normally administered in dose-limiting organic solvents and surfactants, polymeric micelles provide a safer alternative for drug delivery by allowing increased dosing levels, prolonged systemic circulation, and greater tumour accumulation through the enhanced permeability and retention (EPR) effect [37], [137]. Ideally, micelles are monodisperse, <200 nm in diameter, and stable to dilution in the presence of proteins [34], [138]. Notwithstanding the many polymeric micelle formulations that have been studied, many have poor stability both *in vitro* and *in vivo* [37], [52], [137], [139].

The most common polymers used in nanoparticle micelles comprise a biocompatible hydrophobic block (e.g., poly(lactic acid), poly(caprolactone), poly(aspartic acid), poly(lactic-co-glycolic acid)) and a biocompatible hydrophilic block, usually poly(ethylene glycol) (PEG) [54], [140], [141]. For decades PEG has been the polymer of choice for a variety of biomedical applications [142], [143]. It is used clinically in a number of protein formulations to prevent premature clearance by the mononuclear phagocyte system and has been shown to be bioresorbable [73], [144], [145]. Several studies have also demonstrated limited protein adsorption and opsonization of PEG-modified nanoparticles - especially those used in solid particle platforms [77], [79], [146]-[150]. We designed a novel, biocompatible graft polymer of poly(D,L-lactide-*co*-2-methyl-2-carboxytrimethylene carbonate)-*g*-poly(ethylene glycol) (P(LA-co-TMCC)-g-PEG) that self-assembles into micelles in aqueous solution [132], [151]. The graft polymer design exhibits a low critical micelle concentration (CMC) and can be easily modified with functional groups for conjugation of targeting antibodies and peptides by click chemistry, thereby enabling receptor-mediated endocytosis [135], [151], [152].

Polymeric micelle stability is of critical importance during storage, handling and clinical use. Insight into thermodynamic stability can be gained by investigating the CMC and freeze-drying, while insight into kinetic stability can be tested with dynamic studies. Many polymeric micelle formulations are unstable under freeze-drying conditions, requiring the addition of excipients. For example, excipients can prevent nanoparticle fusion by inter-particle bridging during the freeze-drying process, yet can themselves be toxic, dose-limiting and thus ultimately undesirable [6], [7], [153], [154]. To avoid the use of excipients, polymeric micelle formulations are prepared immediately prior to use or stored in aqueous solutions, but this is impractical and limits dosing. Despite the importance of polymeric micelle stability in circulation and the wide use of PEG in amphiphilic copolymers, it is surprising that there are few studies that investigate the effect of PEG density on lyophilization and serum stability of micelles [79], [146], [148], [155].

Polymeric micelles used clinically must remain stable after intravenous (IV) injection in order to be useful for targeted delivery. Upon IV injection, micelles are subject to a number of environmental changes including changes in salt concentration, significant dilution and contact with serum proteins. The CMC, the fundamental parameter of thermodynamic stability, is largely influenced by hydrophobic interactions of the amphiphilic polymer [69]. Polymeric micelles often have CMCs in the micromolar concentration range, yet these are often measured in water, which does not accurately reflect the complexity of serum. Polymeric micelles with lower CMCs are more stable with respect to dilution; however, CMC does not always accurately reflect how quickly the micelles will dissociate under environmental influences. The kinetic stability of a micelle reflects its behaviour over time and during disassembly - a property that dramatically shifts with environmental changes. Micelle kinetic stability has been measured under physiological conditions by methods including FRET and conjugation of fluorogenic probes in the presence of serum proteins [155]-[159]. Although these experiments provide valuable insight into the rate of degradation of the micelles, the external probe itself may change the apparent stability of the formulation. Hammond and co-workers recently reported a probe-free strategy to assess the inherent kinetic stability of micelles in the presence of serum using size exclusion chromatography [37], [105], [137].

Herein, we describe a newly designed amphiphilic polymeric nanoparticle micelle with both high thermodynamic and kinetic stability. Our P(LA-*co*-TMCC)-*g*-PEG polymers are comprised of a gradient backbone of lactide and 2-methyl-2-carboxytrimethylene carbonate (comprised of 90%

LA and 10% TMCC) and grafted PEG chains (grafting is controlled to between 5 and 50% of TMCC backbone repeat units). With control of the graft chemistry, the number of PEG chains conjugated to the hydrophobic backbone is tuned, thereby providing a platform with which to investigate the role of PEG density on micelle stability. Using PEG of molar mass 10 kg/mol, we synthesized amphiphilic polymers having an average of 0.5-6 PEG chains per backbone, the molar mass of which is 12 kg/mol. We demonstrate the benefits of increased PEG density on the long-term storage and handling of micelles and under physiologically relevant conditions. These self-assembled polymeric micelles have a narrow size distribution, similar to other block copolymer amphiphilic polymeric micelles, yet have the advantage of allowing the number of PEG chains along the polymer backbone to be easily varied [109], [110], [127], [156], [160]. This approach provides key insights into design elements of other polymeric nanoparticle micelles. As proof of concept for use in drug delivery, we demonstrate the capacity of these polymeric micelles to encapsulate docetaxel, a potent chemotherapeutic anticancer drug with poor water solubility.

2.3 Materials and Methods

2.3.1 Materials

All solvents and reagents were purchased from Sigma Aldrich and used as received unless otherwise noted. Synthesis of 5-methyl-5-benzyloxycarbonyl-1,3-trimethylene carbonate (TMCC-Bn) was carried out as previously reported [96]. .3,6-dimethyl-1,4-dioxane-2,5-dione (Sigma Aldrich, St. Louis, MO) and 1-[3,5-bis-(trifluromethyl)phenyl]—3-[(1*R*,2*R*)-(-)-2(dimethylamino)cyclohexyl] thiourea (Strem Chemicals, Newburyport, MA) were used as received in the synthesis of P(LA-*co*-TMCC). Boc-NH-PEG(10K)-NHS (Rapp Polymere, Tubingen, Germany) was modified according to previously published protocols [96], [135].

2.3.2 Instruments

^{1}H NMRs were recorded at 400 MHz at room temperature using a Varian Mercury 400 spectrometer. The chemical shifts (δ) are in ppm. Molecular weights and polydispersity of P(LA-*co*-TMCC) were measured by gel permeation chromatography (GPC) in THF (containing 0.25% tetrabutyl ammonium bromide) relative to polystyrene standards at room temperature on a

Waters 515 HPLC pump with a RI detector (VE3580) and a UV detector (KNAUER 2500) at a flow rate of 0.6 mL/min. Fluorescence and absorbance measurements were performed with the Tecan Infinite M200 Pro fluorescent plate reader. Serum stability studies were performed using a GE ÄKTA Purifier 10 Fast Protein Liquid Chromatography System equipped with a UV900 monitor. Docetaxel quantification was determined using an Agilent 1100 HPLC equipped with an AB Sciex API 4000 triple quadropole mass spectrometer with electrospray ionization source detector.

2.3.3 Synthesis of poly(D,L-lactide-co-2-methyl-2-carboxytrimethylene carbonate)-g-polyethylene glycol-furan

P(LA-*co*-TMCC) was synthesized as previously described [132]. The copolymer (100 mg) was dissolved in DMF (5 mL). N,N'-diisopropylcarbodiimide (DIC, 100 uL) and hydroxybenzotriazole (HOBt, 16.88 mg) were added and the solution was stirred for 30 min at room temperature. NH_2-PEG-furan (10 kg/mol) was dissolved in 5 mL of DMF and added to the copolymer solution under argon. Varying equivalents (3-12) of PEG to backbone polymer were used to achieve the different graft densities. The reaction was stirred at room temperature for 24 h, after which 500 uL of borate buffer (pH 9, 500 mM) was added and the solution was dialyzed against distilled water. Unreacted PEG was removed using a Sepharose CL-4B column equilibrated with distilled water. Collected fractions with polymer were combined and lyophilized to give a white solid (~60% yield). ^{1}H NMR ($CDCl_3$): δ1.23 (m, CH_3 from TMCC), 1.57 (m, CH_3 from LA), 3.64 (bs, PEG), 4.34 (m, methylene from TMCC), and 5.16 (m, CH from LA).

2.3.4 Micelle preparation

Micelles were prepared by self-assembly in water as previously described [132]. P(LA-*co*-TMCC)-*g*-PEG (4 mg) was dissolved in DMF (1 mL). 50 uL of borate buffer (pH 9, 500 mM) was added and the solution was left at room temperature for 15 min. 0.5 mL of distilled water was added drop wise at a rate of ~1 drop per 3 s. The solution was dialyzed against distilled water for 24 h, changing the water six times (dialysis membrane: MWCO of 2 kg/mol).

2.3.5 Lyophilization

Polymeric micelles (1.2 mg/mL in water) were prepared and flash frozen in liquid nitrogen with and without the addition of pluronic-F68 (P68) at 0.2 w/w polymer/excipient prior to lyophilization. After freeze-drying, formulations were resuspended in water to their original concentration and characterized by DLS.

2.3.6 Dynamic light scattering (DLS) and zeta potential

The hydrodynamic diameter and zeta potential of micelles was determined using a Malvern Zetasizer Nano ZS, equipped with a 4 mW, 633 nm laser. All samples were prepared at a concentration of 1 mg/mL and filtered through a NY-0.45 μm filter (Progene, QC, Canada) prior to use. Measurements were carried out at 25 °C. Hydrodynamic diameter was measured in polystyrene cuvettes (Küvetten, Germany). Hydrodynamic diameters (d_h) were calculated from the Stokes-Einstein equation $d_h = k_B T/3\pi\eta D$, where k_B is the Boltzmann constant, T is the absolute temperature, η is the solvent viscosity and D is the diffusion coefficient. The autocorrelation functions of the scattered intensity were analyzed by means of the cumulant method to yield the effective diffusion coefficient (D) as a function of the scattered angle. The average of 3-5 individual samples with 36 runs each is reported. Zeta potential was measured using folded capillary cells (Malvern, DTS 1060). The average of three individual samples, prepared under the same conditions with 36 runs each is reported.

2.3.7 Transmission electron microscopy (TEM)

TEM images were obtained with a Hitachi H-7000 conventional transmission electron microscope operated at 75 kV. Samples were prepared by placing three drops of particle solution at a concentration of 1 mg/mL in distilled water on a 400 mesh ultrathin carbon film on holey carbon support film copper grid (Ted Pella, Redding, CA). No heavy metal staining agents were used in grid preparation. The water was allowed to evaporate at room temperature prior to imaging. Particles were sized using ImageJ software, with sizes being an average of three individual batches, prepared under the same conditions with 10 particle measurements each.

2.3.8 CMC measurement

Critical micelle concentrations of polymers in PBS (1x, pH 7.4) were determined using the standard pyrene procedure [161]. Briefly, 100 μL of pyrene solution (2 μg/mL in acetone) was added into glass vials. Acetone was allowed to evaporate overnight to form a pyrene film. 1 mL of polymer solution (from 0.1 μg/mL to 250 μg/mL in 1x PBS) was added into each vial and incubated for 24 h at room temperature while shaking. The fluorescence intensity was measured (excitation at 340 nm, emission 390 nm) as a function of polymer concentration. Micellization causes an abrupt change in quantum yield as the pyrene partitions into the hydrophobic core of micelles and its fluorescence intensity shifts.

2.3.9 Polymer hemolysis and cytotoxicity assays

Hemolysis assays were performed following Hoffman's standard procedure [162]. Briefly, blood was collected from a human donor in 4 mL vacutainers coated with EDTA (BD Biosciences, Mississauga, ON). Serum was removed by centrifugation at 1500 rpm for 10 min. The whole blood was washed with 150 mM NaCl three times. After removing NaCl, the sample was increased to its original sample volume with 100 mM phosphate buffer at pH 7.4. The red blood cell solution was diluted 10x with phosphate buffer to give a suspension of 5 x 10^8 RBC/mL and used immediately. Micelle solutions were diluted with phosphate buffer to a total volume of 800 μL and mixed with 200 μL RBC solution to achieve final polymer concentrations of 1000, 800, 500, 250, 130, 65 and 33 μg/mL. After incubation for 1 h at 37°C with mixing, solutions were centrifuged for 5 min at 5000 rpm. The supernatant was collected and the absorbance of lysed, oxygen-saturated hemoglobin was measured at 541 nm. For negative controls, red blood cells were incubated with 800 μL of phosphate buffer (PB, 100 mM) or 0.5 mg/mL dextran (60 kDa) to ensure that the polymeric material did not affect membrane integrity. For positive controls, red blood cells were incubated with deionized water or 1% Triton X-100, both of which are known to rupture membranes. The percent hemolysis was calculated according to the following equation:

$$\%\ hemolysis = \frac{Abs\ (sample) - Abs\ (blank\ PB)}{Abs\ (positive\ control) - Abs\ (negative\ control)} \times 100\%$$

For cytotoxicity assays, polymeric micelles (at 50 μg/mL polymer concentration) were incubated for 5 h with MDA-MB-231 cells seeded overnight in 96 well plates at a density of 1 x 10^3 cells/well in serum containing media. MDA-MB-231 were maintained (<8 passages) in RPMI 1640 growth medium supplemented with 10% FBS, 10 μg/mL penicillin and 10 μg/mL streptomycin. Lactate dehydrogenase assays were performed following the Roche procedure to determine cytotoxicity of polymers (Roche Applied Science, Laval, QC). The cytotoxicity was calculated relative to a positive control (2% Triton-X) and a negative control (cells alone) based on the absorbance of the samples at 490 nm. The experiment was repeated three times, with four wells per experiment for each polymer formulation.

$$\%\ cytotoxicity = \frac{experimental\ value - negative\ control}{positive\ control - negative\ control} \times 100\%$$

2.3.10 Serum stability

Stability was assessed using Fast Protein Liquid Chromatography in a method adapted from Hammond et al [105]. Samples were run through a Superdex 200 gel filtration column with a flow rate of 1 mL/min and 1x PBS (pH 7.4) as the mobile phase. Micelles at a concentration of 1 mg/mL in 1x PBS were incubated with 20% fetal bovine serum (FBS, HyClone, Thermo Scientific). At specific time points after incubation with serum (0, 6, 24, 48 and 72 h), 500 μL aliquots were removed and injected onto the column. Elution peak areas were calculated using UNICORN software version 5.31.

2.3.11 Docetaxel loaded micelles

Docetaxel (DTX) loaded micelles were prepared using the same micellization procedure as described above for polymer alone, except with the addition of 2.4 mg of DTX to the dissolved polymer solution. Free DTX, which is insoluble in water and forms large aggregates, was removed by filtration through a 0.45 μm nylon filter. To determine drug loading, 10 μL of DTX-loaded micelles were diluted 1000x into a 50:50 mixture of acetonitrile and water and analyzed by high performance liquid chromatography coupled with tandem mass spectrometry (HPLC-MS/MS). The drug loading was quantified by comparing to a DTX standard curve (3.125-200 ng/mL) using paclitaxel as an internal standard (100 ng/mL).

2.3.12 Statistics

All statistical analyses were performed using Graph Pad Prism version 5.00 for Macintosh (Graph Pad Software, San Diego, California, www.graphpad.com). Differences among groups were assessed by one-way ANOVA with Bonferroni *post hoc* correction to identify statistical differences among three or more treatments. Alpha levels were set at 0.05 and a p-value of ≤ 0.05 was set as the criteria for statistical significance. Graphs are annotated where p-values are represented as $*p \leq 0.05$, $**p \leq 0.01$ or $***p \leq 0.001$. All data are presented as mean ± standard deviation.

2.4 Results

2.4.1 Polymer synthesis and micellization

P(LA-*co*-TMCC) was synthesized by a ring opening polymerization of D,L-lactide and benzyl protected TMCC (TMCC-Bn) using a pyrenebutanol initiator and a bifunctional thiourea catalyst as shown in Scheme 2.1 [132]. The polymer backbone was characterized by GPC to have an M_n of 12,500 g/mol and a polydispersity index of 1.13 relative to polystyrene standards. ^{1}H NMR showed a composition of 10 mol% TMCC and 90 mol% LA by comparing the integration of peaks at 4.33 ppm (27) and 5.17 ppm (123), respectively. After deprotection of the benzyl group on TMCC, PEG was grafted onto the backbone using DIC and HOBt. The graft density was controlled by varying the molar equivalents of PEG to the hydrophobic backbone. PEG density was calculated by ^{1}H NMR (Figure 2.1) by comparing the proton peak associated with the ethylene oxide of PEG (δ 3.64 ppm) to that associated with the lactide of PLA (δ 5.17 ppm). By ^{1}H NMR, we observed no evidence of PLA backbone cleavage, demonstrating that NH_2-PEG reacted with activated TMCC esters, as expected. Seven batches of polymers were synthesized with densities ranging from 0.5 to 6 PEGs per backbone (representing between 30-80 wt% of the total polymer). A maximum density of 6 PEGs/backbone was obtained (representing 50% of the free carboxylic acids along the backbone), with maximum conjugation likely due to steric hindrance of the large molar mass PEG chains.

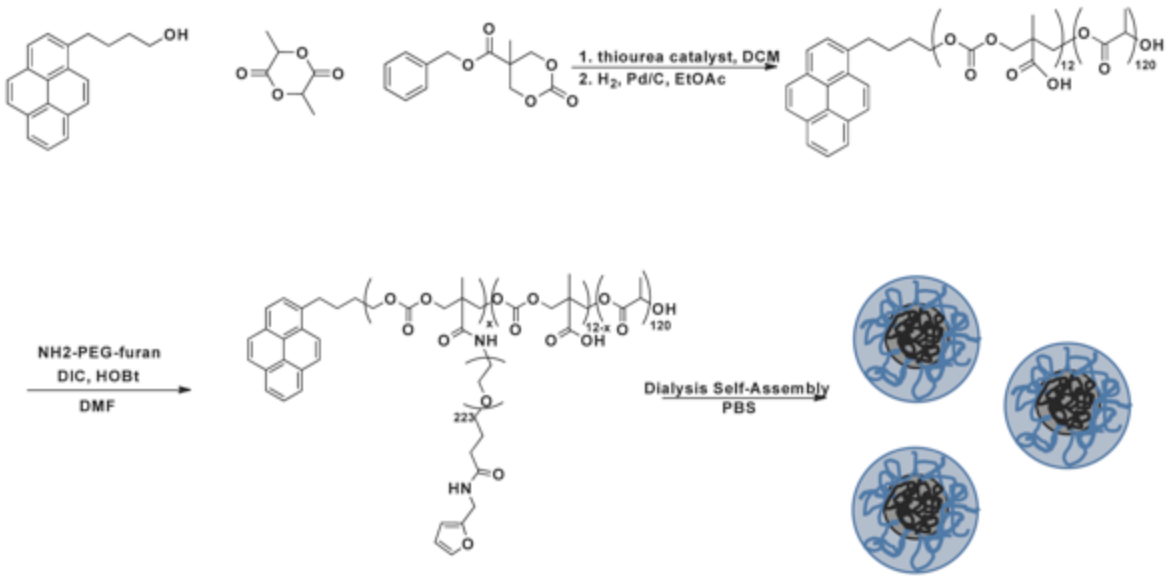

Scheme 2.1: Synthesis of P(LA-*co*-TMCC)-*g*-PEG followed by preparation of polymeric micelles by dialysis. The co-polymer backbone is synthesized by a ring opening polymerization of the monomers D,L-lactide and 5-methyl-5-benzyloxycarbonyl-1,3-trimethylene carbonate (TMCC-Bn) initiated by 1-pyrenebutanol and catalyzed by a bifunctional thiourea. Following benzyl deprotection by palladium-catalyzed hydrogenolysis, bifunctional furan-polyethylene glycol-amine (NH_2-PEG-furan) is grafted onto P(LA-*co*-TMCC) using diisopropylcarbodiimide (DIC) and hydroxybenzotriazole (HOBt) coupling chemistry. The resulting polymer is 90 mol% LA and 10 mol% TMCC, up to half of which have PEG grafted thereon. Micelles were formed by a dialysis self-assembly procedure against phosphate buffered saline (1x, PBS).

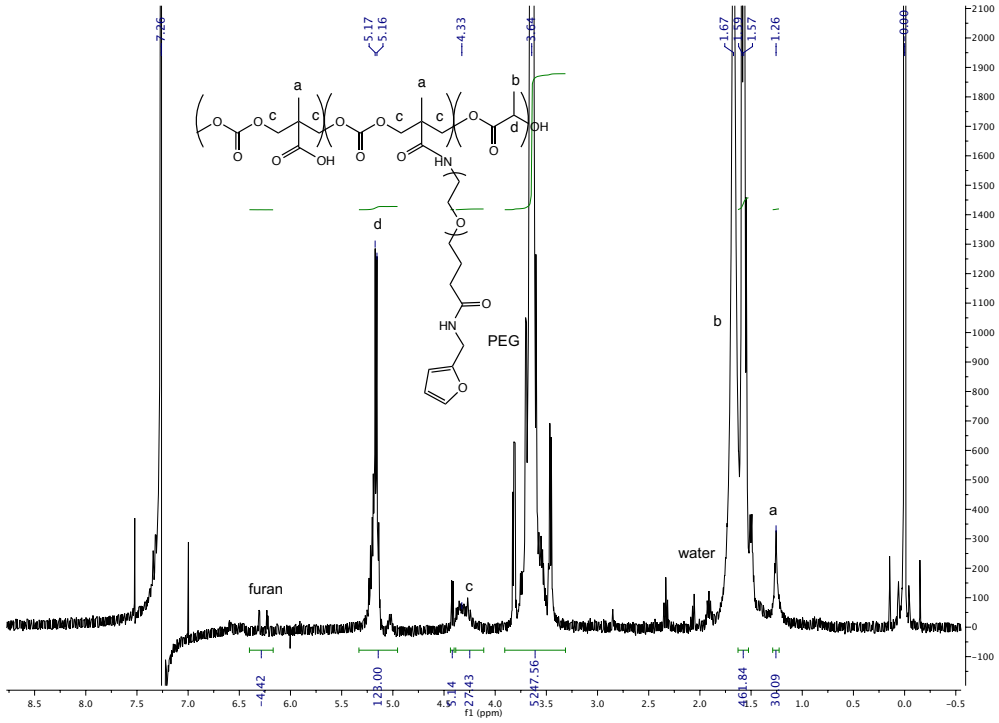

Figure 2.1: ^{1}H NMR of P(TMCC-*co*-LA)-*g*-PEG with ~6 PEG/backbone. ^{1}H NMR ($CDCl_3$): δ 1.41 (m, CH_3 from TMCC), 1.57-1.59 (m, CH_3 from LA), 3.64 (t, CH_2 from PEG, satellite peaks at 3.46 and 3.82), 4.32 (m, CH_2 from TMCC), 5.00-5.19 (m, CH from LA) and 6.23 (m, furan).

Micelles were formed by self-assembly whereby the water-insoluble P(LA-*co*-TMCC)-*g*-PEG is dissolved in DMF and dialyzed against water [132], [151]. The process is likely entropically driven; water molecules bound to the hydrophobic P(LA-*co*-TMCC) backbone are freed as the backbone aggregates together to form the micelle core [74]. The hydrophilic PEG chains form the micelle corona, thereby stabilizing the hydrophobic-hydrophilic interface by limiting the interaction between the core and the aqueous solution [74].

2.4.2 Micelle lyophilization and resuspension

Since excipients, such as P68, have been shown to protect micelles against aggregation through lyophilization [163], we studied lyophilization of our polymeric particles with and without P68 as a function of PEG substitution. Micelles with low PEG densities (i.e., 0.5 or 1 PEG/backbone) form large polydisperse aggregates upon freeze-drying that cannot be disrupted by sonication to polymeric micelles upon re-suspension in aqueous solutions. These low density PEG micelles

require the addition of P68 for re-suspension after lyophilization, as shown in Figure 2.2 and Figure 2.3.

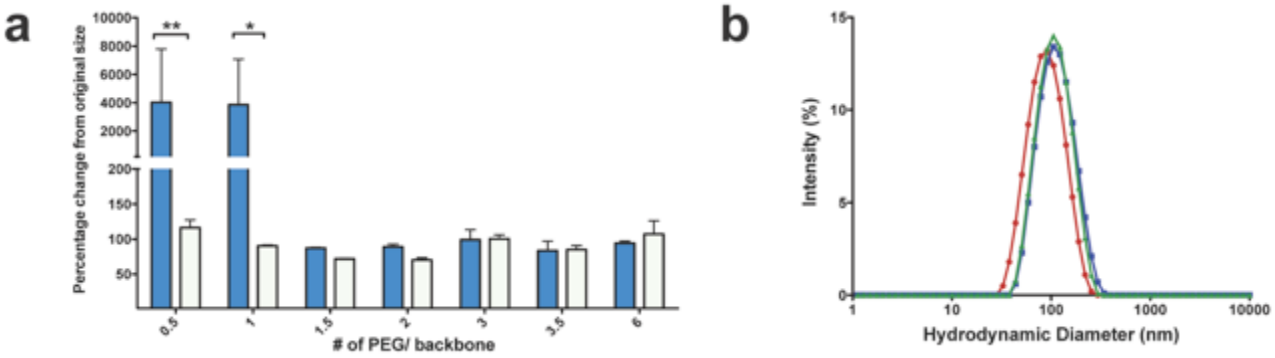

Figure 2.2: Effect of PEG density on nanoparticle micelle stability after lyophilization. (A) As measured by dynamic light scattering, the percent change in diameter of polymeric nanoparticle micelles upon reconstitution in aqueous solution after freeze-drying (□) with or (■) without the excipient Pluronic-F68 (P68) (n=3, mean ± standard deviation, ** p< 0.05, * p<0.01 determined by one way ANOVA and Bonferroni post-hoc test). (B) Size distribution of high PEG (6 PEG/backbone) density nanoparticle micelles: (—●—) before freeze-drying, (—★—) after freeze drying with the excipient P68 and (—■—) after freeze drying without excipients.

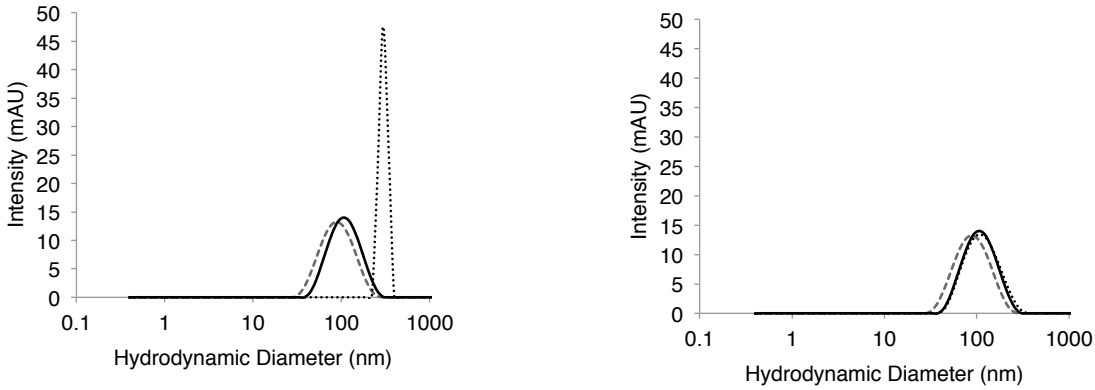

Figure 2.3: Size distribution of low PEG (1 PEG/backbone) and medium PEG (3.5 PEG/bb) density particles before (—) and after freeze-drying with (----) or without (.....) the excipient P68.

As the PEG density increases, the addition of P68 is unnecessary as freeze dried micelles are resuspended to their original micelle size without evidence of aggregation. Micelles with docetaxel encapsulated showed an identical trend, as shown in Figure 2.4.

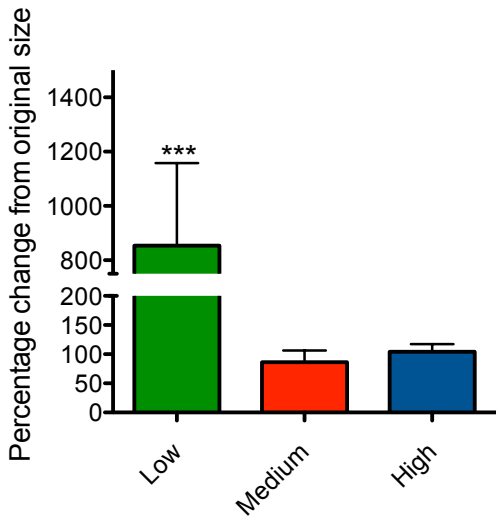

Figure 2.4: Effect of PEG density on nanoparticle micelle stability after lyophilization. As measured by dynamic light scattering, the percent change in diameter of polymeric nanoparticle micelles with DTX encapsulated upon reconstitution in aqueous solution after freeze-drying (n=3, mean ± standard deviation). A similar trend is observed between empty nanoparticle micelles (Fig 2.2) and drug-loaded micelles shown here.

2.4.3 Micelle optimization

In order to better assess the influence of PEG density on nanoparticle micelle stability, three micelle formulations were chosen for further characterization in terms of micelle diameter, micelle size distribution/polydispersity and stability in protein rich aqueous solutions, as shown in Table 2.1: 1 PEG/backbone (low PEG density), 3.5 PEG/backbone (medium PEG density), and 6 PEG/backbone (high PEG density).

Table 2.1: Characterization of low (1 PEG/backbone, bb), medium (3.5 PEG/bb) and high (6 PEG/bb) PEG density polymers and micelles.

PEG Density	PEG/bb[a]	M_n (kg/mol)[a]	CMC (μM)[b]	N_{agg} (x10^3)[c]	Micelle distribution[d]
Low	1	22	0.54±0.06	1.32	0.156
Medium	3.5	47	0.55±0.05	3.37	0.158
High	6	72	0.37±0.04	5.98	0.093

[a]Average PEG number per backbone and total polymer molar mass were obtained by ^{1}H NMR. [b]CMC was measured by the pyrene method, n=4, mean±standard deviation [c]N_{agg} is an estimate of the number of polymer chains aggregated in one micelle [d]Distribution of micelles in PBS is determined by dynamic light scattering

The CMCs of polymers, summarized in Table 2.1, were determined using the standard pyrene procedure as shown in Figure 2.5 [105], [161]. The CMCs of P(LA-*co*-TMCC)-*g*-PEG polymers ranged from 0.37-0.54 μM, with the high PEG density polymer having the lowest CMC. The trend in decreasing CMC and increasing aggregation number is attributed to the decrease in carboxylic acids within the core, making the core more hydrophobic and reducing repulsion between backbone polymer chains [132].

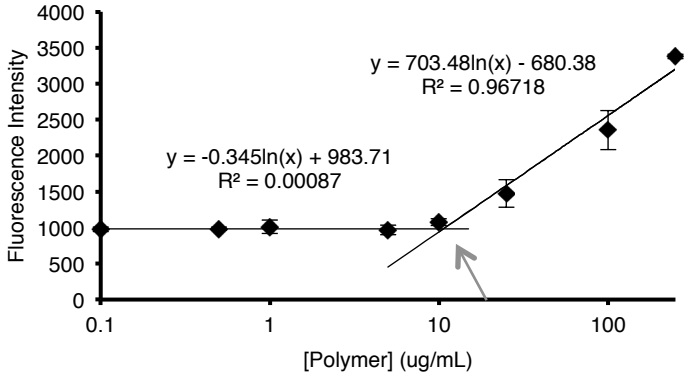

Figure 2.5: CMC determination using pyrene fluorescence intensity (excitation 340 nm, emission 390 nm), where pyrene fluorescence changes as a function of its environment. Representative graph shown with low PEG density (1 PEG/bb) polymer shown.

The negative surface charge of polymeric micelles with low PEG density increased toward neutral with increased PEG density, as measured by zeta potential (Figure 2.6A). There are two contributing reasons for this phenomenon: (1) with increased PEG density there are fewer free TMCC carboxylate ions within the core that normally contribute to the negative surface potential; and (2) with increased PEG density, the remaining TMCC carboxylates within the core are better shielded.

Size measurements by DLS and TEM showed an increase in diameter with an increase in PEG density (Figure 2.6 B,C). TEM measurements were smaller than those by DLS, consistent with the dehydrated state of the micelles when they are measured using this technique. Notably, low PEG density micelles tended to aggregate during dehydration and form thin films making them difficult to image, an effect that was not seen when dehydrating high PEG density micelles. Even in areas of poor dispersion on the TEM grid, micelles of high PEG density polymers did not flocculate or form thin films (Figure 2.6D). All polymeric micelles had diameters <150 nm, suggesting that they are suitable for studies that rely on the EPR effect.

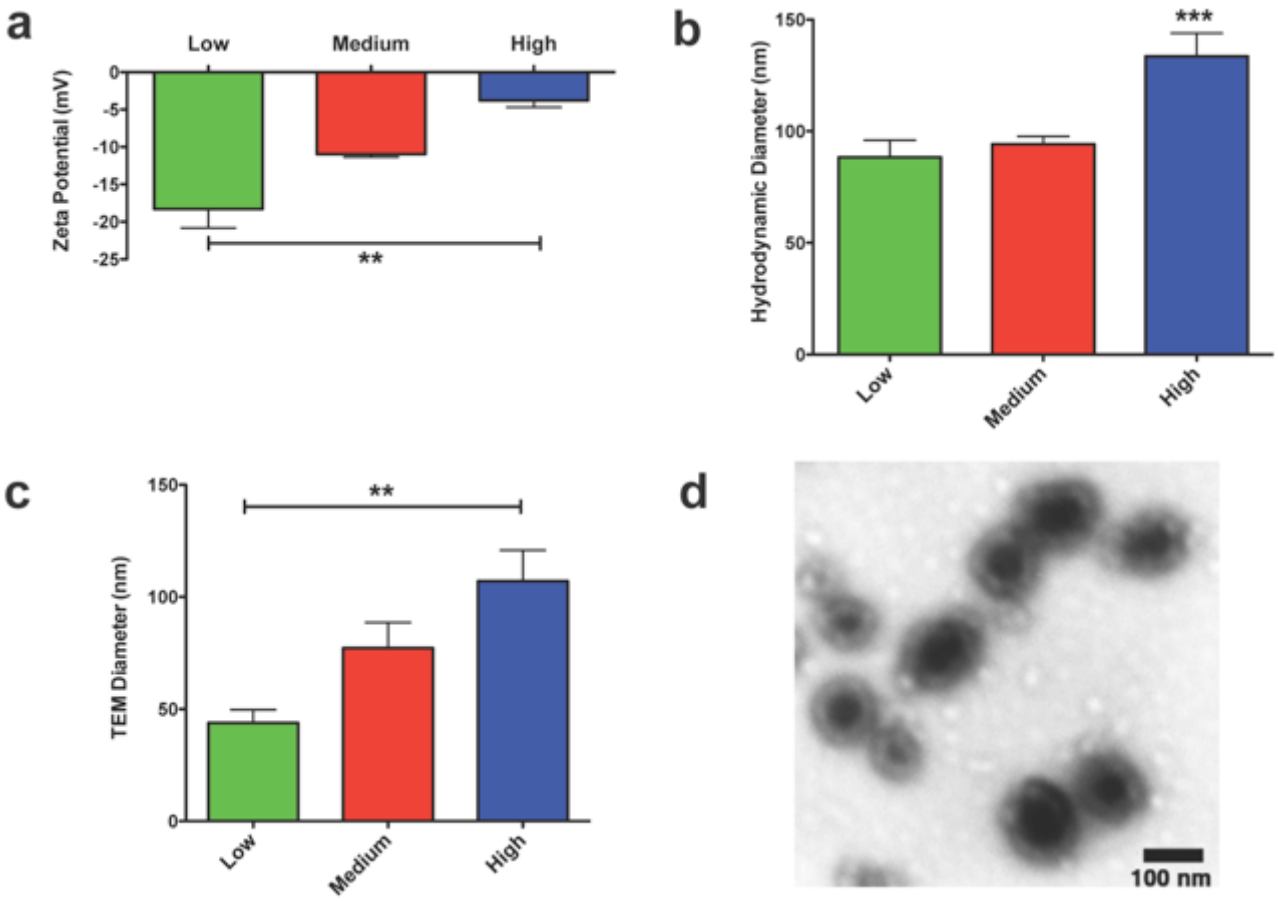

Figure 2.6: Micelle characterization (A) Zeta potential measurements of micelles in water at 1 mg/mL: zeta potential increases towards neutral with increased PEG density. (B) Hydrodynamic diameter determined by DLS: polymeric nanoparticle micelle diameter increases at high PEG density. (C) Nanoparticle micelle diameter measured by TEM increases with increased PEG density. TEM diameters are less than DLS diameters because TEM measures the dry state whereas DLS measures the hydrated state. (D) Representative TEM image of high PEG density nanoparticle micelles clearly shows individual nanoparticle micelles (scale bar is 100 nm). No heavy metal staining agents were used in TEM image. For (A), (B), (C): n=3 independent batches of micelles, mean + standard deviation, ** p<0.01 and ***p<0.001 by one-way ANOVA.

2.4.4 Hemolysis and cytocompatibility of polymeric micelles

P(LA-*co*-TMCC)-*g*-PEG micelles of low, medium and high PEG densities were evaluated for hemolysis with red blood cells and cytotoxicity with metastatic breast cancer MDA-MB-231

cells. Since common excipients to solubilize chemotherapeutics can cause undesirable side effects, we wanted to ensure that the nanoparticles micelles themselves are not cytotoxic and are good candidates for use as drug delivery vehicles. Micelles were incubated with human red blood cells to check for hemolysis. All three formulations showed no hemolysis, as quantified relative to the amount of heme released into pure water and detected by absorbance at 451 nm (Figure 2.7). Cytotoxicity was assessed by the lactate dehydrogenase (LDH) assay after incubation of the micelles with MDA-MB-231 cells. All formulations showed no cytotoxicity relative to a positive control (2% Triton-X) and a negative control (untreated cells) (Figure 2.7). These data demonstrate that all three micelle formulations are cytocompatible.

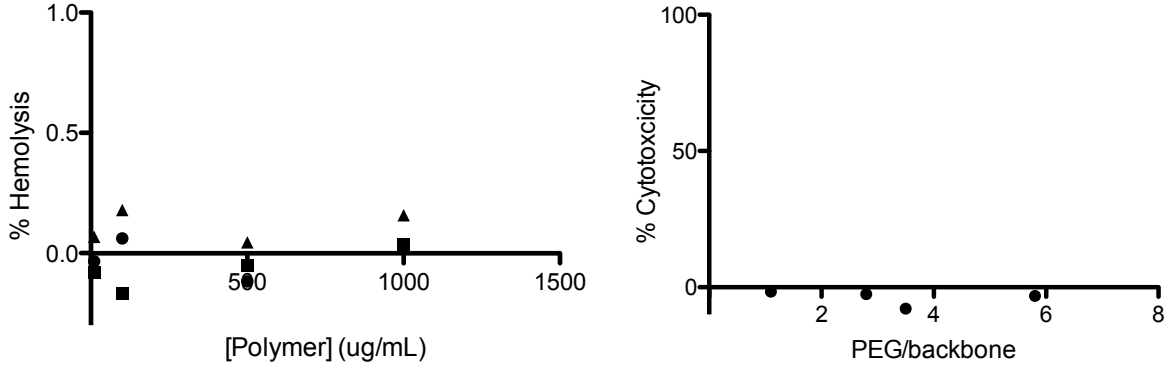

Figure 2.7: (a) Hemolytic activities of micelles (• low peg density, ■ medium peg density and ▲ high peg density) as a function of polymer concentrations demonstrate that all formulations are cytocompatible with red blood cells (under 0.2% hemolysis relative to a positive control of DI water). (b) LDH cytotoxicity results. Cytotoxicity is calculated relative to a high control (2% TritonX) and a low control (untreated cells) based on absorbance of reagent at 490 nm. (n=3 independent experiments, mean ± standard deviation)

2.4.5 Kinetic stability

In order to assess the kinetic stability of micelles with varying PEG densities, micelles (1 mg/mL) were incubated in the presence of FBS (20 vol%) at 37 °C. 20% serum represents a good proxy for both in vitro and in vivo studies, while still allowing micelles to be separated and quantified by FPLC as a direct measure of their stability. At selected times, up to 72 h, the micelles were separated from serum proteins using size exclusion chromatography (SEC) on a

Superdex 200 column. The micelle stability was associated with the peak intensity at 280 nm at 12 mL eluant: a decrease in peak area indicates micelle dissociation.

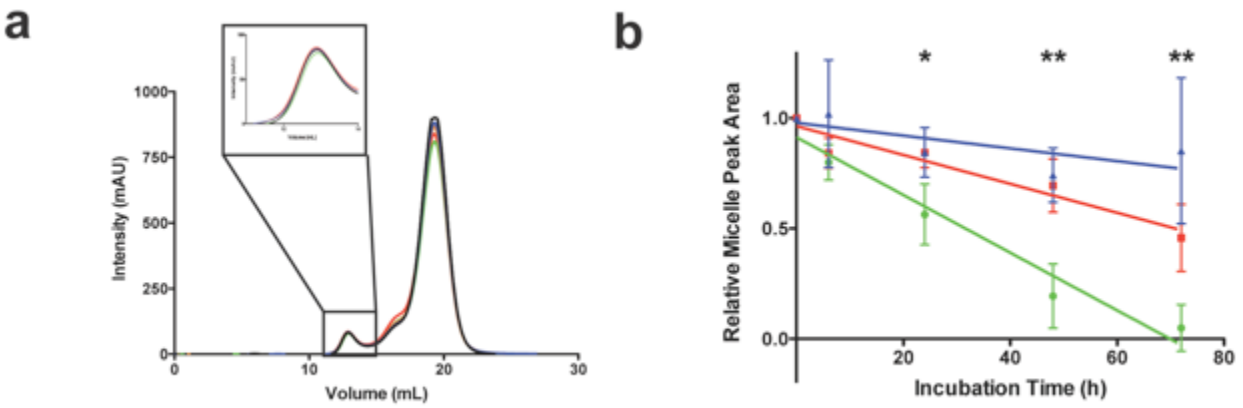

Figure 2.8: (A) SEC traces at 280 nm of high PEG density micelles incubated with 20 vol% FBS for different time periods (— 0 h, —6 h, —24 h, —48 h, and —72 h) at 37 °C show clear separation of the polymeric nanomicelles (eluent at 12 mL) from FBS proteins (eluent at 18 mL). (B) Change in peak area of micelles as a function of incubation time. Decrease in peak area indicates micelle dissociation: (—■—) high PEG density micelles are the most stable, followed by (—●—) medium and then (—▲—) low PEG density micelles (n=4, mean ± standard deviation, * p<0.05, ** p<0.01 by one-way ANOVA followed by Bonferroni post-hoc test).

As shown in Figure 2.8a, the peak at 12 mL corresponds to the micelle peak, while the peak at 18 mL corresponds to the various serum proteins in FBS as well as dissociated, free polymer chains (Figure 2.9). The micelle formulations were compared by relative micelle peak area over time, as shown in Figure 2.8B. At high PEG density, the micelle peak did not change significantly as a function of time ($p>0.05$), suggesting little micelle dissociation over the 72 h period. The low PEG density micelle peak area decreased significantly over time due to the dissociation of micelles in the presence of serum proteins, with no micelles detectable at 72 h. Linear regression analysis shows that the slopes representing the dissociation of the three PEG density formulations were significantly different ($p<0.002$). Significant differences were detected between formulations at 24 ($p<0.05$), 48 and 72 h ($p<0.01$), while there was no significant difference at 6 h. Half-lives of the formulations (i.e., when 50% of the micelles are dissociated) were estimated by the time at which the micelle peak area had decreased to 50% of its initial value. The low PEG density micelles have a half-life of 32 ± 5 h and medium PEG density

micelles have a half-life of 71 ± 12 h. A half-life for the high PEG density micelles could not be estimated over this time period, as the slope of the line for the decrease in peak area was not significantly different from zero.

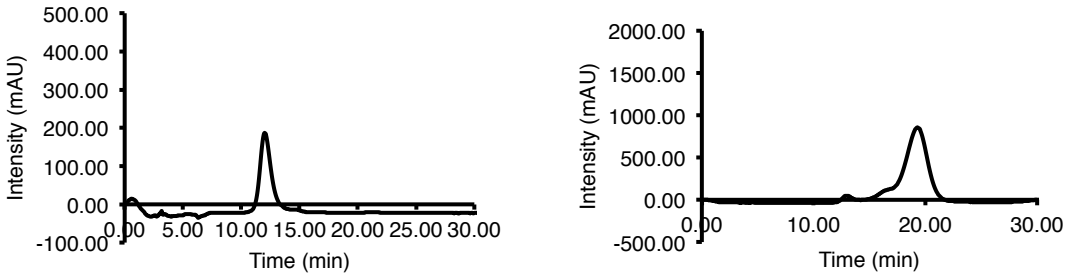

Figure 2.9 Elution peaks of (A) nanoparticle micelles and (B) FBS showing background absorbance intensity from FBS at 280 nm.

2.4.6 DTX loading

To understand whether these P(LA-*co*-TMCC)-*g*-PEG micelles would be effective drug delivery vehicles, the loading of a hydrophobic chemotherapeutic, docetaxel, was assessed using HPLC-MS/MS. There was no significant difference in terms of drug loading as a function of PEG density (Figure 2.10A), suggesting that loading of this hydrophobic drug is dictated only by the hydrophobic interactions within the core. Since the core molar mass and chemical structure were not changed by PEG grafting density, the drug loading was constant for all formulations at approximately 10 wt% relative to the hydrophobic core; however, when compared to the total mass of the polymer micelle, percent loading necessarily decreases with increased PEG density (Figure 2.10B).

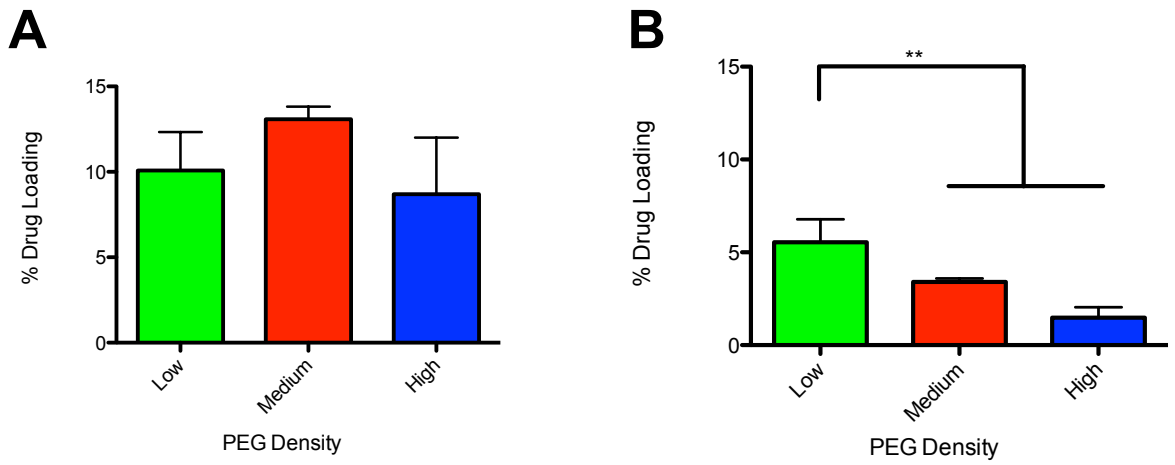

Figure 2.10 (A) Percent drug loading relative to the mass of the hydrophobic backbone, P(LA-co-TMCC). The level of PEG density did not significantly affect the relative amount of drug loaded per micelle (n=4, mean ± standard deviation, p=0.15 by one-way ANOVA between all groups) (B) While percent drug loading relative to the hydrophobic core is unchanged for all three formulations with low, medium and high PEG density polymers, when the total mass of the polymer micelle is considered, the percent loading decreases relative to the mass of the total polymer, P(LA-co-TMCC)-g-PEG. (n=3, mean ± standard deviation, ** p<0.01 by one-way ANOVA followed by Bonferroni post-hoc test)

2.5 Discussion

PEG is known to prevent protein adsorption and particle opsonization, and for this reason has been integrated into a variety of particle platforms intended for clinical use [164], [165]. Despite the prevalence of PEG as the hydrophilic block in polymer micelles, there has been limited research on the effect of PEG density on nanoparticle micelle stability, which is critical to their ultimate success clinically. Several groups have shown the shielding effect associated with increased PEG molecular weight, but even with high molecular weight PEG, polymeric micelles often requires the use of excipients for stabilization [79], [153]. Composition of the copolymer used here, P(LA-*co*-TMCC), provides a convenient platform to control the graft density of high molecular weight PEG. In addition, PEG grafting to TMCC carboxylic acid groups can be achieved throughout the backbone and is not limited to terminal polymer modification with higher molecular weight or branched PEGs, as is required by other systems [79], [166]. This

unique graft architecture allows us to control PEG conjugation along the polymer chain in order to produce brush-like polymer morphologies that self-assemble into well-defined nanoparticle micelles.

The ability to lyophilize micelles and resuspend them without aggregation enables dry product storage, eliminating concerns of solution stability of polymer, micelle and drug. Numerous micelle formulations have had limited use due to the necessity for fresh preparation prior to use [167]. To overcome this, micelle syntheses often require the addition of excipients as stabilizers for the freeze drying process, which increases both the complexity and potential cytotoxicity of the formulation. Common excipients used to stabilize nanoparticle micelles are known to cause a number of side effects such as rupturing cell membranes, hypersensitivity reactions, erythrocyte aggregation and peripheral neuropathy [6], [168]-[170]. Moreover, PEG-based micelles are particularly notorious for crystallizing during freeze drying, causing significant aggregation even with the addition of polysaccharides [171], [172]. Prud'homme and colleagues successfully lyophilized several different micelle formulations, including PLA-co-PEG, with the addition the P68 [154]. In this study, we found that only the low PEG density P(LA-*co*-TMCC)-*g*-PEG micelles required P68 in order to prevent aggregation of particles during lyophilization. P68 is a block terpolymer of poly(ethylene oxide)-poly(propylene oxide)-poly(ethylene oxide), (PEO-PPO-PEO). Its proposed mechanism of stabilization is based on the PPO adsorbing onto the particle surface and the PEO intercalating between the nanoparticle micelle PEG chains, thereby causing the PEG chains to adopt a more extended conformation [173]. This extended brush-like conformation sterically stabilizes the particles [174]. Higher PEG densities incorporated into our polymeric micelles appear to have the same effect as this excipient, but without the added complexity and toxicity concerns associated with P68. The crowded surface prevents coalescence at high polymer concentrations during freeze-drying, critical for re-suspension without changes in either size or polydispersity. This effect was confirmed by TEM where high PEG density micelles were easily imaged, even in areas of high polymer concentration on the grid, as they maintained their structure without aggregating into a film. In summary, the architecture of our copolymer facilitates the stabilization of micelles through both freeze-drying and concentrating procedures.

Interestingly, all PEG density formulations had CMCs between 0.37 and 0.54 μM, suggesting that they are thermodynamically stable. This is of particular interest considering the increase in

hydrophilic PEG between formulations (from 30 to 80 wt%) - an effect which contrasts what is seen in linear systems, where it has been shown that an increase in the length of the hydrophilic block also increases the CMC [74]. Since all of our P(LA-*co*-TMCC)-*g*-PEG copolymers differ only in the number of PEG chains, the low CMCs of all formulations suggest that micelle thermodynamic stability is dictated not by the hydrophilic corona, but rather the length, hydrophobicity and cohesion of the hydrophobic polymer within the core of our graft copolymers [141], [175]. The CMCs of our polymers, measured using the standard pyrene method, are all lower than Pluronics and many common amphiphilic polymers, such as PLA-PEG diblock copolymers, indicating that they are less susceptible to disassembly upon dilution, which is key for administration by intravenous injection [137].

Colloidal systems typically flocculate because they lack electrostatic repulsion at neutral zeta potential [176]. However, our polymeric nanoparticle micelles are stable as zeta potential increases to neutral, which is likely due to steric repulsion among the higher density of PEG chains that forces an extended brush-like conformation in the corona [177]. By reducing contact between micelles, the higher PEG density also may diminish van der Waals forces of attraction between the particles that usually account for their flocculation [176]. As negatively charged species are often cleared more rapidly than neutral species by immune cells [178]-[180], we anticipate that our micelles will result in less opsonization and longer resident circulation times *in vivo*.

To test kinetic stability, we assessed the dissociation of micelles over time in the presence of serum containing cell culture media. The more physiological composition (protein, salt, pH etc.) of this medium can shift the equilibrium between the free polymer chains and the micelle, resulting in more rapid dissociation. As expected, low PEG density micelles, while still having a half-life greater than 30 h, began dissociating almost immediately after incubation. In contrast, high PEG density micelles are more kinetically stable, with almost no dissociation over a 72 h incubation at 37 °C. The presence of proteins in the blood upon intravenous injection is well known to destabilize micelles due to protein adsorption on the surface, so the improved kinetic stability of high PEG density micelles is likely beneficial for future *in vivo* studies.

While the kinetic and thermodynamic stability of the polymeric nanoparticle micelles are influenced by the hydrophilic corona, the loading of a hydrophobic drug is predominantly

influenced by the hydrophobic block composition. Here, increasing the graft PEG density did not significantly change the drug loading of the potent chemotherapeutic docetaxel, which has a similar drug loading to that achieved with other polymeric micelles [75], [141], [181]. To further enhance drug loading, polymeric nanoparticle micelle core modifications may be investigated with this system [106], [108], [110], [129].

2.5.1 Conclusions

With our gradient copolymers of P(LA-*co*-TMCC)-*g*-PEG, we have demonstrated both near monodisperse synthesis and control over PEG graft density. Subsequent self-assembly into polymeric micelles allowed us to study the role of PEG graft density on both thermodynamic and kinetic stability. Although choosing an 'optimal' PEG density will depend on many factors, here we show a unique graft polymer morphology that can be used to prepare polymeric micelles with desirable drug delivery properties (low CMC, kinetic and thermodynamic stability, minimal cytotoxicity). In future work, PEG can be functionalized with targeting ligands to provide a strategy for either receptor-mediated endocytosis [37], [67], [134], [182] or enhanced stealth evasion of the native immune system [183], [184]. Overall, controlling unimer composition by tuning PEG graft density has clear implications for enhancing micelle stability and thus presents a strategy that can be broadly applied to other amphiphilic self-assembling polymeric systems intended for drug delivery applications.

2.6 Acknowledgements

We thank Professor Robert Prud'homme (Princeton University) for insight into lyophilization of polymeric micelles and Professor Mitchell Winnik and Peng Liu (both at the University of Toronto) for the use of their GPC. We are grateful for partial funding from the Natural Sciences and Engineering Research Council of Canada (MSS, PGSD to JL and PDF to CKM) and the Canadian Institutes of Health Research (MSS).

3 Leveraging colloidal aggregation for drug-rich nanoparticle formulations

*This chapter was submitted to *Molecular Pharmaceutics*. #These authors contributed equally to this work.

Ganesh, A.G.#, Logie, J.#, McLaughlin, C.K.#, Barthel, B.L, Koch, T.H., Shoichet, B.K. and Shoichet, M.S. (2016) Leveraging colloidal aggregation for drug-rich nanoparticle formulations.

A.G., J.L., C.K.M. and M.S.S. designed research; A.G. performed experiments with fulvestrant; J.L. performed experiments with PPD; C.K.M. performed transmission electron microscopy experiments for all formulations; and A.G., J.L., C.K.M. and M.S.S. wrote and edited the manuscript.

3.1 Abstract

While limited drug loading continues to be problematic for chemotherapeutics formulated in nanoparticles, we found that we could take advantage of colloidal drug aggregation to achieve high loading when combined with polymeric excipients. We demonstrate this approach with two drugs - fulvestrant and pentyl-PABC Doxazolidine (PPD) – a crosslinking, anthracycline prodrug of doxorubicin; and two polymers, respectively - polysorbate 80 (UP80) and poly(D,L-lactide-co-2-methyl-2-carboxytrimethylene carbonate)-graft-poly(ethylene glycol) (P(LA-co-TMCC)-g-PEG) – a custom-synthesized, self-assembling, amphiphilic polymer. In both systems, drug-loaded nanoparticles had diameters <200 nm, were stable for up to 2 days in buffered saline solution, and for up to 24 h in serum-containing media at 37°C. While colloidal drug aggregates alone are typically unstable in saline and serum-containing media, we attribute colloid stability herein to the polymeric excipients and consequent decreased protein adsorption. We expect that this strategy of polymer-stabilized colloidal drug aggregates to be broadly applicable in delivery formulations.

3.2 Introduction

The inefficient formulation of hydrophobic small molecule drugs continues to be a barrier between drug development and clinical use. Although excipients can solubilize drugs for in vivo delivery, the high excipient concentrations necessary are associated with dose-limiting adverse effects, such as hypersensitivity and hemolysis[170], [185], [186]. While nanoparticle delivery systems have been developed to overcome this toxicity and to improve drug bioavailability and

biodistribution[54], [187], [188], these strategies are themselves limited by low drug loading[41], [43], [49], [189], [190].

To produce more drug-rich systems and to overcome the limitations of excipient toxicity, an alternative approach has emerged to exploit the intrinsic physicochemical properties of a drug directly in formulation. These formulations generally take advantage of the immiscibility of hydrophobic drugs in aqueous media, which results in self-aggregation to produce a particle core[122], [191]. More recently, co-formulation strategies have been developed that use macromolecules, either during or after particle formation, to suppress Ostwald ripening through stabilization of the drug-particle surface[192]. However, less attention has been given to the potential self-assembly parameters of the drugs themselves.

In the past decade, many drugs have been shown to self-assemble into colloidal drug aggregates. In early drug discovery[115] this leads to artifacts including both false positives in biochemical[118], [193] and false negatives in cellular assays[112], [113]. Though hard to predict[194], the mechanism of self-assembly for these colloidal aggregators is governed by a critical aggregation concentration (CAC) and leads to the generation of amorphous liquid-liquid phase-separated particles[115], [116]. While the assembling properties have been well studied, the utility of these aggregates is hindered by their instability[113], [117]. We and others have attempted to stabilize colloidal drug aggregates in order to further study both their biological implications and use in drug delivery[121], [192]. Previously, we demonstrated that co-aggregation with azo-dyes can stabilize colloids, resulting in a maintenance of structural integrity in high ionic strength solutions and serum-containing media[121]. The incorporation of polymeric excipients, such as pluronics and polysorbates, remains an attractive method to stabilize colloidal aggregates due to the chemical diversity of polymers available and their ubiquity in pharmaceutical formulations. Work by Taylor et al. has shown that polymeric excipients can modulate the colloidal properties of drug aggregates, however only modest improvements in stability (less than 2 h) have been achieved thus far[120], [195].

Here, we investigate how small molecule colloidal drug aggregation properties can be combined with polymeric excipients to substantially improve particle stability. Using pharmaceutical excipients and biocompatible amphiphilic polymers, we demonstrate that colloidal drug aggregates can be formulated for multi-day stability in both buffered saline and serum-containing

media. With this strategy, we not only stabilize colloidal drug aggregates, but overcome the low drug loading typically found in traditional polymeric nanoparticle systems. Monodisperse and stable colloidal formulations are achieved using polymeric excipients of two chemotherapeutics: the estrogen receptor antagonist fulvestrant[113], [196] and the novel anthracycline-derived prodrug of doxorubicin, pentyl-p-aminobenzylcarbamate doxazolidine (PPD)[15]. After screening a series of polymers, we found that the optimal polymer-colloid combination is specific to each drug; however, this approach should be broadly applicable to other colloidal drug aggregators. As a proof of concept for use in drug delivery, we investigate the stability in serum-containing media, variations in protein adsorption properties and interactions with cancer cells of these colloidal formulations.

3.3 Materials and Methods

3.3.1 Materials

PPD was synthesized from expired clinical samples of doxorubicin (FeRx Inc, Aurora, CO) as previously described [15]. Fulvestrant was purchased from Selleckchem. Poly(D,L-lactide-co-2-methyl-2-carboxy-trimethylene carbonate)-graft-poly(ethylene glycol) (P(LA-co-TMCC)-g-PEG) was synthesized by a ring-opening polymerization and conjugated with an average of 3 PEG chains/backbone as previously described [197]. Polysorbate 80 (H2X, UP80) was purchased from NOF America Corporation. Vitamin E-PEG 1000 (VitEPEG), Pluronic F68, Pluronic F127, Brij L23 and Brij 58 were purchased from Sigma Aldrich. McCoy's 5A cell culture media, CholEsteryl BODIPY 542/563 C11, Hoechst 33342 were purchased from Thermo Fisher Scientific. The SKOV-3 cell line was purchased from ATCC. Charcoal stripped fetal bovine serum and Hank's balanced salt solution were purchased from Wisent Bioproducts.

3.3.2 Colloid formation

Colloids of both fulvestrant and PPD were formulated upon dilution of organic stock solutions into an aqueous phase. Fulvestrant colloids were prepared by adding double-distilled water (880 μL) to DMSO stock solution (10 μL at 5 mM) followed by the addition of 10X PBS (100 μL). Final fulvestrant drug and organic concentrations were 50 μM and 1% (v/v), respectively. PPD colloids were prepared in a similar manner with drug stock solution at 12.5 mM in DMF leading to formulations with a final drug concentration of 500 μM and an organic concentration of 4% (v/v). Excipients were incorporated into formulations prior to colloid formation. P(LA-co-

TMCC)-g-PEG was added to the organic phase while all other excipients studied were dissolved in the aqueous phase. Amounts of polymers were chosen based on the initial concentration of drug being formulated. For fulvestrant colloids formulated at 50 μM excipients were used at the following concentrations: 0.001% (w/v) UP80, 0.01% F127, 0.01% F68, 0.01% Brij L23, 0.01% Brij 58, 0.01% VitEPEG and 0.004% P(LA-co-TMCC)-g-PEG. For PPD colloids formulated at 500 μM excipients were used at the following concentrations: 0.01% UP80, 0.05% F127, 0.05% F68, 0.01% Brij L23, 0.01% Brij 58, 0.01% VitEPEG and 0.04% P(LA-co-TMCC)-g-PEG.

3.3.3 Colloid characterization

Colloid diameter, polydispersity and normalized scattering intensity were measured by dynamic light scattering (DLS) using a DynaPro Plate Reader II (Wyatt Technologies) with a laser width optimized for colloidal aggregate detection (i.e., particles in the 100 to 1000 nm radius range) by the manufacturer. Operating conditions were 60 mW laser at 830 nm wavelength and detector angle of 158°. Samples were measured in a 96-well format with 100 μL and 20 acquisitions per sample.

Colloids (5 μL) were deposited from 50 μM and 500 μM solutions of fulvestrant and PPD, respectively, onto glow discharged transmission electron microscope (TEM) grids and allowed to adsorb for 5 min. The solution was then wicked away and the grid was washed briefly with water (5 μL). Grids were then allowed to dry and negatively stained with either uranyl acetate (5 μL, 10 sec, 2 % solution, pH ~4) for PPD colloids or ammonium molybdate (5 μL, 30 sec, 1% solution, pH 7) for fulvestrant colloids prior to imaging on a Hitachi H-7000 microscope operating at 75 kV.

3.3.4 In vitro serum stability

The stability of fulvestrant and PPD colloids under serum conditions was determined using fast protein liquid chromatography (FPLC) using a previously established method [105], [190]. Colloids were incubated with 20% fetal bovine serum (FBS, Charcoal stripped) and 1% penicillin - streptomycin at 37°C. At 0, 6, 12, 24 and 48 h, 500 μL aliquots were removed and injected onto a Superdex 200 gel filtration column. Samples were run with a flow rate of 1.5 mL/min and 1x PBS as the mobile phase. For fulvestrant, colloids were co-formulated with the FRET pair of CholEsteryl BODIPY FL and BODIPY 542/563 (500 nM) and fluorescent emission at 575 nm was determined using a Tecan plate reader followed by integration of colloid

peak area using GraphPad software version 6.0. For PPD, elution peak areas at 480 nm were calculated using UNICORN software version 5.31. Neither the polymer nor the FBS contribute to the absorbance at 480 nm or the fluorescence at 575 nm. Without polymer, PPD and fulvestrant colloids precipitate rapidly in PBS and thus their stability cannot be assessed by FPLC.

3.3.5 In vitro protein adsorption

Fulvestrant and PPD colloids were prepared at 50 μM as before in the presence or absence of UP80 and P(LA-co-TMCC)-g-PEG, respectively. Colloids were then incubated with 50 nM bovine serum albumin, human immunoglobulin G or fibrinogen for 10 min. Colloids were then pelleted by centrifugation for 1 h at 16000x *g* at 4 ^{o}C. Proteins were then separated by sodium dodecyl sulfate polyacrylamide gel electrophoresis and identified used Coomassie Blue G-250 staining. Protein band intensities were quantified using ImageJ software.

3.3.6 In vitro cell uptake

SKOV-3 cells were maintained at 37 ^{o}C in 5% CO_2 in McCoy's 5A media supplemented with 10% FBS, 10 UI/mL penicillin, and 10 μg/mL streptomycin. SKOV-3 cells were seeded at 12,000 cell/well in 8-well borosilicate glass chamber slides and allowed to adhere overnight. Cells were incubated with 50μM of appropriate formulations for 45 min in serum-free or 10% serum conditions. Fulvestrant colloids were co-formulated with CholEsteryl BODIPY 542/563 C11 (500 nM) for visualization. Following incubation, cells were rinsed and counterstained with Hoechst. Cells were imaged on an Olympus FV1000 confocal laser-scanning microscope at 60X magnification under live-cell imaging conditions. Excitation and emission wavelengths were as follows: for Hoechst, excitation at 405 nm, emission at 460 nm; for fulvestrant colloids co-formulated with BODIPY, excitation at 559 nm, emission at 572; for PPD colloids and DOX formulations, excitation at 488 nm, emission at 520 nm.

3.4 Results

3.4.1 Polymer-stabilized colloids

Hydrophobic chemotherapeutics, such as fulvestrant and PPD, form colloidal aggregates, with critical aggregation concentrations (CACs) of 0.5 nm [112] and 14 μM (Figure 3.1), respectively.

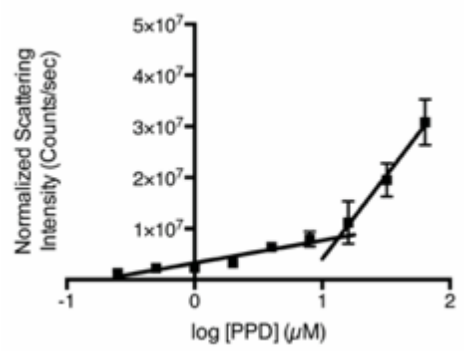

Figure 3.1: The critical aggregation concentration of PPD is 14 μM in PBS as determined by dynamic light scattering. Formulations contain 2% DMF. (n=3, mean ± SD).

Consistent with other colloidal drug aggregates [117], the addition of salt causes massive aggregation and precipitation of both drugs (Figure 3.2C and D, pink bars). In an effort to prevent colloid precipitation and improve stability in the presence of salts, each drug was co-formulated with one of seven different polymers ranging from clinically used excipients (polysorbate 80, Pluronics F68 and F127, Brij 58 and L23) to amphiphilic polymers used in micelle systems (P(LA-co-TMCC)-g-PEG, VitEPEG). Polymers were used at 0.001-0.05% (w/v), a low weight percent versus traditional drug formulations that are orders of magnitude higher [198]. All formulations in water had an initial diameter of <200 nm regardless of the presence of excipient or type of excipient used (Figure 3.2C, 3.2D and 3.3). When formulated in PBS buffer, the addition of polymers prevented or reduced the aggregation of colloids. In contrast, the absence of polymers led to the formation of drug aggregates larger than 1 μm, which precipitated from solution within minutes. In the presence of polymeric excipients, colloids were stable over 48 h at 37 ^{o}C (Figure 3.2E and 3.2F). For fulvestrant, formulation with polysorbate 80 (UP80) resulted in homogeneous colloids stable over 48 h. Fulvestrant-UP80 colloids had initial diameters of 109±7 nm, which increased to 168±18 nm over 48 h. Other polymers, such as P(LA-co-TMCC)-g-PEG, partially inhibited the growth rate of fulvestrant colloids in high salt buffer compared to the drug alone; however, the initial fulvestrant colloid diameter doubled over a 48 h period, demonstrating that UP80 was a more effective stabilizing agent. In contrast, P(LA-co-TMCC)-g-PEG was the optimal polymer to stabilize PPD colloids over 48 h. PPD- P(LA-co-TMCC)-g-PEG colloids had initial diameters of 93±8 nm, which grew to 122±6 nm.

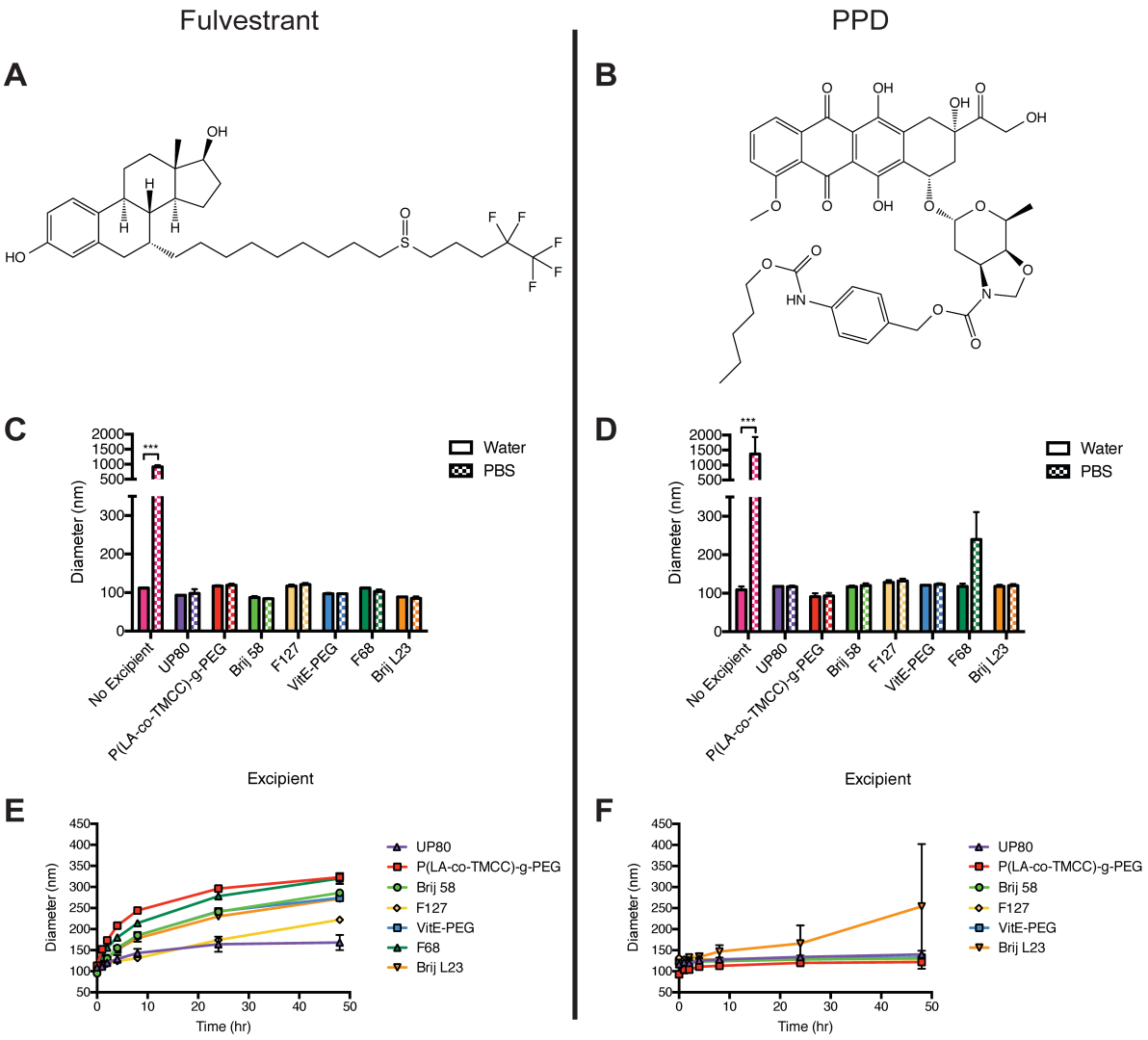

Figure 3.2: (A) Fulvestrant and (B) PPD were selected for their intrinsic chemotherapeutic efficacy and aggregation properties. Formulation of (C) fulvestrant and (D) PPD colloids in water or PBS in the presence of the following polymeric excipients: UP80, P(LA-co-TMCC)-g-PEG, Brij 58, Pluronic F127, VitE-PEG, Pluronic F68 and Brij L23. Incubation of (E) fulvestrant and (F) PPD formulations at 37°C over 48 h. UP80 was the optimal polymer to maintain the size of fulvestrant overtime in buffered salt solution (PBS) compared to other polymers. P(LA-co-TMCC)-g-PEG was the optimal polymer to maintain the size of PPD, with the smallest nanoparticle size over the incubation period. (n=3, mean + SD, *** p<0.001)

While other polymers stabilized PPD colloids, they were not as effective as P(LA-co-TMCC)-g-PEG. For example, Pluronic F68 showed a doubling in size within minutes of exposure to a high salt buffer (Figure 3.2). Both fulvestrant-UP80 and PPD- P(LA-co-TMCC)-g-PEG remain monodisperse over the incubation period (PDI<0.2). Fulvestrant-UP80 and PPD- P(LA-co-TMCC)-g-PEG formulations have drug loadings of 75 and 50%wt, respectively.

We characterized the morphology of our most stable and monodisperse formulations, fulvestrant-UP80 and PPD- P(LA-co-TMCC)-g-PEG, using TEM. Imaging confirmed the spherical morphology of the resulting particles, with multiple fields of view used to determine particle size distributions for each formulation (Figure 3.3). Specifically, fulvestrant-UP80 colloids had diameters of 53±15 nm and PPD- P(LA-co-TMCC)-g-PEG had diameters of 60±16 nm. By TEM, we observed smaller diameters than those determined by DLS, which is consistent with the drying effects of TEM vs. DLS. Even small amounts of polymer excipients (0.001% UP80 and 0.04% P(LA-co-TMCC)-g-PEG) for these two formulations significantly improved stability in buffered aqueous solutions. This prompted us to investigate stability in more biologically relevant conditions, such as serum-containing media.

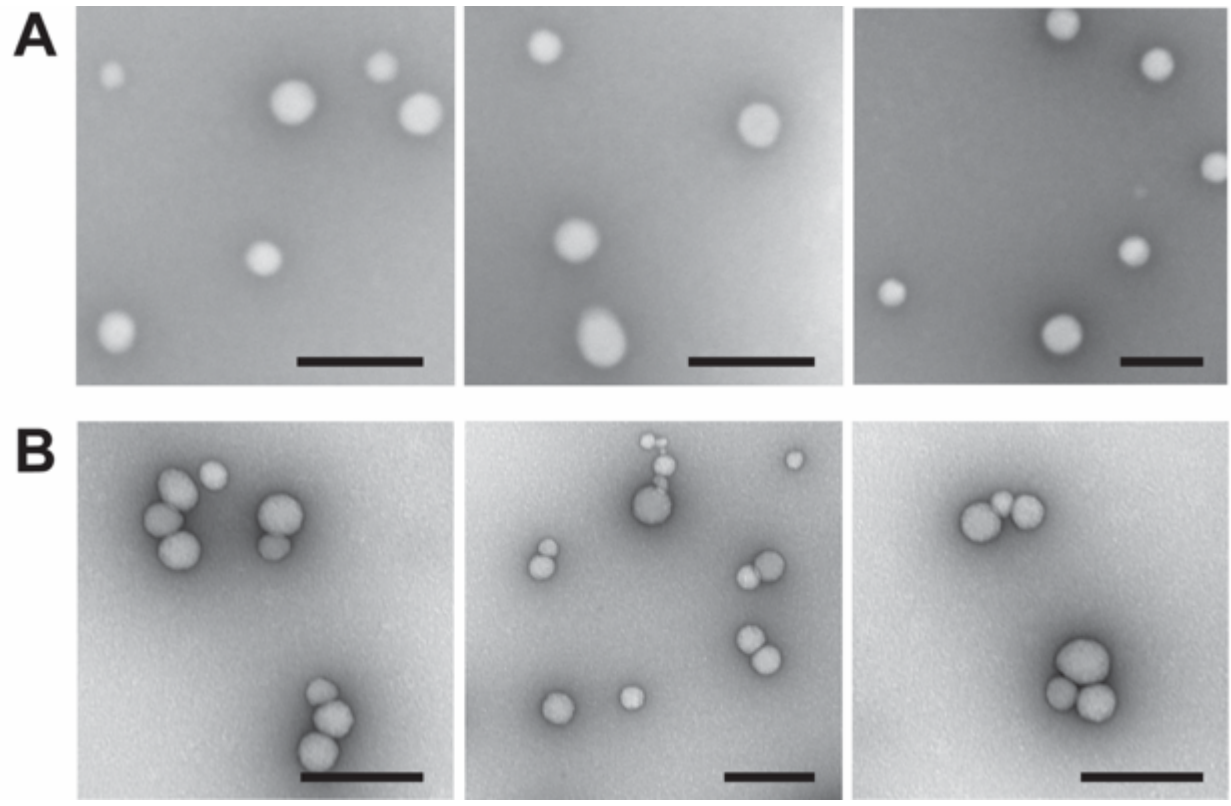

Figure 3.3: Representative fields of view of (A) fulvestrant-UP80 and (B) PPD- P(LA-co-TMCC)-g-PEG colloids in PBS. Scale bar represents 200 nm.

3.4.2 Serum stability

Encouraged by the enhanced stability of fulvestrant-UP80 and PPD- P(LA-co-TMCC)-g-PEG colloids in buffered solutions, we sought to better assess the structural integrity and stability of these formulations over time in serum-containing media, using both TEM imaging and FPLC separation. Representative fields of view from TEM imaging (Figure 3.4A, 3.4B) show that both formulations are present in 10% serum over a 48 h time period; fulvestrant-UP80 colloids (Figure 3.4A and 3.4C) increased in size and dispersity during the incubation, from an initial diameter of 67±17 nm to a final diameter of 222±77 nm (Figure 3.4C). PPD- P(LA-co-TMCC)-g-PEG colloids maintained their size and distribution over time (Figure 3.4B and 3.4D), with initial and final diameters of 36±10 nm and 36±11 nm, respectively. Importantly, the spherical morphology of the colloids was retained for both formulations over the incubation period.

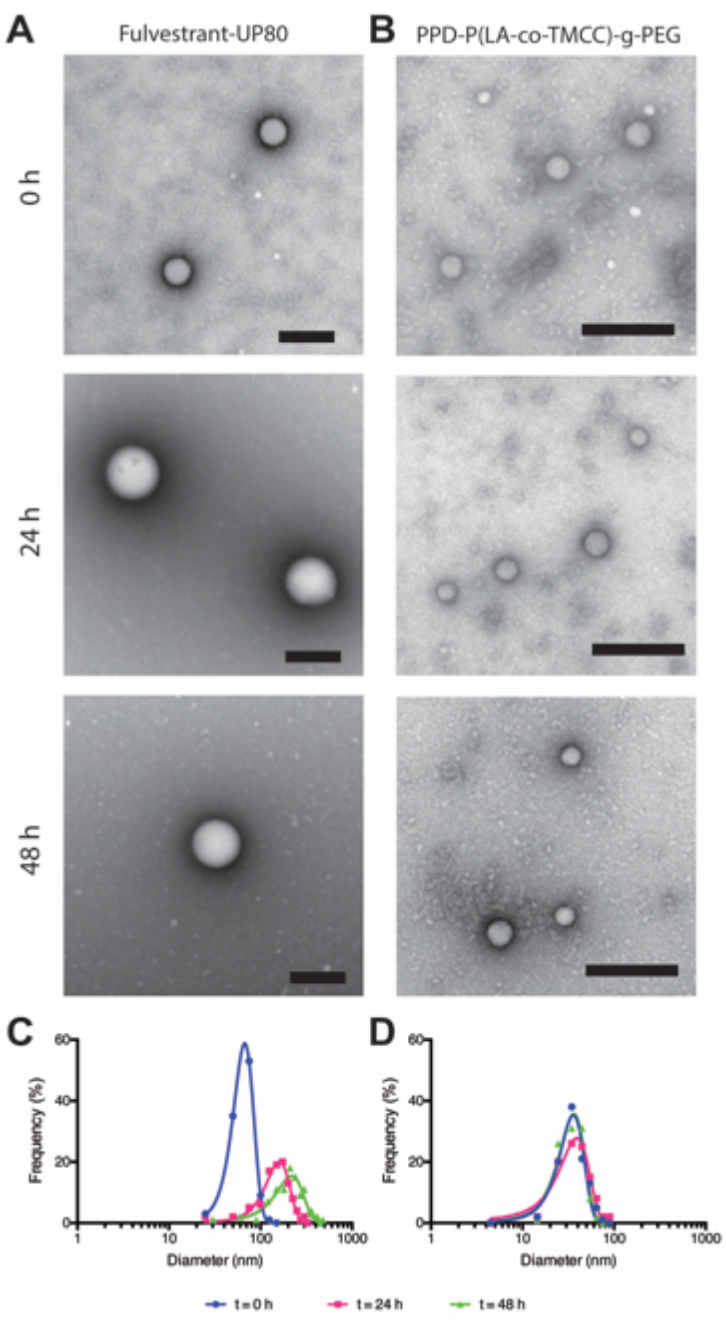

Figure 3.4: Fulvestrant-UP80 and PPD- P(LA-co-TMCC)-g-PEG characterization in 10% serum. (A) Representative TEM images of particles in serum at 0, 24 and 48 h. Fulvestrant-UP80 colloids were stained with ammonium molybdate while PPD- P(LA-co-TMCC)-g-PEG colloids were stained with uranyl acetate, scale bars are 200 nm. (B) Frequency distribution shows peak broadening of fulvestrant-UP80 colloidal aggregates over time, while PPD- P(LA-co-TMCC)-g-PEG maintain size and dispersity over time.

The protein corona that forms on particle surfaces can cause premature drug release due to partitioning of the drug into the hydrophobic pockets of proteins, and so we investigated drug release in the stabilized colloidal formulations in serum. To quantify the drug release, our two formulations were incubated in 20% serum, which is representative of in vivo conditions and allows colloids to be separated and quantified by FPLC directly [197]. At selected time points, up to 48 h, the colloidal population was separated from serum proteins and free drug using size exclusion chromatography (SEC) and the colloid peak area was used as a proxy for drug concentration (Figure 3.5A and 3.5B). Notably, bare colloids could not be separated by this method due to their rapid precipitation in salt conditions. Fulvestrant-UP80 was co-formulated with BODIPY FRET pair, enabling fluorescence emission detection while PPD- P(LA-co-TMCC)-g-PEG colloids were quantified by absorbance at 480 nm. Both formulations showed little dissociation over a 24 h time period (Figure 3.5C). Fulvestrant-UP80 colloidal aggregates began to dissociate after this time, with almost 50% of the drug being released at 48 h. PPD-P(LA-co-TMCC)-g-PEG aggregates showed no dissociation over the 48 h time period. Encouragingly, the stability data obtained for the colloids by FPLC separation reflects the trends observed by TEM (Figure 3.4).

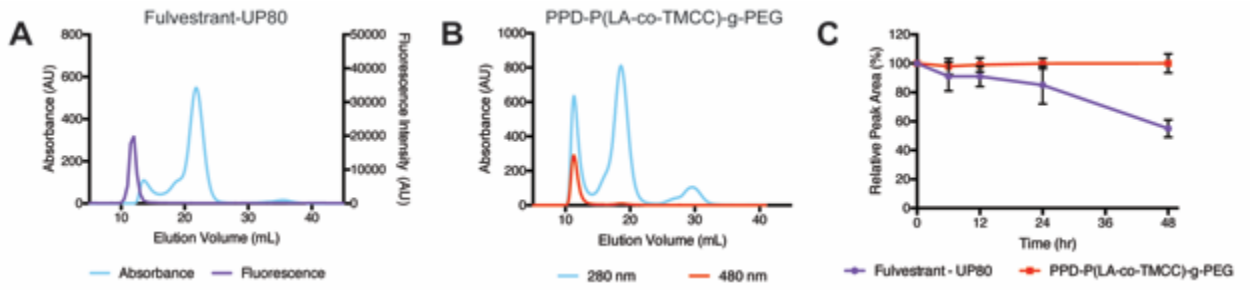

Figure 3.5: Serum stability assessment of colloidal formulations by FPLC. Traces show separation between serum proteins (absorbance at 280 nm) and (A) fulvestrant-UP80 colloids (tracked by fluorescence using a BODIPY FRET pair) and (B) PPD- P(LA-co-TMCC)-g-PEG colloids (unique absorbance at 480 nm) at t=0. (C) The peak area under the colloid curve over time is compared to the area at t=0 h to determine colloid stability as a function of time. Both colloids are stable up to 24 h, with fulvestrant-UP80 colloids dissociating between 24 and 48 h and PPD- P(LA-co-TMCC)-g-PEG colloids showing no evidence of dissociation over 48 h.

We hypothesize that the polymeric excipients used to stabilize the colloidal formulations reduce protein adsorption and thereby provide stability in serum. To test this hypothesis, we used a previously reported method of centrifugation and gel electrophoresis of colloidal formulations to identify surface-bound proteins [118]. We studied the interaction of a series of proteins, which comprise the main proteins of serum with colloidal aggregates of fulvestrant vs. fulvestrant-UP80 and PPD vs. PPD- P(LA-co-TMCC)-g-PEG: albumin (BSA), immunoglobulin G (IgG) and fibrinogen. Colloids were incubated with each protein and pelleted by centrifugation. Proteins in the supernatant were separated from those in pelleted, colloid fractions by gel electrophoresis (Figure 3.6).

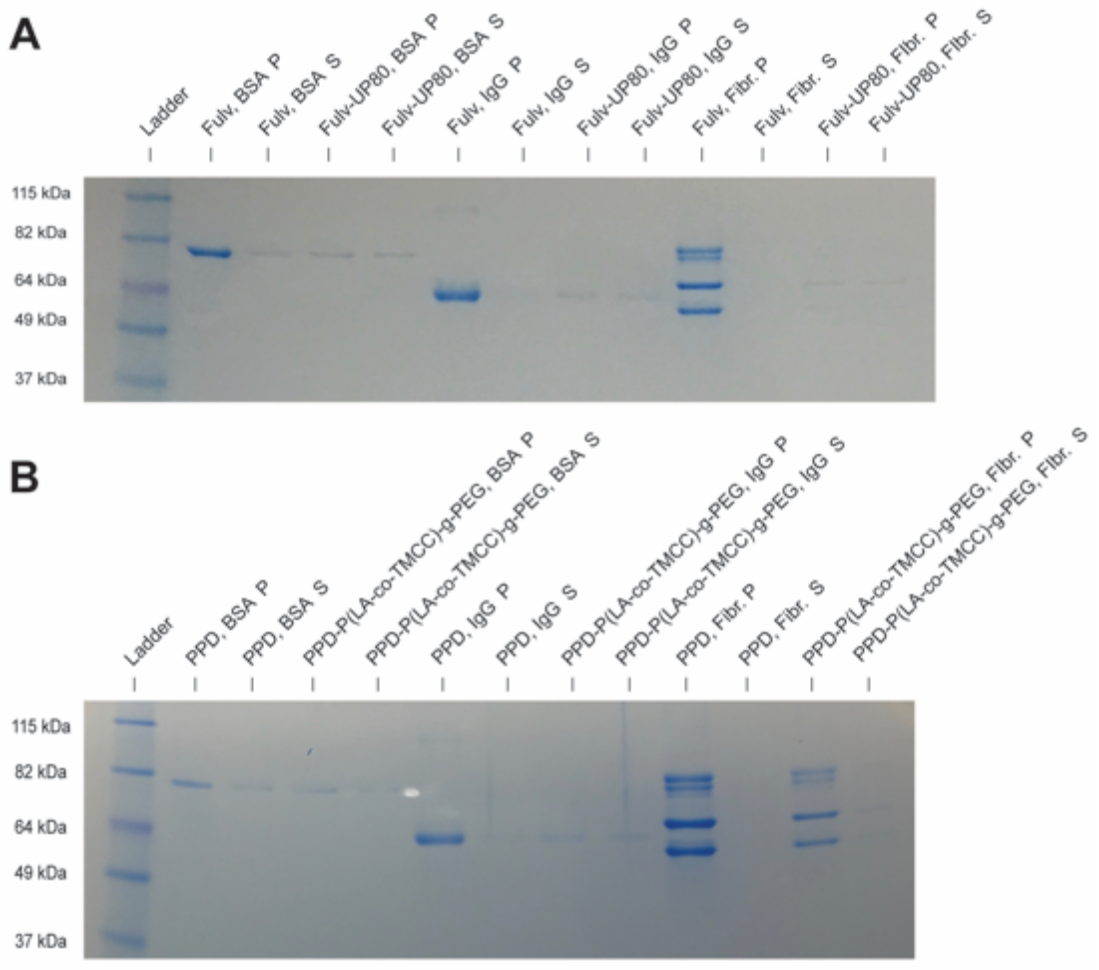

Figure 3.6: Representative SDS-PAGE images of (A) fulvestrant and (B) PPD colloids after incubation with 50 nM bovine serum albumin (BSA), immunoglobulin G (IgG) and fibrinogen (Fibr.). Pellet (P) and supernatant (S) fraction were separated by centrifugation of formulation at 16000x *g* for 1 h at 4 ^{o}C. Representative image of 3 repeats.

All three proteins studied were concentrated (at a 5-15 fold increase) in the pelleted fraction when incubated with bare colloids, indicating significant adsorption to the colloid surface (Figure 3.7). In contrast, none of the three proteins studied were concentrated in the pelleted fraction when incubated with polymer-stabilized colloidal formulations of both fulvestrant-UP80 and PPD- P(LA-co-TMCC)-g-PEG, demonstrating minimal protein adsorption (Figure 3.7). These data are consistent with several other particle systems that use high-density PEG surfaces to prevent protein adsorption and particle opsonization [77], [177], [199].

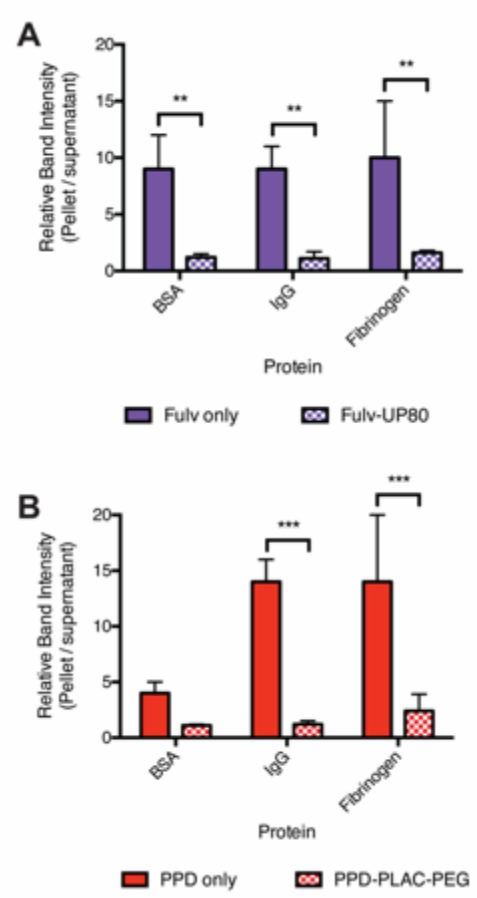

Figure 3.7: Formulation of colloids with excipient polymers reduces protein adsorption. BSA, IgG and fibrinogen (50 nM) adsorption are significantly increased on the surface of bare colloids of (A) fulvestrant and (B) PPD (filled bars) compared to colloids stabilized with the appropriate polymer (white bars): fulvestrant-UP80 and PPD- P(LA-co-TMCC)-g-PEG (n=3, mean + SD, **p<0.01, ***p<0.001).

3.4.3 Cell uptake

In order to understand cell uptake of colloidal aggregates vs. drug monomers, which typically diffuse across cell membranes, fulvestrant-UP80 and PPD- P(LA-co-TMCC)-g-PEG were incubated with the human epithelial ovarian cancer SKOV-3 cell line (Figure 3.8) both in the presence and absence of serum. Doxorubicin, an anthracycline chemotherapeutic from which PPD is derived, does not form colloidal aggregates and was used as a positive control as it can freely permeate cell membranes. Doxorubicin and PPD were directly tracked by excitation at 488 nm while fulvestrant-UP80 colloids were co-formulated with a BODIPY dye that was visualized by excitation at 559 nm. Fluorescence of the non-colloid forming doxorubicin was observed diffusely, co-localizing with cell nuclei under both serum-free and serum conditions. Conversely, intracellular fluorescence of fulvestrant-UP80 and PPD- P(LA-co-TMCC)-g-PEG colloids was only observed under serum-free conditions. Even then, the fluorescence was observed as punctate features within the cell body. In serum-containing media, little to no fluorescence was observed for the colloidal formulations.

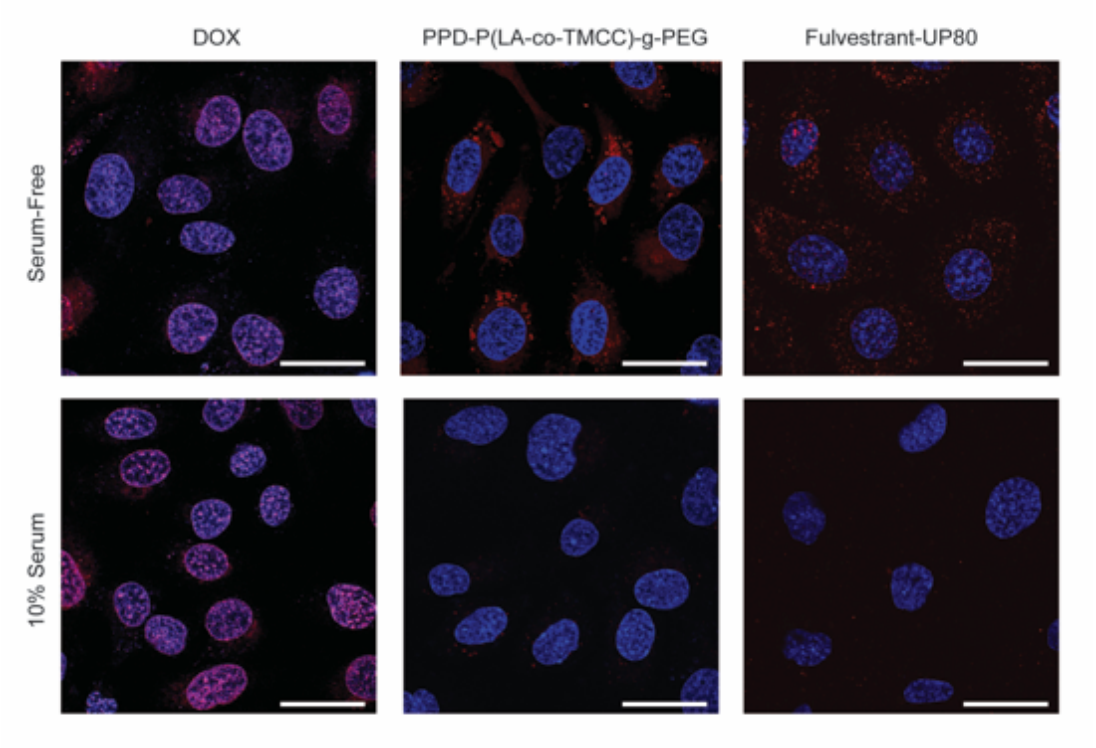

Figure 3.8: Representative images of cell uptake of doxorubicin (monomer) and the colloidal formulations of PPD- P(LA-co-TMCC)-g-PEG and fulvestrant-UP80 (tracked by BODIPY). SKOV-3 cells were used for all experiments. Doxorubicin monomer freely permeates the cell membrane, showing localized fluorescence within the cells' nuclei. PPD and fulvestrant colloids show uptake only in serum-free conditions, with punctate fluorescence within the cell body. There is no evidence of cell uptake of colloids in serum-containing media. (scale bar is 30 µm).

3.5 Discussion

The intrinsic colloidal aggregation properties of hydrophobic molecules are often thought of as limitations in drug screening, and can be problematic for delivery. While the aggregation of these small molecules is unpredictable, this phenomenon can be exploited and controlled with the addition of excipients. By formulating colloidal aggregates with polymeric excipients, we can produce stable high drug loaded particles resistant to changes in salt and serum conditions. Absolute drug loadings of our two formulations, fulvestrant-UP80 (75 wt%) and PPD- P(LA-co-TMCC)-g-PEG (50 wt%), are an order of magnitude higher than conventional micelle formulations (<10wt%)[43]. By incorporating polymeric excipients, the particles are stabilized

and aggregation is prevented through steric repulsion between hydrophilic polymer chains[177], [197]. In the absence of polymer, the presence of salts leads to charge shielding at the surface of colloidal species causing particle fusion and rapid aggregation[176]. The use of amphiphilic polymers allows hydrophobic segments of the polymer to interact with the colloidal surface and hydrophilic segments of the polymer to extend into the aqueous phase to provide steric stability.

At present the limited number of colloid-polymer combinations studied here prevent general predictions on optimal drug-polymer pairs. We hypothesize that the solubility parameters play an important role in determining which polymer would be best suited to stabilize a drug colloid, as has been shown by computational approaches used in other studies[200], [201]. The concentration of polymer used in these formulations plays an important role in stabilizing colloidal species[174], [202]. If the polymer concentration is too low, there is insufficient coverage of the colloidal surface to prevent aggregation and coalescence of the drug colloids. If the polymer concentration is too high and above the critical micelle concentration (CMC), the polymers themselves form micelles and solubilize the drug rather than stabilize the colloid. Accordingly, polymer concentrations just below their CMCs were chosen for this study, providing adequate surface coverage without colloid disruption.

While the stability in salts is essential, we sought to characterize these colloidal aggregates in biologically relevant serum-containing media. Blood proteins destabilize particles, and premature drug release often results from drugs partitioning into the hydrophobic pockets of proteins adsorbed to the particle surface[85]. By monitoring the drugs using their spectral properties, we show that polymers stabilize these colloidal particles for at least 24 h in 20% fetal bovine serum. We hypothesized that this stability was due to a reduction in protein adsorption to the colloidal surface, consistent with the use of hydrophilic polymers, such as PEG, in other particle platforms[77], [79]. To evaluate the interaction between the main components of serum – albumin, globulins and fibrinogens – and the particle surface, we used a centrifugation method to identify surface-bound proteins as previously used to study the inhibition of enzymes by colloid surface sequestration[114], [118]. While this method is limited by the concentration of proteins that can be evaluated, non-stabilized colloids showed significant adsorption of proteins to their surface, whereas polymer stabilization of colloids reduced protein adsorption.

To further probe the stability of the colloidal aggregates, we investigated their interactions with cells in vitro. Under serum-free conditions, distinct punctate fluorescence was observed intracellularly for both fulvestrant and PPD colloidal formulations, which is typical of internalized particles that are trafficked through the endo-lysosomal pathway[203], [204]. Corroborating previous literature, doxorubicin, a compound that does not form colloidal aggregates, freely permeated lipid membranes and localized in the nucleus[205]. In serum-containing media, while the cellular uptake of DOX was not significantly influenced, fulvestrant-UP80 and PPD- P(LA-co-TMCC)-g-PEG colloids were not internalized by cells, consistent with previous observations[113]. The presence of proteins precludes the non-specific uptake of particles and supports the need for cellular targeting agents on the particles[80], [189].

It is clear from this study that the combination of hydrophobic drug and polymer strongly influences particle size and stability over time. This is consistent with other polymer-based nanoparticle formulations where similar drug and vehicle compatibility leads to optimized drug loading and stability[76], [126], [206]-[208]. Of the formulations tested here, the combinations of fulvestrant-UP80 and PPD- P(LA-co-TMCC)-g-PEG are optimal for colloidal stability in both high ionic strength aqueous and serum containing solutions. Chemical modifications of both the drug and the polymeric excipient have been used previously to enhance molecular interactions that provide improved particle stability[122], [123], [191]. However, this strategy often requires re-validation of materials, especially with respect to the drug. Directly screening for and exploiting the colloidal aggregation properties of drugs, as demonstrated here, can provide a mechanism to significantly increase drug loading and stability, without the need for chemical modification or reassessment. With a continued increase in chemical diversity of both colloid-forming drugs and polymeric excipients, the methods outlined here will find further application in formulating drug-rich nanoparticle delivery systems.

3.6 Conclusions

By incorporating polymeric excipients into colloidal formulations of two clinically relevant chemotherapeutics, fulvestrant and PPD, we demonstrated stability in both salt and serum containing-media. This enhanced stability can be attributed to reduced serum protein adsorption to the surface of the particles. Overall, the use of polymers to stabilize fulvestrant and PPD has

clear implications for their efficient delivery, and presents a strategy that should be broadly applicable to formulate the large subset of colloid-forming compounds.

3.7 Ongoing Work

PPD- P(LA-co-TMCC)-g-PEG nanoparticles are currently being tested against a N-HepG2 subcutaneous liver cancer model in Nude *Nu/Nu* mice. In this study, the nanoparticles are being compared against Doxorubicin, an anthracycline used clinically against a wide range of cancers. PPD has been shown to overcome resistance mechanisms against Doxorubicin through a secondary mechanism involving inhibition of topoisomerase II. Interestingly, the incorporation of P(LA-co-TMCC)-g-PEG into the formulation protects the drug from premature cleavage in the mouse serum, where carboxyesterase II is prevalent. This allows increased dosing regimens when delivered in the nanoparticle, as tail vein damage due to drug toxicity is averted.

3.8 Acknowledgements

This work was supported by grants from the Canadian Cancer Society Research Institute (to M.S.S and B.K.S), the US National Institutes of General Medical Sciences (GM71630 to B.K.S. and M.S.S.) and the US National Cancer Institute (CA143549 to T.H.K.). A.N.G. and J.L. were supported in part by Natural Sciences and Engineering Research Council (NSERC) Postgraduate Research Scholarships and C.K.M was supported in part by an NSERC postdoctoral fellowship. We thank S. Boyle and B. Calvieri from the University of Toronto Microscopy Imaging Laboratory for assistance with TEM imaging and members of the Shoichet labs for thoughtful discussion.

4 Innovative use of the taxol binding peptide overcomes key challenges of stable and high drug loading in polymeric nanomicelles

*This chapter was published in Chemical Communications.

Logie, J., McLaughlin, C.K., Tam, R.Y., and Shoichet, M.S. (2015) Innovative use of the taxol binding peptide overcomes key challenges of stable and high drug loading in polymeric nanomicelles. *Chemical Communications.* 51:12000-12003.

Reprinted with permission from the Royal Society of Chemistry. J.L., C.K.M., R.Y.T. and M.S.S. designed research; J.L. performed research and analyzed data with the exception of transmission electron microscopy, performed by C.K.M.; and J.L. and M.S.S. wrote the manuscript.

4.1 Abstract

Despite widespread clinical use, delivery of taxane chemotherapeutics remains a challenge due to poor solubility and lack of selectively. Polymeric nanomicelle strategies have been pursued to overcome these issues; however current formulations are often limited by low drug loading and poor serum stability. To achieve a drug delivery system that addresses these issues, poly(D,L-lactide-co-2-methyl-2-carboxytrimethylene carbonate)-g-poly(ethylene glycol) was covalently modified with the taxol binding peptide - a peptide from the β-tubulin-taxane binding site - to achieve increased loading for docetaxel. This modification resulted in drug loadings five times higher than unmodified polymers, which is significantly higher than typical hydrophobic modifications, including with benzyl and docetaxel functionalization. Unlike many formulations with high drug loading, these nanomicelles were stable in serum for up to 24 h and maintained docetaxel cytotoxicity. By incorporating the taxane binding peptide into the polymer chemistry, a new twist was applied to an old problem, which is broadly applicable to other polymeric micelle systems and drug-peptide combinations in general.

4.2 Introduction

Taxanes, such as docetaxel (DTX) and paclitaxel, are used clinically against a wide range of cancers including breast, lung and pancreatic, and are one of the most prescribed cancer chemotherapeutics. Docetaxel is arguably the biggest oncology product ever developed, with a global market value of over $3 billion in 2010 [9], and sales of Taxotere (Sanofi) at $500 million

in 2013 even after being off-patent for three years [209]. Despite their widespread use, delivery remains a challenge. Current formulations are poorly soluble and thus require the use of excipients, such as Polysorbate 80 or Cremophor EL, that cause a number of side effects such as hypersensitivity and hemolysis [168], [170]. Furthermore, these potent drugs lack specificity, and cause a variety of dose-limiting side effects such as neutropenia and thrombocytopenia [8].

Polymeric nanoparticle micelles, comprised of a hydrophobic core and hydrophilic corona, have been widely investigated to improve the pharmacokinetics of taxanes; however, low drug encapsulation and limited serum stability have hindered their clinical translation [43], [104], [108], [110], [189], [210]. To address these issues, both the formulation and the affinity of the drug in the micelle have been pursued. On the one hand, while techniques such as nanoprecipitation have been shown to produce high drug loadings, encapsulation is transient and often comes at the cost of micelle stability [154]. Modifications to the polymer core, on the other hand, have shown great promise at increasing drug loading without jeopardizing the stability of the delivery vehicle itself [211], [212].

Several strategies have been pursued to improve loading in polymeric nanomicelles. Traditionally, increasing the ratio of hydrophobic to hydrophilic polymer block lengths has improved loading efficiency [74]; however, this reduces the amount of shielding and often results in rapid micelle dissociation upon dilution [101], [102]. Moreover, high drug loading often comes at the expense of stability in serum conditions, resulting in nanomicelles that release drug prematurely [107], [213]. More specific chemical modifications have shown increased loading without hindering the stability of the vehicles. For example, Hennink et al. increased taxane loading by covalently bonding aromatic groups to the core that facilitated pi-pi stacking between drug and polymer [110]. Yang et al. exploited hydrophobic interactions by incorporating cholesterol onto a polycarbonate backbone to increase paclitaxel loading [104]. Others have explored direct drug conjugation to the hydrophobic block of an amphiphilic polymer, which increased loading of free drug by inducing crystallinity within the core [106], [108], [109]. While these systems resulted in loadings greater than those previously achieved, even higher loadings are required to achieve optimal dosing and overcome excessive use of excipients required for solubility and stability in serum. To this end, we designed a core modification in our polymeric nanomicelles that is specific to taxanes, thereby using a known structural motif in a new way to solve a problem that has been plaguing the field for decades.

4.3 Materials and Methods

4.3.1 Materials

All solvents and reagents were purchased from Sigma-Aldrich and used as received unless otherwise noted. 5-methyl-5-benzyloxycarbonxyl-1,3-trimethylene carbonate (TMCC-Bn) was synthesized as previously reported. [96] 3,6-dimethyl-1,4-dioxane-2,5-dione) and 1-[3,5-bis-(trifluromethyl)phenyl]—3-[(1*R*,2*R*)-(-)-2(dimethylamino)cyclohexyl] thiourea (Strem Chemicals, Newburyport, MA) and NH_2-PEG-OMe (10 kg/mol, Rapp Polymere, Tubingen, Germany) were used as received. Docetaxel was purchased from LC Laboratories (Woburn, MA). Peptide synthesis reagents, including Fmoc-Amino Acids, were purchased from AnaSpec (Fremont, CA).

4.3.2 Instruments

^{1}H NMR spectra were recorded at 500 MHz at room temperature using an Agilent DD2 spectrometer. Molecular weights and polydispersity of P(LA- co-TMCC) were measured by gel permeation chromatography (GPC) in THF (containing 0.25% tetrabutyl ammonium bromide) relative to polystyrene standards at room temperature on a Waters 515 HPLC pump with a RI detector (VE3580) and a UV detector (KNAUER 2500) at a flow rate of 0.6 mL/min. Chemicals shifts (δ) are in ppm. Fluorescence and absorbance measurements were performed with the Tecan Infinite M200 pro fluorescent plate reader. Docetaxel was quantified using an Agilent 1100 HPLC equipped with an AB Sciex API 4000 triple quadropole mass spectrometer with electrospray ionization source detector. Serum stability studies were performed on a GE AKTA purifier 10 Fast Protein Liquid Chromatography System equipped with a UV900 monitor.

4.3.3 Synthesis of P(LA-co-TMCC)-g-PEG

P(LA-*co*-TMCC) was synthesized as previously described [132]. Briefly, 3,6-dimethyl-1,4-dioxane-2,5-dione (10.4 mmol) and 5-methyl-5-benzyloxycarbonyl-1,3-trimethylene carbonate (2.3 mmol) were co-polymerized for 7 days in dry, distilled dichloromethane (10 mL) under argon by a ring opening polymerization initiated with 1-pyrenebutanol (0.0625 mmol) and catalyzed by 1-[3,5-bis-(trifluromethyl)phenyl]—3-[(1*R*,2*R*)-(-)-2(dimethylamino)cyclohexyl] thiourea (0.35 mmol). GPC analysis revealed a backbone M_n of 12,869 and a PDI of 1.09. Following purification by silica column to remove the catalyst, the copolymer was deprotected

for 7 days using Pd/C catalyst (20 wt%) in 50:50, v/v THF:EtOAc under hydrogen gas (91% yield). NH_2-PEG-OMe was grafted to the backbone at 3 PEG/backbone, as previously described[197]. P(LA-co-TMCC) (100 mg) was dissolved in DMF (5 mL) to which N,N'-diisopropylcarbodiimide (DIC, 100 uL) and hydroxybenzotriazole (HOBt, 16.88 mg) were added, and the solution was stirred for 30 min at room temperature. NH_2-PEG-OMe (PEG, 10 kg/mol, 416 mg) was dissolved in DMF (5 mL) and added to the copolymer solution under argon. The reaction was stirred at room temperature for 24 h, after which 500 uL of borate buffer (pH 9, 500 mM) was added and the solution was dialyzed against distilled water (2 kg/mol MWCO). Unreacted PEG was removed using a Sepharose CL-4B column equilibrated with distilled water. Collected fractions with polymer were combined and lyophilized to give a white solid (~60% yield). ^{1}H NMR ($CDCl_3$): δ1.23 (m, CH_3 from TMCC), 1.57 (m, CH_3 from LA), 3.64 (bs, CH_2 from PEG), 4.34 (m, CH_2 from TMCC), and 5.16 (m, CH from LA). Average PEG conjugation was calculated by end group analysis comparing area under the curve for PEG (3.64 ppm) vs. LA (5.17 ppm) as previously reported [132].

4.3.4 Synthesis of P(LA-co-TMCC-co-TMCC-Bn)-g-PEG (P_{Bn})

P(LA-*co*-TMCC-Bn) was synthesized as described above with controlled deprotection of the benzyl group. Deprotection by palladium-catalyzed hydrogenolysis was monitored by ^{1}H NMR in order to control the number of pendant benzyl groups. Copolymers were synthesized with 2 or 5% benzylated monomers (20 or 50% Bn-TMCC). 3 PEGs were grafted onto the benzylated copolymer as described above, and purified by Sepharose CL4B column to remove free PEG. The final product, P_{Bn}, was lyophilized and characterized by ^{1}H NMR (72% yield). ^{1}H NMR (DMSO-d_6): δ1.28 (m, CH_3 from TMCC), 1.47 (m, CH_3 from LA), 3.51 (bs, CH_2 from PEG), 4.29 (m, CH_2 from TMCC), 5.22 (m, CH from LA), 7.36 (m, aromatic protons from Bn-TMCC).

4.3.5 Synthesis of P(LA-co-TMCC)-g-PEG,DTX (P_{DTX})

P(LA-*co*-TMCC) was synthesized as previously described. A Steglich esterification was performed to graft docetaxel onto the backbone as previously reported [109]. Briefly, the copolymer (100 mg) was dissolved in distilled DCM (5 mL) and pre-activated with N,N'-dicyclohexylcarbodiimide (DCC, 17.2 mg) and 4-dimethylaminopyridine (DMAP, 10.2 mg) for 30 min with stirring under Ar. Docetaxel was dissolved in DCM (5 mL) and added dropwise to the polymer solution over ice. The solution was sealed under argon and stirred for 2 h over ice

followed by 22 h at room temperature. The solution was filtered to remove dicyclohexylurea, and then extracted against water (3 times) and 0.5 M ammonium chloride (1 time). The organic fraction was collected and dried with magnesium sulfate and filtered. The dichloromethane was removed by rotary evaporation, the polymer precipitated into cold hexane and dried under vacuum (with any remaining docetaxel removed in the subsequent step of PEG grafting). PEG was grafted as reported above (3 PEG/polymer backbone), and dialyzed against water, prior to purification by Sepharose CL4B column to remove free PEG. The final product, P_{DTX}, was lyophilized and characterized by ^{1}H NMR (81% yield, 2.5 DTX/polymer backbone). ^{1}H NMR ($CDCl_3$): δ1.25 (m, CH_3 from TMCC), 1.58 (m, CH_3 from LA), 3.64 (bs, CH_2 from PEG), 4.26 (m, CH_2 from TMCC), 5.17 (m, CH from LA), 8.12 (br, ortho-aromatic Hs on DTX).

4.3.6 Synthesis of P(LA-co-TMCC)-g-PEG, TBP (P_{TBP}) or P(LA-co-TMCC)-g-PEG, Scrambled (P_{SCR})

P(LA-*co*-TMCC) was synthesized as previously described. The copolymer (200 mg, 12,000 g/mol) was dissolved in distilled DCM (5 mL) and pre-activated for 30 min with DIC (15.5 uL) and HOBt (13.5 mg). 3,3'-dithiobis(propionic hydrazide) (23.8 mg) [214] was pre-dissolved in 5 mL of distilled DCM with a few drops of DMF to increase solubility, before being added dropwise to the pre-activated polymer. The solution was sealed under argon and stirred. After 24 h, DCM was removed by rotary evaporation and the product was precipitated into hexane and dried under vacuum. PEG was grafted as described above (3 PEG/polymer backbone). After Sepharose CL4B purification to remove unreacted PEG, the polymer was reduced using DTT (50 eq) in PBS (1x, pH 7.5) for 6 h. The product was dialyzed against dilute HCl (pH 4.5) to ensure free thiols remain stable and to remove byproducts. An Ellman's assay was used to quantify free thiols against an L-Cysteine standard curve (1.1 thiols/backbone). 3-maleimidopropinoic-taxol binding peptide (Mal-PGFAPLTSRGSQQYAAG) and 3-maleimidopropinoic-scrambled peptide (Mal-PRSAYAIFGGSQPQTLG) were synthesized by conventional solid-phase microwave peptide synthesis techniques (CEM Liberty 1). The peptide was dissolved in phosphate buffer (0.1 M, pH 8) with a small amount of acetonitrile to increase solubility. The polymer-SH solution was added dropwise to the peptide, and the pH of the final solution was increased to 7 using NaOH. The polymer was allowed to react with the peptide for 48 h, followed by quenching of the unreacted thiols with N-(2-hydroxyethyl) maleimide (20 eq) for 24 h. The final solution was dialyzed for 2 days against 0.1 M Arginine and 0.1 M NaCl to remove unreacted peptide (20

kg/mol MWCO) followed by dialysis against water for 24 h to remove salts. The final products, P_{TBP} or $P_{Scr,}$ were lyophilized and characterized by amino acid analysis (84% and 62% yield respectively, 0.8 peptide/polymer backbone).

4.3.7 Nanomicelle formation by dialysis

Polymer (4 mg) and DTX (2.4 mg) were dissolved in DMF (1 mL) to which 50 uL of borate buffer (pH 9, 500 mM) was added and the solution left at room temperature for 15 min. The borate buffer is added to reduce nanomicelle size as described in detail previously. [2] 0.5 mL of distilled water was added dropwise at a rate of ~1 drop every 3 s. The solution was dialyzed against distilled water for 24 h, changing the water six times (MWCO 2 kg/mol). The solution was centrifuged to remove free DTX aggregates prior to use and characterization. DTX concentration was quantified by HPLC-MS/MS by diluting micelle solutions into 80:20 v/v acetonitrile: water and comparing to a DTX standard curve (3.125 ng/mL-200 ng/mL) using paclitaxel as an internal standard (100 ng/mL). Loading was normalized between groups by calculating based on the molecular weight of the modified-hydrophobic backbone (P(LA-co-TMCC)) in order to avoid measuring differences due to a shift in the hydrophobic-hydrophilic balance.

4.3.8 Dynamic light scattering (DLS), Zeta Potential and Transmission electron microscopy (TEM)

The hydrodynamic diameter was quantified at 25°C using a Malvern Zetasizer Nano ZS, equipped with a 4 mW, 633 nm laser. All samples were prepared at a concentration of 1 mg/mL and centrifuged to remove aggregates prior to use. Hydrodynamic diameters (d_h) were measured in polystyrene cuvettes (Kuvetten, Germany) and calculated using the Strokes-Einstein equation $d_h = k_BT/3\pi\eta D$, where k_B is the Boltzmann constant, T is the absolute temperature, η is the solvent viscosity and D is the diffusion coefficient. The autocorrelation functions of the scattered intensity were analyzed by means of the cumulant method to yield the effective diffusion coefficient (D) as a function of the scattered angle. Micelles prepared from P_{TBP} were concentrated to ~13 mg/mL polymer using a centrifugal filter device (Millipore, MWCO 30 kg/mol). Zeta potential was measured using folded capillary cells (Malvern, DTS 1060). The average of three individual samples, prepared under the same conditions with 36 runs each is reported. For TEM, a sample (5 μL) was deposited onto a freshly glow-discharged 400 mesh

carbon coated copper TEM grid (Ted Pella, Inc.) and allowed to adhere for 4 min. Excess liquid was removed with filter paper and particles then stained with 2% uranyl acetate (w/v, 5 µL, pH 4.3) for 15 seconds. The stain was removed and samples imaged using a Hitachi H-7000 microscope operating at 75 kV. Images were captured using an Advanced Microscopy Techniques (AMT) XR-60 CCD camera with typical magnifications between 50,000 – 100,000x. Particles (360 over 14 images) were analyzed using ImageJ 64 software.

4.3.9 In vitro serum stability

The stability of docetaxel-loaded micelles was determined using fast protein liquid chromatography by previously established method [105], [197]. Docetaxel micelles at a polymer concentration of 1 mg/mL in 1x PBS (pH 7.4) were incubated with 20% fetal bovine serum (FBS, Charcoal Stripped) at 37 °C. At 0, 24 and 48 h, 500 µL aliquots were removed and injected onto a Superdex 200 gel filtration column. Samples were run with a flow rate of 1.5 mL/min and 1x PBS as the mobile phase. 1 mL fractions from the middle of the micelle peak (11 mL elution volume) were collected and DTX concentration was analyzed by HPLC-MS/MS. The drug loading was quantified as described above.

4.3.10 Cell culture cytotoxicity assay

SKBR-3 cells were cultured in McCoy's 5A media supplemented with 10% FBS and 1% penicillin-streptomycin in a humidified 37 °C incubator at 5% CO_2. Cells were seeded into 96-well flat-bottomed tissue culture plates at a density of 5,000 cells per well, and incubated for 24 h before use. Control and P_{TBP} micelles were synthesized as described, and dose-matched with free docetaxel to a concentration of 10 ng/mL (determined to be the IC_{50} of docetaxel in SKBR-3 cells). Dilutions of micelles were done with blank polymeric micelle solutions in McCoy's media (100 ug/mL polymer). Treatment with DTX was left on for 5 h, followed by media replacement and incubation for 48 h. At 48 h, the cell culture medium was replaced with 110 uL of Presto Blue solution (Life Technologies) [215], [216]. The plate was incubated for 2 h at 37°C, allowing viable cells to reduce the resazurin dye to the highly red fluorescent resorufin derivative. The fluorescence of individual wells was measured with an excitation at 560 nm and an emission at 590 nm by a microplate reader. Each measurement is an average of 6 repeat wells/plate, with 3 plates of separate passages of SKBR-3 cells.

4.3.11 Statistics

All statistical analyses were performed using Graph Pad Prism version 5.00 for Macintosh (Graph Pad Software, San Diego, California, www.graphpad.com). Differences among groups were assessed by one-way ANOVA with Bonferroni *post hoc* correction to identify statistical differences among three or more treatments. Alpha levels were set at 0.05 and a p-value <0.05 was set as the criteria for statistical significance. Graphs are annotated where p-values are represented as $*p<0.05$, $**p<0.01$ or $***p<0.001$. All data are presented as mean + standard deviation.

4.4 Results and Discussion

4.4.1 Polymer Modification Strategies

Taxanes achieve their potency by interacting specifically with β-tubulin and arresting cell division. The native binding site of the taxanes has been identified as a specific taxol binding peptide (TBP) sequence, PGFAPLTSRGSQQYAA, on the M-loop of β-tubulin [13], [14]. We hypothesized that incorporation of this taxol binding peptide (TBP) into the hydrophobic backbone of our polymeric nanomicelles would enhance docetaxel loading without compromising serum stability. To test this hypothesis, we covalently modified the carboxylic acid functional groups of poly(D,L-lactide-co-2-methyl-2-carboxy-trimethylene carbonate)-graft-poly(ethylene glycol), P(LA-co-TMCC)-g-PEG, with TBP and compared its drug loading to more common hydrophobic modification strategies, including the use of benzyl and docetaxel groups (Figure 4.1). Polymer-TBP (P_{TBP}) nanomicelles were further investigated for serum stability and in vitro cytotoxicity.

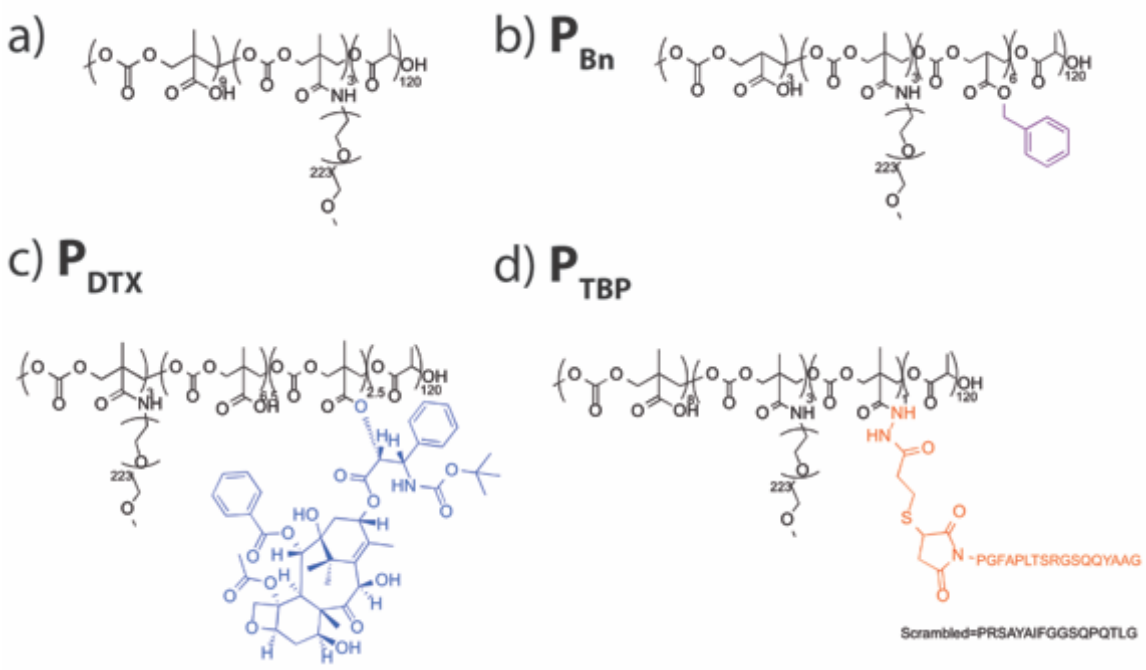

Figure 4.1 Hydrophobic backbone modifications of (a) P(LA-*co*-TMCC)-*g*-PEG with (b) benzyl groups (P_{Bn}), (c) docetaxel (P_{DTX}), and (d) taxol binding peptide (P_{TBP}) *PGFAPLTSRGSQQYAAG* or the TBP scrambled control peptide (P_{SCR}) *PRSAYAIFGGSQPQTLG*.

To modify P(LA-co-TMCC) carboxylic acids, a series of strategies were exploited. To achieve the benzylated polymer backbone, the palladium catalyzed hydrogenolysis conditions for TMCC benzyl deprotection were controlled (Scheme 4.1). The highest degree of substitution achieved was six benzyl groups per backbone, representing 50% of the TMCC monomers or 5% of all monomers (Figure 4.2).

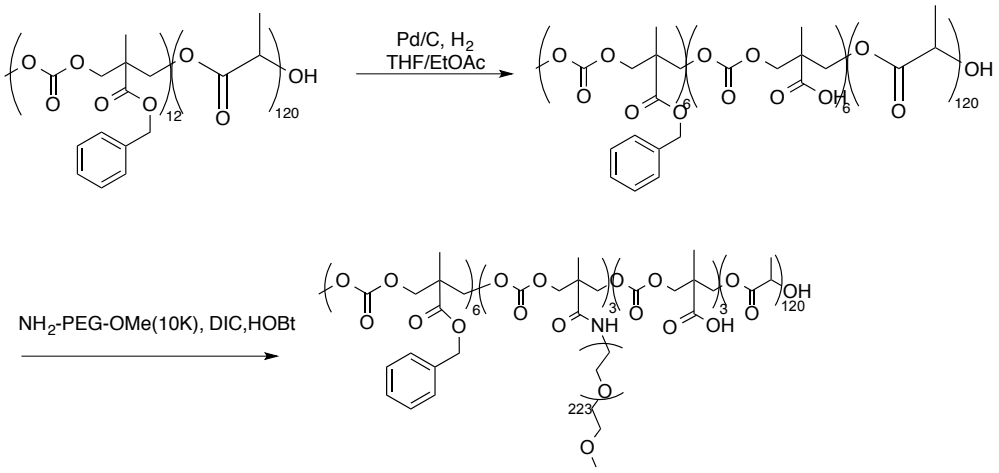

Scheme 4.1: By controlling the palladium catalyzed deprotection of benzyl groups, we achieved P(LA-*co*-TMCC-Bn) with as many as 6 benzyl groups per polymer backbone (50% of the TMCC groups or 5% of the polymer backbone)

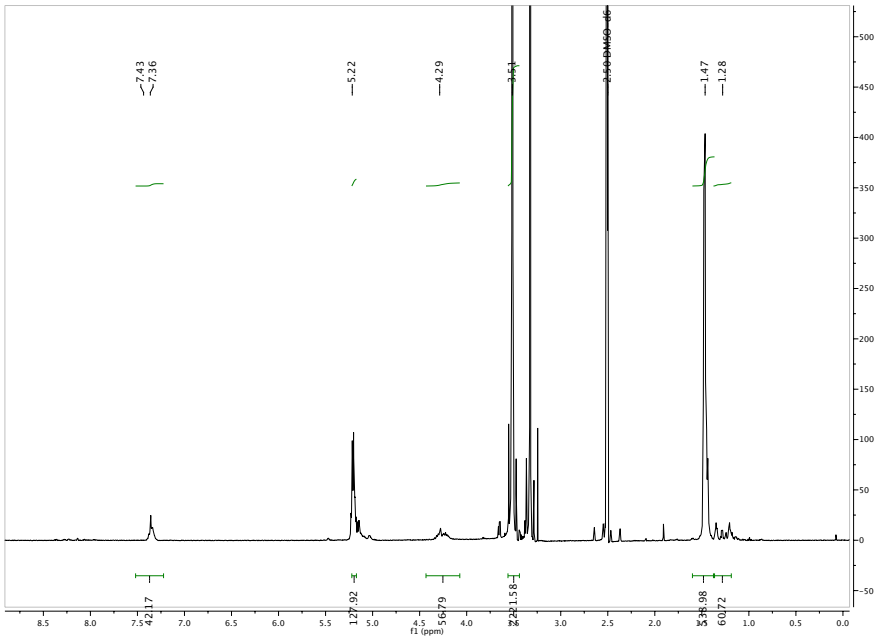

Figure 4.2: ^{1}H NMR of P_{Bn} (DMSO-d_6): δ1.28 (m, CH_3 from TMCC), 1.47 (m, CH_3 from LA), 3.51 (bs, CH_2 from PEG), 4.29 (m, CH_2 from TMCC), 5.22 (m, CH from LA). 7.36 (m, aromatic protons from Bn-TMCC).

To synthesize the docetaxel modified polymer backbone, Steglich esterification conditions were used whereby the 2' hydroxyl groups of DTX were coupled to the P(LA-co-TMCC) carboxylic acids by carbodiimide chemistry (Scheme 4.2) [109]. An average of 2.5 DTX per backbone was

achieved, as calculated by ^{1}H-NMR (Figure 4.3). P(LA-co-TMCC), with either benzyl (P_{Bn}) or docetaxel (P_{DTX}) modifications, was subsequently modified by grafting terminally functionalized MeO-PEG-NH_2 (10,000 g/mol) to the P(LA-co-TMCC) carboxylic acids backbone using N, N'-diisopropylcarbodiimide (DIC) and hydroxybenzotriazole (HOBt) coupling, followed by purification through a Sepharose CL4B column to remove unreacted PEG. Three PEG chains per backbone were grafted in all cases to achieve high stability [197].

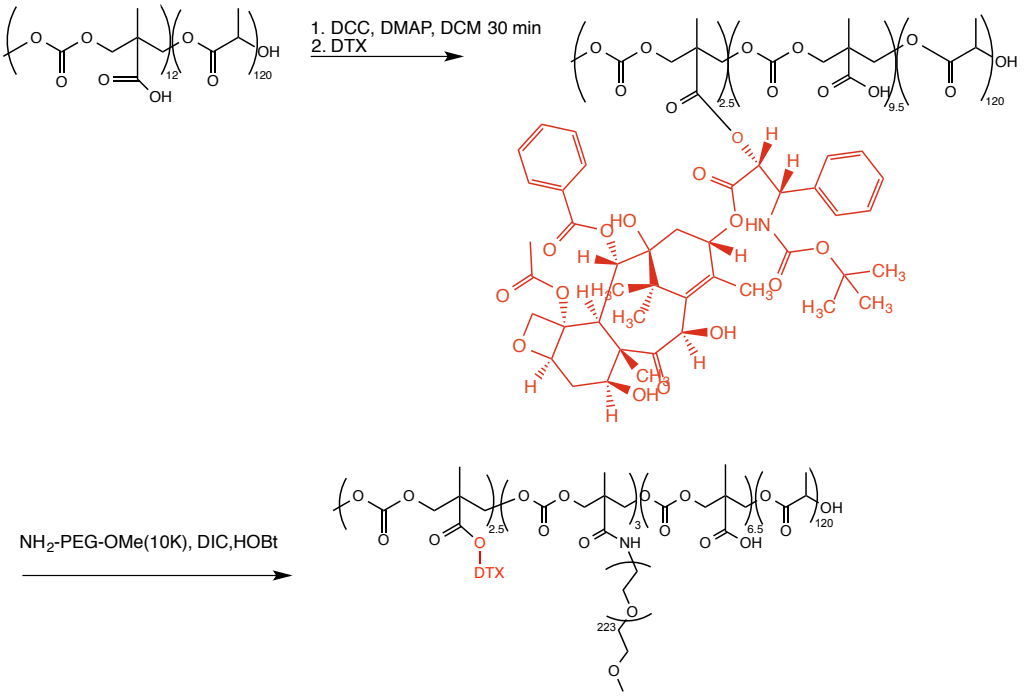

Scheme 4.2: Steglich esterification was used to conjugate docetaxel (DTX) to P(LA-*co*-TMCC) backbone carboxylic acid functional groups, after which NH_2-PEG-OMe was coupled.

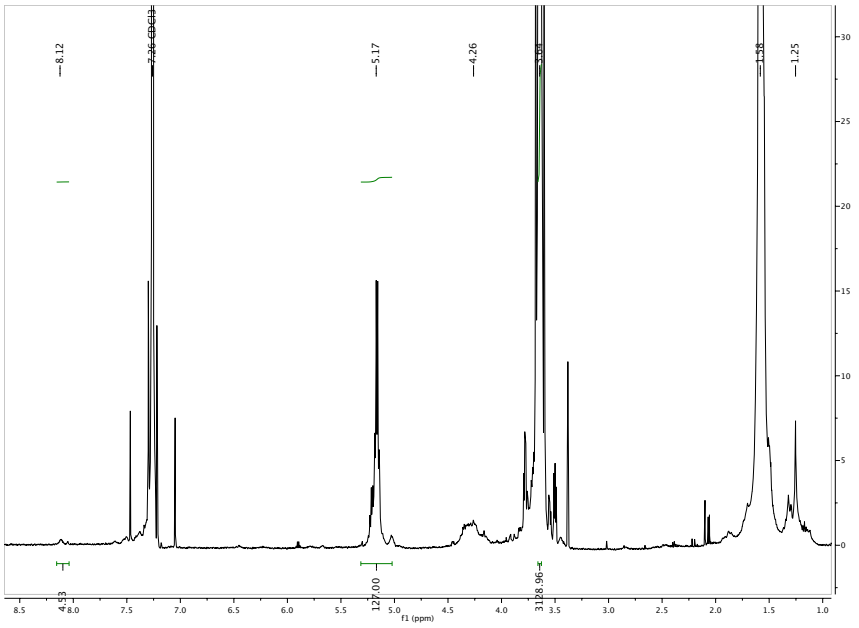

Figure 4.3: ^{1}H NMR of P_{DTX} ($CDCl_3$): δ1.25 (m, CH_3 from TMCC), 1.58 (m, CH_3 from LA), 3.64 (bs, CH_2 from PEG), 4.26 (m, CH_2 from TMCC), 5.17 (m, CH from LA). 8.12 (b, o-Bz on DTX).

An alternate synthetic route was required to covalently modify the P(LA-co-TMCC) carboxylic acids with TBP due to potential cross-reactivity of the amino acid side chains (Scheme 4.3). Here, the backbone carboxylic acid groups were first modified with 3,3'dithiobis(propionic dihydrazide) (DTP) [214], [217] using DIC and HOBt as coupling agents, thereby introducing protected thiol functional groups, followed by MeO-PEG-NH_2 grafting, as described above. After purification, reduction of the disulfides using dithiolthreitol (DTT) produced a thiolated polymer, which was then reacted with maleimide-functionalized TBP by a Michael addition reaction to produce P_{TBP} with an average of 0.8 peptides per backbone (Figure 4.4). Unreacted thiols were quenched with N-(2-hydroxyethyl)-maleimide.

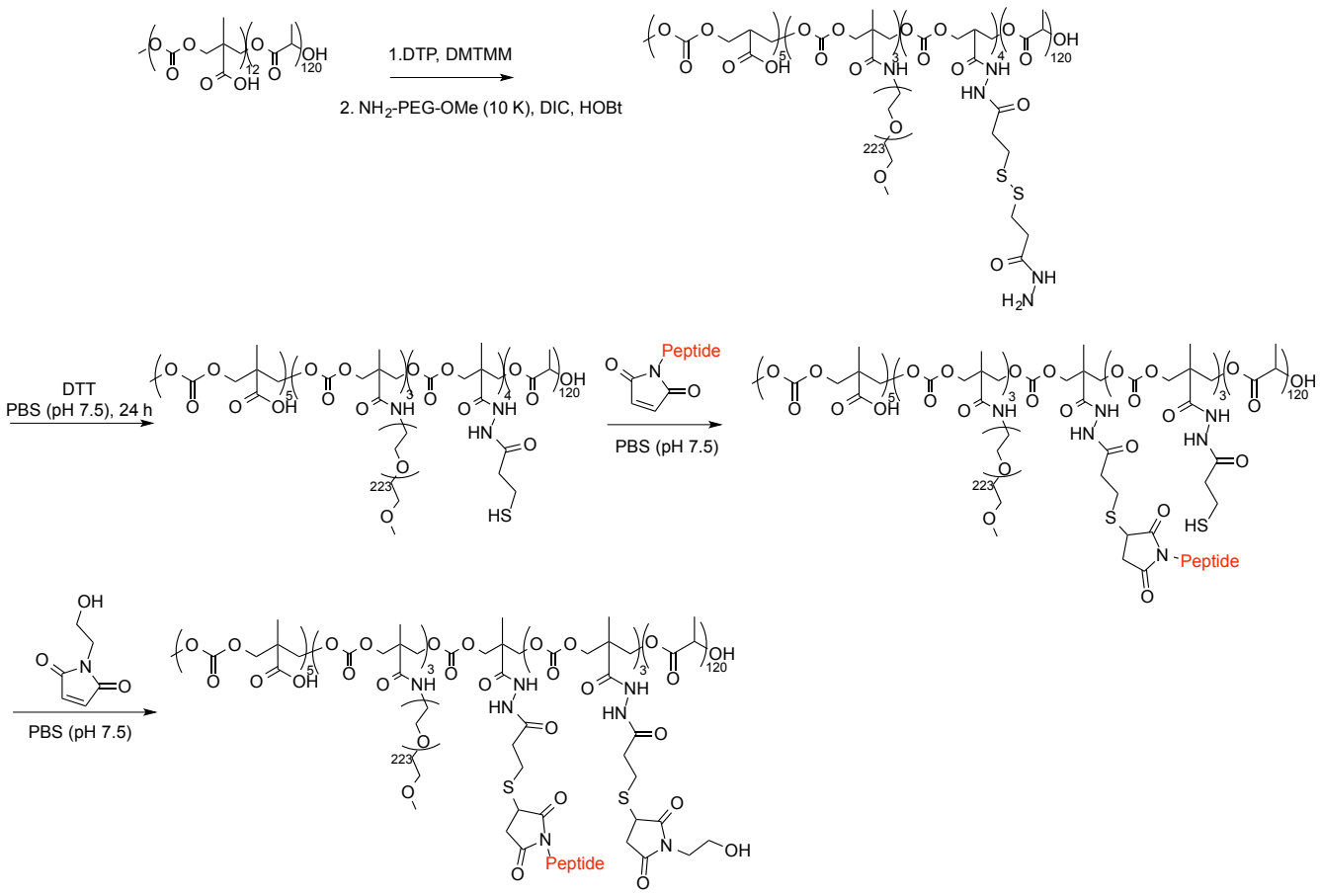

Scheme 4.3: Synthesis of P_{TBP} and the scrambled analog, P_{SCR}, were achieved by first modifying P(LA-co-TMCC) backbone carboxylic acid groups with DTP and NH_2-PEG-OMe followed by reduction of the DTP with DTT to expose thiol groups for Michael addition of maleimide-modified peptides: either (a) taxol binding peptide (TBP) – PGFAPLTSRGSQQYAA; or (b) scrambled peptide control (SCR) - PRSAYAIFGGSQPQTLG.

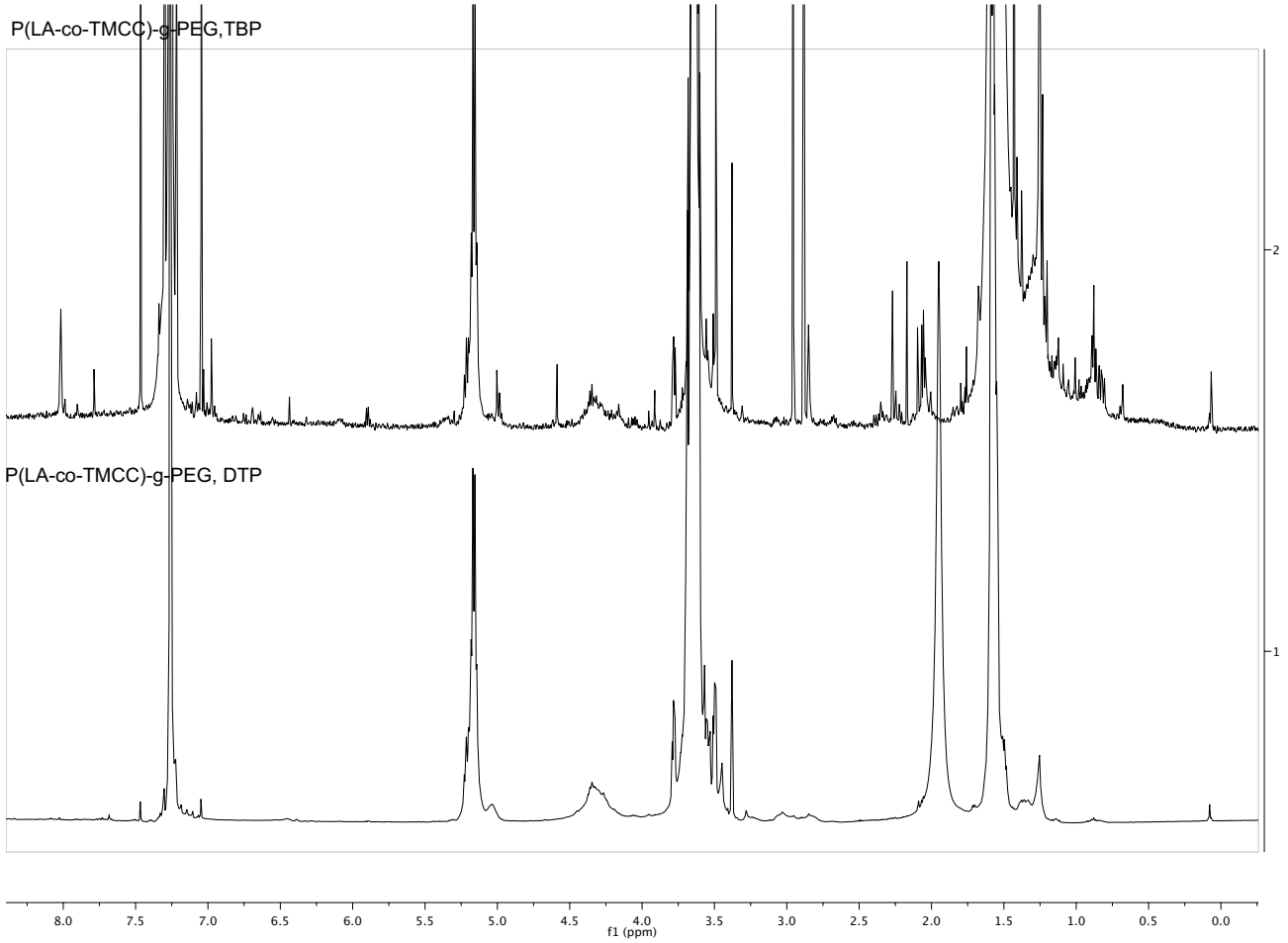

Figure 4.4: ^{1}H NMR of P(LA-*co*-TMCC)-g-PEG, DTP (bottom) and P(LA-co-TMCC)-g-PEG,TBP (top) showing successful conjugation of the PEG and peptide ($CDCl_3$): δ1.25 (m, CH_3 from TMCC), 1.58 (m, CH_3 from LA), 3.64 (bs, CH_2 from PEG), 4.26 (m, CH_2 from TMCC), 5.17 (m, CH from LA). Peptide conjugation was determined by amino acid analysis to be 0.8 peptides/backbone.

4.4.2 Polymeric micelle characterization

All modified polymers, represented in Figure 4.1, self-assembled by dialysis to form uniform polymeric micelles with diameters <200 nm and polydispersity indexes <0.2, as determined by dynamic light scattering (DLS, Table 4.1).

Table 4.1: Average molar mass of polymers (measured by ^{1}H NMR end group analysis) and the corresponding diameters of self-assembled polymeric nanomicelles as measured by dynamic light scattering.

Polymeric Micelle	M_n (^{1}H NMR)*	Size (nm, mean ± SD)
Unmodified P(LA-*co*-TMCC)-*g*-PEG	40800	94.2 ± 3.5
P_{Bn}	37500	99.0 ± 7.6
P_{DTX}	41000	148.0 ± 0.4
P_{TBP}	39700	108.4 ± 15.9

*calculated by end group analysis comparing area under the curve for PEG (3.64) vs. LA (5.17) with backbone M_n calculated as previously reported[132].

Additionally, P_{TBP} micelles were further characterized by transmission electron microscopy (TEM), exhibiting a spherical shape and size under dehydrated conditions of 36 ± 11 nm, and a zeta potential of -2.41 ± 0.06 mV (Figure 4.5).

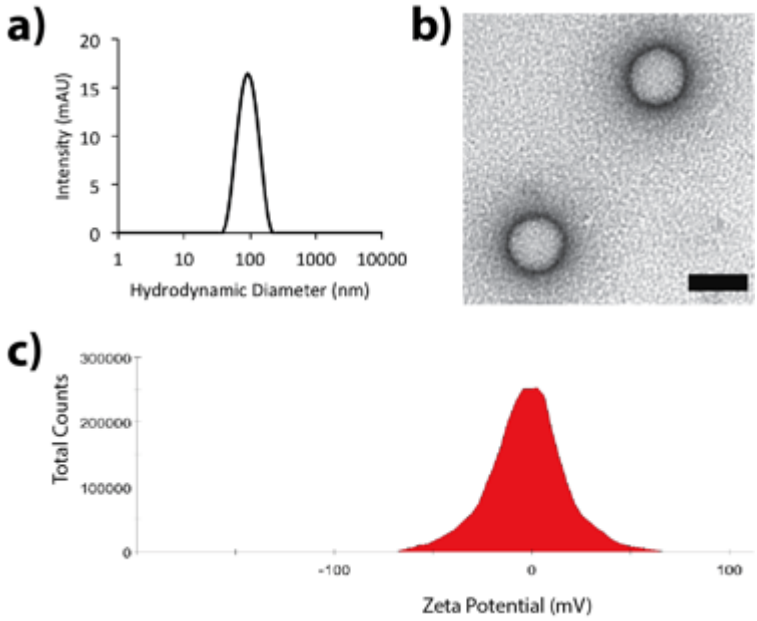

Figure 4.5: Characterization of P_{TBP} micelles show: (a) narrow distribution of 0.15 and diameter of 108 nm by DLS, (b) representative fields of view obtained by TEM (scale bar is 50 nm) and (c) zeta potential characterization showing neutral zeta potential.

To investigate differences in drug loading between modified polymers, micelles were formulated by dialysis with docetaxel, and the encapsulated drug was quantified using high performance liquid chromatography coupled with tandem mass spectrometry (HPLC-MS/MS). To eliminate differences due to changes in molar mass, and thus the hydrophilic-hydrophobic ratio after chemical modification, all loadings were normalized to the mass of the hydrophobic backbone (Figure 4.6).

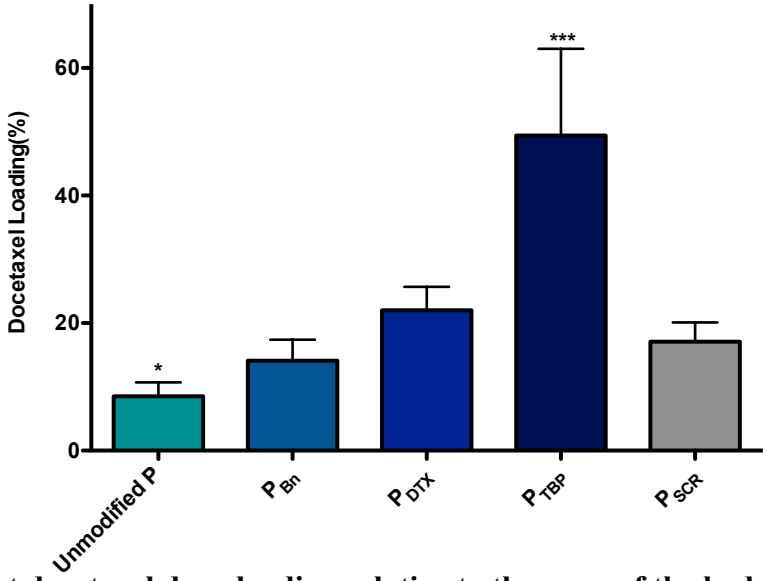

Figure 4.6: Percent docetaxel drug loading relative to the mass of the hydrophobic backbone. Relative to P(LA-co-TMCC)-g-PEG nanomicelles (unmodified P), a significant increase in drug loading was achieved with all hydrophobic modification strategies (benzyl, P_{Bn}; docetaxel, P_{DTX}; and scrambled peptide, P_{SCR}), with the greatest increase observed for nanomicelles formulated with taxol binding peptide-modified polymer, P_{TBP} (n = 4-6, mean + standard deviation, * p<0.05, ***p<0.001 by one-way ANOVA followed by Bonferroni post-hoc test).

As shown in Figure 4.6, all of the polymer modifications formed nanomicelles with significantly higher docetaxel loadings compared to the unmodified polymer ($p<0.05$, Figure 3). P_{Bn} and P_{DTX} showed loadings consistent with those observed with other polymer systems, including polycaprolactone-PEG and polyhydroxypropyl methacrylamide-PEG [109], [110]. Impressively, P_{TBP} formed micelles with loadings significantly higher than all other hydrophobically-modified formulations ($p<0.05$) and five times higher than the control (49 ± 14%, $p<0.001$), suggesting a high affinity of the drug with the peptide-polymer core.

4.4.3 Mechanism of TBP loading

To further explore whether the increased docetaxel loading in the P_{TBP} formulation was due to a specific multivalent interaction or simply due to increased hydrophobicity, we synthesized a scrambled peptide sequence that had the same overall hydrophobicity and isoelectric point (of 9.34) as the TBP, but with the taxane-specific PLTSR amino acid sequence scrambled. In

addition, the phenylalanine residue, which is known to interact with the 3' phenyl ring of docetaxel, was scrambled within the peptide sequence. Notably, cell lines with point mutations in the microtubule at either the phenylalanine or within PLTSR are DTX resistant [218], [219]. Interestingly, the scrambled peptide-polymer conjugate (P_{SCR}) showed significantly less encapsulated docetaxel than P_{TBP} and only a modest increase in drug loading relative to unmodified polymer controls (two times higher, Figure 4.6), which is similar to that of P_{Bn} and P_{DTX}. Given that hydrophobic interactions in general can increase loading and we specifically maintained a similar hydrophobicity in the scrambled vs. normal taxol binding peptide, we attribute this modest increase in loading in P_{SCR} nanomicelles to general hydrophobic interactions with the drug, similar to those observed with P_{Bn} and P_{DTX}. Importantly, these data suggest that a specific interaction between TBP and docetaxel accounts for the significantly greater docetaxel loading in P_{TBP}.

The high loading of the P_{TBP} suggests multivalent interactions within the core, in which binding of the peptide to the drug facilitates drug-drug stacking. Characterizing the specific interaction between the taxol binding peptide and the drug is an analytical challenge due to the poor solubility of both the docetaxel and the peptide. Classic techniques for measuring affinity, such as isothermal titration calorimetry, require aqueous experimental conditions that are not achievable with these molecules. Organic solvents required to solubilize the binding partners in techniques such as ^{1}H NMR neither reflects the native environment within the polymeric nanomicelle nor the cell, and have been reported to cause a change in the conformation of both short peptide sequences and docetaxel itself [220], [221].

4.4.4 Serum stability of P_{TBP} micelles

As higher drug loadings can result in reduced micelle stability in the presence of serum proteins [189], we were particularly interested in characterizing the stability of these high docetaxel loaded nanomicelles. The reduction in stability is typically associated with protein adsorption onto the nanoparticle surface which can cause premature drug release due to a partitioning effect between the hydrophobic core and hydrophobic pockets of the proteins [85]. This lack of stability limits *in vivo* efficacy and is evident with *in vitro* studies. To determine whether the high docetaxel loading observed with P_{TBP} alters micelle stability, we investigated their in vitro serum stability relative to unmodified polymeric nanomicelles. Nanomicelles were incubated with fetal bovine serum (FBS) in phosphate buffered saline (PBS, 1X) at 37 °C [105], [197]. At 0, 24 and

48 h, an aliquot of the nanomicelle solution was taken and separated from serum proteins using fast protein liquid chromatography (FPLC). The docetaxel in the nanomicelle fraction was quantified using HPLC-MS/MS. The compiled data in Figure 4.7 is presented: (A) as docetaxel amount that is encapsulated, relative to time zero, as a function of time; and (B) as absolute drug loading over time, assuming no polymer is lost to protein adsorption. Drug loaded P_{TBP} nanomicelles showed no significant differences ($p=0.89$) in docetaxel release compared to the unmodified polymer (Figure 4.7A), demonstrating that the higher docetaxel loaded P_{TBP} nanomicelles were as stable in serum as the unmodified formulations. This is noteworthy because nanomicelles loaded with more chemotherapeutic are often less stable in serum [213], [222], [223]. Moreover, the absolute drug loading was higher at all time points up to 48 h in P_{TBP} nanomicelles (Figure 4.7B) and remained relatively unchanged up to 24 h. Importantly, stable drug loadings in serum solutions for 24 h is considered long, and provides sufficient time for tumour accumulation in vivo.[1] After 24 h, a decrease in docetaxel is observed (to ~35% at 48 h), suggesting release of payload due to micelle dissociation [197]. Importantly, these data show that the increased drug loading observed with P_{TBP} micelles does not come at the expense of kinetic nanomicelle stability, which is key to ultimate use *in vivo*.

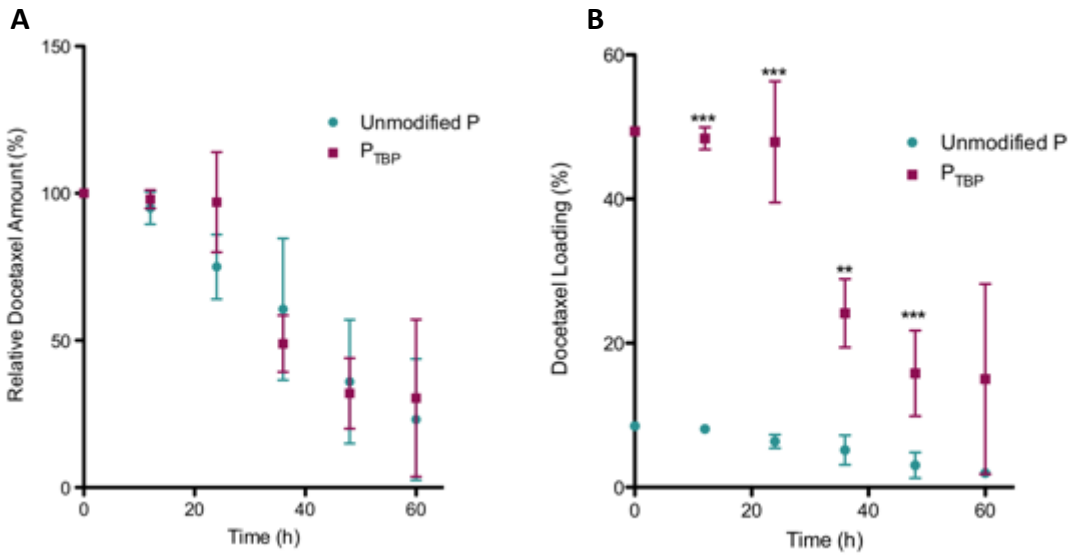

Figure 4.7: Serum stability of docetaxel-loaded P_{TBP} vs. unmodified P(LA-*co*-TMCC)-*g*-PEG was compared over 60 h in terms of: (A) the amount of docetaxel encapsulated relative to time 0; and (B) the total docetaxel loaded (as a percentage of the polymeric backbone). As shown in (A), there was no significant difference between the stability of unmodified P(LA-*co*-TMCC)-*g*-PEG and P_{TBP} over 60 h (n=3-6, mean ± standard deviation, p=0.89 comparing slopes). As shown in (B), the percent of docetaxel loaded drug is significantly higher in P_{TBP} than unmodified polymer control nanomicelles at all time points up to 48 h (p<0.01***p<0.001), and relatively unchanged at 24 h, assuming no polymer loss due to degradation or dissolution (n=3-6, mean ± standard deviation).**

4.4.5 Cytotoxicity of P_{TBP} micelles

Polymeric cytocompatibility and docetaxel-loaded nanomicelle cytotoxicity are both critical for future *in vivo* applications. To demonstrate the cytocompatibility of the P_{TBP} (without encapsulated docetaxel) and the cytotoxicity of docetaxel loaded P_{TBP} micelles, polymeric nanomicelles were incubated with the human epithelial breast cancer line, SKBR-3 cells. Cell viability was assessed after 48 h and normalized to untreated cells (Figure 4.8).

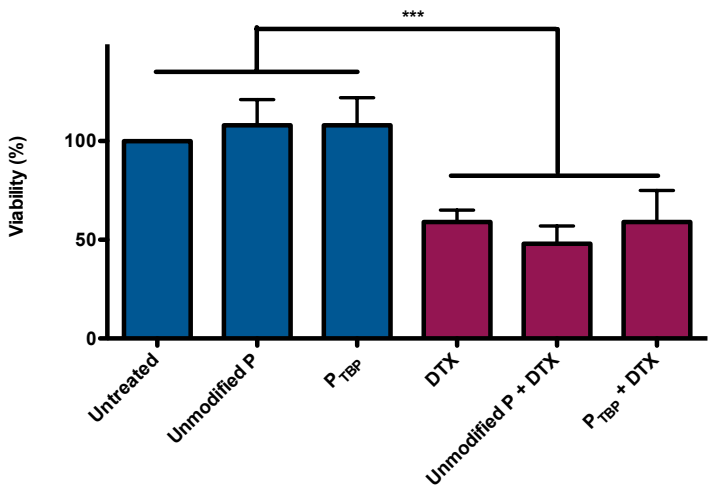

Figure 4.8: Cytotoxicity of various treatments against SKBR-3 cells was measured using the Presto Blue assay after 48 h incubation and normalized to untreated control SKBR-3 cells. Both P_{TBP} and unmodified P(LA-*co*-TMCC)-*g*-PEG nanomicelles are cytocompatible, showing 100% viability as compared to untreated cell controls. Both drug loaded nanomicelles (unmodified P(LA-*co*-TMCC)-*g*-PEG + DTX and P_{TBP} + DTX) show similar cytotoxicity to free DTX (n=3 separate cultures, mean + standard deviation, ***p<0.001, by one-way ANOVA followed by Bonferroni post-hoc test).

Importantly, both unmodified polymeric nanomicelles and P_{TBP} nanomicelles, without encapsulated docetaxel, showed no cytotoxicity relative to untreated cells, demonstrating cytocompatibility of both polymers. Since free DTX is highly toxic with an IC_{50} of 10 ng/mL (Figure 4.9), it was used as a positive control to test the cytotoxicity of DTX when loaded in both unmodified and P_{TBP} nanomicelles. Using dose-matched controls, we observed no significant difference between DTX and the encapsulated DTX, suggesting that encapsulation did not impede the mechanism of action of the drug within the cell. Importantly, all DTX formulations were cytotoxic compared to controls.

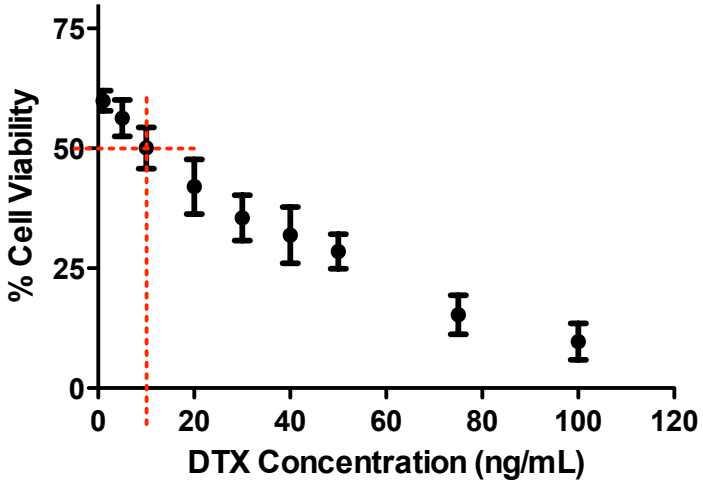

Figure 4.9: *In vitro* cytotoxicity of docetaxel in SKBR-3 breast cancer cells. Cells were exposed to the different concentrations of docetaxel for 4 h, followed by media replacement and growth for 48 h. % Cell viability was determined by the Presto Blue assay as described in Methods. Red dashed line identifies the IC_{50} determined. (n=3 separate cultures, mean ± standard deviation)

4.5 Conclusion

Achieving high drug loading while maintaining both serum stability and cytocompatibility are critical for ultimate use as clinically relevant polymeric nanomicelle formulations. Here we show, for the first time, that by incorporating the natural binding site of the drug with the β-tubulin peptide into our polymeric nanomicelle design, we achieve enhanced loading without jeopardizing either kinetic serum stability or drug toxicity. This strategy has broad applicability to other polymeric systems. The affinity demonstrated with P(LA-co-TMCC)-g-PEG is not specific to this polymer, but rather to the taxol binding peptide and taxanes. By incorporating this peptide onto other polymer scaffolds, the delivery of taxanes chemotherapeutics can be enhanced. Furthermore, a rational design approach using known peptide mimetics could form the basis for the encapsulation of other drugs[34], thereby overcoming key limitations of high drug loading (without the usual loss of serum stability) of polymeric nanomicelles.

4.6 Acknowledgements

We thank Professor Mitchell Winnik and Joey Hang Zhou (University of Toronto) for use of their GPC, Mr. Steven Doyle and Mr. Battista Calvieri (University of Toronto Microscopy Imaging Laboratory) for assistance with TEM imaging, and Pearson Wu who helped with benzyl deprotection experiments. We wish to acknowledge the Canadian Foundation for Innovation and the Ontario Research Fund for funding of the Centre for Spectroscopic Investigation of Complex Organic Molecules and Polymers, and Dr. Darcy Burns (CSICOMP) who helped us with NMR. We are grateful for partial funding from the Natural Sciences and Engineering Research Council of Canada (MSS, PGSD to JL and PDF to CKM) and the Canadian Institutes of Health Research (MSS).

5 Preclinical evaluation of taxol binding peptide-modified polymeric micelles loaded with docetaxel in an orthotopic breast cancer mouse model

*This chapter was submitted to *Biomaterials.*

Logie, J., Ganesh, A.N., Aman, A.M., Al-awar, R.S., Shoichet, M.S. (2016) Preclinical evaluation of taxol-binding peptide modified-polymeric micelles loaded with docetaxel in an orthotopic breast cancer mouse model. Submitted October 11, 2016 to Biomaterials.

J.L., A.M.A., R.S.A. and M.S.S. designed research; J.L. performed research; A.N.G. assisted with animal experiments; J.L. and A.M.A. analyzed data; and J.L. and M.S.S. wrote the manuscript.

5.1 Abstract

We developed a novel taxol-binding peptide (TBP) modified, biodegradable polymeric micelle that overcomes limitations of drug loading and poor serum stability typically seen with micelle delivery, leading to enhanced pharmacokinetics and tumour distribution of docetaxel (DTX). The use of the taxol binding peptide to increase docetaxel loading is particularly compelling as it takes advantage of a known intracellular binding mechanism in a new way. Docetaxel is a potent chemotherapeutic with a therapeutic index limited by the toxicity of the excipients that are necessary to enhance its solubility for intravenous delivery. Our polymeric micelle has terminal furan groups that enable facile antibody Fab conjugation by Diels-Alder chemistry for targeted delivery. Compared to the conventional ethanolic polysorbate 80 formulation (Free DTX), our nanoparticle (NP DTX) formulation exhibited a two-fold increase in exposure and tumour accumulation. Notably, the reduced toxicity of the NP DTX formulation increased the therapeutic index and allowed for higher dosing regimens, with a maximum tolerated dose (MTD) 1.6-fold higher than that of the Free DTX formulation, which is significant and similar to enhancements observed in clinical products for other drugs. These improved properties led to enhanced mouse survival in an orthotopic model of breast cancer, however, the targeted formulation of Fab-NP DTX did not further improve efficacy. Together, these results clearly demonstrate the benefits of the TBP-modified polymeric micelles as promising carriers for docetaxel.

5.2 Introduction

Despite widespread clinical use, taxane chemotherapeutics, like docetaxel (DTX), represent a formulation challenge. Current clinical formulations have dose-limiting systemic side effects, such as neutropenia [224] and hypersensitivity reactions [7] associated with the high concentrations of toxic excipients (e.g. polysorbate 80). To circumvent these issues, nanoparticle delivery strategies have been pursued with biocompatible amphiphilic polymers that solubilize drugs within their hydrophobic core during self-assembly.

While several polymeric micelle strategies have been explored, these systems are plagued by low drug loadings and poor stability that can limit their translation in vivo [43], [107], [189]. By facilitating intermolecular interactions within the micelle core, high drug loadings and stability in serum conditions can be achieved [105], [110], [190], [211]. Furthermore, enhanced drug-carrier compatibility has been shown to improve nanotherapy efficacy [208], [225]. Our novel polymer, poly(D,L-lactide-co-2-methyl-2-carboxytrimethylene carbonate)-graft-polyethylene glycol (P(LA-co-TMCC)-g-PEG, Figure 5.1A), forms stable micelles, and is amenable to chemical modification through carboxylic acids along the backbone and end group PEG modification on the corona [135], [155]. In order to increase docetaxel (DTX) loading, we incorporated the taxol binding peptide (TBP) into our polymer design, thereby taking advantage of a known intracellular binding pathway. We were successful and achieved DTX loading in the polymeric micelles that was double compared to typical nanoparticle formulations [190]. Notably, this docetaxel-micelle system was stable in serum with a half-life of greater than 24 hours [190].

Herein, we test the in vivo efficacy of this new polymeric micelle formulation (P_{TBP}) with encapsulated DTX and evaluate the utility of active targeting with the incorporation of a novel anti-human epidermal growth factor receptor 2 (HER2) fragment antibody, Fab 73J (Figure 5.1B). The use of Fab has been shown to mitigate the premature clearance associated with antibody engagement of Fcγ receptors on immune cells [226]. Compared to the clinically used trastuzumab, Fab 73J binds to a unique epitope of the HER2 receptor and has comparable binding and trafficking [29].

We assessed the preclinical efficacy of this formulation in a clinically relevant orthotopic tumour model. In the current study, we used an established orthotopic breast cancer model in NOD-SCID-*IL-2Rγ*null (NSG) mice to better recapitulate the human disease [227]. Compared to

subcutaneous xenograft models, orthotopic models more accurately represent the vasculature and metastatic potential of patient tumours and better predict clinical results [61], [62], [227]-[229]. Here we report the enhanced tolerability and efficacy of a taxol-binding peptide conjugated polymeric micelle formulation of DTX in this mouse model of breast cancer.

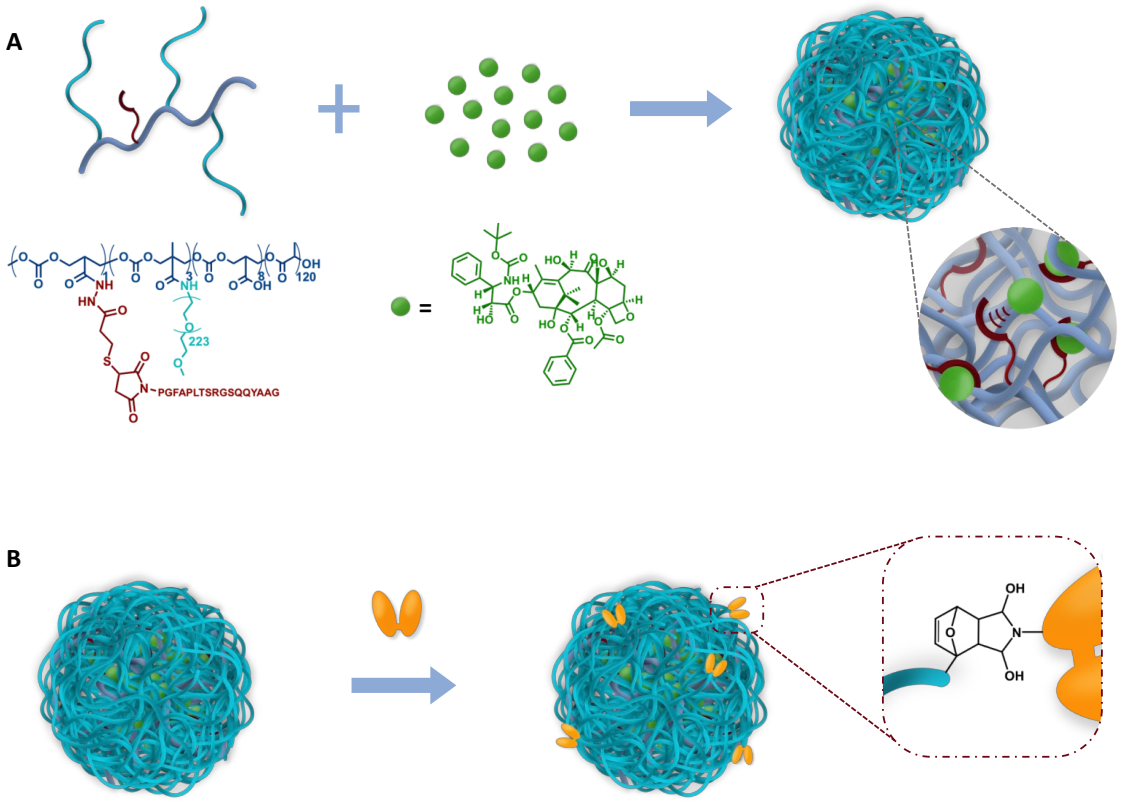

Figure 5.1: (A) Schematic of NP DTX formation from self-assembly of P_{TBP} (P(LA-co-TMCC)-g-PEG,TBP) with docetaxel. Docetaxel binds specifically to TBP, facilitating high drug loading. (B) Fab 73J conjugation to NP by furan-maleimide Diels-Alder click chemistry.

5.3 Materials and Methods

5.3.1 Free DTX and NP DTX formulations

Free DTX was prepared by dissolving DTX in a mixture of ethanol and polysorbate 80 and then diluting in saline to a final solution of 7.5% polysorbate 80, 10% ethanol, 82.5% saline. The 1.25 mg/mL stock was injected directly or diluted to the desired concentration.

P(LA-co-TMCC)-g-PEG-Furan (P_{furan}) and P(LA-co-TMCC)-g-PEG, TBP (P_{TBP}) were synthesized following previously established protocols[132], [197]. Briefly, backbone is

synthesized by a ring opening polymerization of D,L-lactide and 2-methyl-2-carboxy-trimethylene carbonate catalyzed by a thiourea and initiated by a pyrenebutanol. PEG chains are grafted onto the backbone by carbodiimide chemistry, and peptide is conjugated onto backbone using a Michael addition between a thiolated backbone and a maleimide modified peptide [190]. After purification by dialysis and size exclusion chromatography, polymers were lyophilized and further characterized. Both polymers were characterized by ^{1}H NMR and P_{TBP} was further analyzed by amino acid analysis. For NP DTX formulations, polymer was a mix of 90% P_{TBP} and 10% P_{furan}. NP DTX were formed by co-dissolving polymer (4 mg) and DTX (2.4 mg) in DMF (1 mL) to which 50 μL of borate buffer (pH 9, 500 mM) was added. The solution was left at room temperature for 15 min before 0.5 mL of distilled water was added dropwise. Batches were scaled up to 15 mL of DMF depending on the scale of material needed for individual studies. Scale-up had no impact on drug loading or NP size. Solutions were dialyzed against distilled water for 24 h, changing the water two times (MWCO 2 kg/mol). The solution was centrifuged to remove DTX aggregates prior to use and characterization (5000 rpm, 15 min). Particles were characterized by dynamic light scattering (DLS). DTX concentration was quantified by HPLC-MS/MS using a Waters XTerra C18 column (3.5 μm) on an Agilent 1100 HPLC equipped with an AB Sciex API 4000 triple quadrupole mass spectrometer with electrospray ionization source detector. Solutions were diluted into 80:20 v/v acetonitrile: water and compared to a DTX standard curve (3.125-200 ng/mL) using paclitaxel as an internal standard (100 ng/mL). NP DTX solutions were lyophilized and stored at -20°C prior to use. Immediately prior to injection, NP DTX was resuspended in saline to desired concentrations for dosing. Solutions were sonicated in a water bath at 25°C for 10 min to ensure complete dissolution.

5.3.2 Cell maintenance and preparation

MDA-MB-231/H2N cells were a generous gift from Dr. Robert Kerbel (Sunnybrook Research Institute, Toronto, ON, Canada). The cells were maintained in house in RPMI 1640 culture medium supplemented with 10% heat-inactivated fetal bovine serum (FBS), 50 units/mL penicillin and 50 μg/mL streptomycin under a humidified 5% CO_2 environment. To prepare cells for injection, cells were rinsed with PBS and detached using trypsin-ethylenediamine tetraacetic acid (trypsin-EDTA). Once suspended, cells were pelleted and washed 3 times in PBS before resuspension at a concentration of 31.25 x 10^6 cells/mL. Cells were kept on ice prior to injection.

5.3.3 Orthotopic breast cancer model

The protocols used in these in vivo studies were approved by the University Health Network Animal Care Committee and performed in accordance with current institutional and national regulations. Animals were housed in a 12 h light and 12 h dark cycle with free access to food and water. NOD scid gamma (NSG) mice were bred either in-house (for PK and efficacy study) or purchased from Jackson (for MTD study). 7-9 week old female mice were selected for tumour xeno-transplantation. To form orthotopic mammary fat pad tumours, mice were inoculated with 1.5×10^6 MDA-MB-231-H2N cells suspended in 50 μL of sterile PBS. Prior to surgery, mice were anaesthetized with isoflurane-oxygen. The surgical area was depilated and swabbed with betadine before making an incision in the skin of the lower abdomen to the right of the midline, uncovering the mammary fat pad in the right inguinal region into which the cells were injected. The incision was then sutured closed and lactated Ringer's solution and buprenorphine were given post-operatively for recovery and pain management.

5.3.4 DTX injections

For all studies, mice were injected through the tail vein with 200 μL of specified formulation using a BD324702 insulin syringe. Syringes were pre-coated with either 0.01% polysorbate 80 in saline (for free DTX formulations) or with 1 mg/mL polymer in saline to prevent drug loss. Syringes were pre-coated by drawing and withdrawing solutions 3 times prior to filling with desired formulation.

5.3.5 Maximum tolerated dose study

Maximum tolerated doses were determined in a dose escalation study between 2 and 10 mg/kg docetaxel. Mice bearing orthotopic MDA-MB-231/H2N tumours (2 weeks post cell impant) were randomized into treatment groups and given three injections at selected doses at days 0, 5 and 8. Mice were monitored daily for weight loss and signs of distress (unresponsive, labored breathing, discharge). At day 15 post-injection, mice were euthanized and organs (tumour, kidney, liver, thigh muscle) were collected for histology (H&E). All sections were examined by a trained pathologist at the CMDH Pathology Core.

5.3.6 Pharmacokinetics and biodistribution study

The PK and biodistribution of NP DTX was compared to free DTX at 5 mg/kg in mice 2 weeks post cell implantation (tumours palpable). Groups of 16 mice were randomly assigned to each formulation, with groups being subdivided into three groups of three (terminal end points at 2, 4 and 7 h) and one group of six (terminal end point at 24 h). Mice were placed on a staggered blood sampling schedule (10 min, 30 min, 1, 2, 4, 7 and 24 h) via a femoral blood draw (<30 μL) such that each mouse was sampled for blood no more than three times prior to a terminal cardiac puncture. Blood was collected using EDTA tubes (Sarsdet 16.444.100) and immediately centrifuged to collect the plasma fraction. At terminal time points animals were sacrificed by CO_2 asphyxiation and blood was collected via cardiac puncture. The plasma fraction was immediately isolated by centrifugation. Tissues samples (heart, lung, liver, kidney, spleen, and tumour) were collected by dissection, rinsed in PBS, placed in vials and snap frozen.

5.3.7 Plasma and tissue preparation

To prepare plasma for quantification by HPLC-MS/MS, samples were thawed and 10 μL was removed and diluted with 10 μL of 1% formic acid in water. To this solution, 10 μL of 100% acetonitrile containing paclitaxel, the internal standard, at 1 μg/mL was added. The sample was vortexed (15 sec, 2x) prior to the addition of 70 μL cold acetonitrile. After an additional vortex, samples were centrifuged at 16,000g for 15 min at 4°C to spin down precipitated protein. Supernatant was removed for quantification by LC-MS/MS as described above.

To prepare the tissues for quantification, samples were thawed, accurately weighed, and 1.0 mm diameter zirconia beads were added to the tubes (~20 beads/tube) to facilitate homogenization. 200 μL of 1% formic acid and 200 μL of acetonitrile containing 500 ng/mL of the internal standard were added. Samples were homogenized for 1 minute (2x) using a bead beater, with cooling over ice between homogenization steps. 600 μL of cold acetonitrile was added to the tube, followed by an additional two homogenization steps. Samples were then spun down at 16,000xg for 15 min in the cold room to remove precipitated protein. Supernatant was removed for quantification by LC-MS/MS.

5.3.8 DTX concentration measurement

Chromatographic separations were carried out using the LC-MS/MS as described in the above section to quantify drug loading. The mobile phase was 0.1% formic acid in water (solvent A) and methanol (solvent B). The column was held for 0.5 min at 50% solvent A, with a drop to 5% over 0.5 min, holding for 0.5 min, and moving back to 50% in 0.1 min, with a final hold for 3.2 min. Docetaxel was quantified by comparing to a docetaxel standard curve (3.125 ng/mL-200 ng/mL), using paclitaxel as an internal standard (100 ng/mL). Docetaxel was monitored at 830.20 and 549.20 *m/*z; paclitaxel was monitored at 876.20 and 308.10 *m/z.* When necessary, samples were diluted further to be within the linear standard curve.

5.3.9 Fab-73J conjugation

Fab-73J was modified with a maleimide (average 1.9 maleimide/Fab quantified using SAMSA fluorescein) using sulfo-SMCC chemistry previously described [29]. Upon resuspension of NP DTX in saline (pH 5.5), 23 μL of a 4.4 μM solution of Fab-73J-maleimide (10 eq to NP) was added to the solution and allowed to react via Diels-Alder (between the Fab-73J-maleimide and PEG-furan) for 4 h prior to injection. We have previously shown that an average of 10 antibodies/particle results in optimal fractional coverage of HER2 overexpressing cells [230]. Previous work has shown the Diels-Alder reaction was confirmed to go to completion at low equivalents using Alexa Fluor-488 labelled Fabs [29], so a purification step (and subsequent loss of drug) can be avoided.

5.3.10 Efficacy study

Mice bearing orthotopic MDA-MB-231/H2N tumours were checked biweekly to monitor tumour progression and body weight. When tumours were palpable, mice were randomized into five groups (n=9) by tumour size and body weight, and treated by intravenous tail vein injection with one of (1) NP Control (6 mg/mL polymer NP in saline) (2) NP DTX (5 mg/kg DTX in the NP, dissolved in saline) (3) Free DTX (5 mg/kg DTX, dissolved in 7.5% polysorbate 80, 10% ethanol in saline) (4) NP DTX (8 mg/kg DTX in the NP, dissolved in saline) (5) Fab-NP DTX (8 mg/kg DTX in the Fab-73J-NP, dissolved in saline) on days 0, 5, and 8. Tumour dimensions and body weight were measured biweekly. The tumour volume was calculated using the formula: $V=(\pi \times (\text{short diameter})^2 \times (\text{long diameter}))/6$. Mice with tumour volumes >1500 mm^3 or weight loss of over 20% were sacrificed.

5.3.11 PK and statistical analyses

PK parameters were assessed with Phoenix WinNonlin. All statistical analyses were performed using Graph Pad Prism version 5.00 for Macintosh (Graph Pad Software, San Diego, California, www.graphpad.com). Differences among 3 or more groups were assessed by one-way ANOVA with Bonferroni post hoc correction to identify statistical differences among three or more treatments. Analysis of survival curves was done using a Log-rank Mantel-Cox Test. Alpha levels were set at 0.05 and a p value of <0.05 was set as the criteria for statistical significance. Graphs are annotated where p-values are represented as $*p<0.05$, $**p<0.01$, or $***p<0.001$.

5.4 Results

5.4.1 Synthesis and characterization of NP DTX

The polymers used to prepare nanoparticles (NP DTX) were synthesized by an organocatalyzed ring opening polymerization of D,L-lactide (LA) and 5-methyl-5-benzyloxycarbonyl-1,3-trimethylene carbonate (TMCC-Bn) followed by benzyl deprotection to produce the poly(D,L-lactide-co-2-methyl-2-carboxytrimethylene carbonate) (P(LA-co-TMCC)) backbone [132] that was then grafted with 10,000 g/mol PEG chains by carbodiimide chemistry [197]. Polymers were characterized by ^{1}H NMR and showed an average of 3 PEGs/backbone. P(LA-co-TMCC)-g-PEG-furan (P_{furan}) was synthesized using a PEG modified with a furan end group, while P(LA-co-TMCC)-g-PEG, TBP (P_{TBP}) used methoxy-terminated PEG groups. P_{TBP} was synthesized by Michael addition between the maleimide-TBP peptide and a thiolated backbone, and showed an average of 1 peptide/backbone by amino acid analysis [190]. NP DTX was formed by co-dissolving polymers (10% P_{furan}, 90% P_{TBP}) and docetaxel in DMF and then dialyzing against water for 24 h. The Z-average particle size was measured by dynamic light scattering (DLS) to be 121 ± 25 nm with a distribution of 0.15 ± 0.03. The particle size is larger than particles without docetaxel (108 ± 16 nm), consistent with observations from other systems [109], [225]. Absolute drug loading of particles used in the three in vivo studies was $18.5 \pm 1.1\%$, which is double that achieved by any other micellar formulations of docetaxel [181], [231] and reflects the importance of the incorporation of the taxol-binding peptide to drug loading.

To assess the benefit of actively targeting the cancer cells, we included a targeted arm in our efficacy study. NP DTX was targeted by conjugating Fab 73J, a novel HER2-binding Fab, using Diels-Alder click chemistry between furan end groups of the PEG and maleimide-modified Fab

73J to achieve an average of 10 Fab/NP (Figure 5.1B). We have previously shown that this Fab increases intracellular uptake of NPs in vitro in HER2+ breast cancer cell lines [29].

5.4.2 Maximum tolerated dose

Before evaluating the pharmacokinetics and efficacy of our formulation, we evaluated its tolerability compared to a clinically relevant surfactant-based formulation. Taxotere, the clinically used formulation of docetaxel, is comprised of docetaxel in a solution of 20% polysorbate 80 and 13% ethanol in saline. Notably, as this formulation caused severe toxicity upon injection into the NSG mice, we reduced the excipients to 7.5% polysorbate 80 and 12.5% ethanol for the Free DTX formulation in this study. Even this scaled-down formulation caused mild lethargy immediately following injection in many of the animals. In contrast, injections of NP DTX and NP alone (i.e., particles without docetaxel) caused no adverse reaction upon injection, and injection of NP alone was comparable to that of no injection in terms of animal activity level and tail vein damage.

Strikingly, the maximum tolerated dose (MTD) of DTX is 1.6-times higher in the NP DTX formulation compared to the free formulation (8 mg/kg vs. 5 mg/kg, Figure 5.2). Significant weight loss was seen in animals receiving high doses of Free DTX (>5 mg/kg). In contrast, NP DTX up to 8 mg/kg caused only minor weight loss (<10%) and a rapid 3-5 d recovery without any abnormality in the histology of clearance organs, such as the kidney and liver. The number of injections was limited to three due to severe tail vein damage from the high percentage of polysorbate 80 (7.5%) used in the Free DTX formulation. The improved tolerability of the NP DTX formulation gives a greater therapeutic index and allows for higher dosing in the efficacy study. Before assessing the efficacy, we characterized the two formulations in terms of pharmacokinetics and biodistribution.

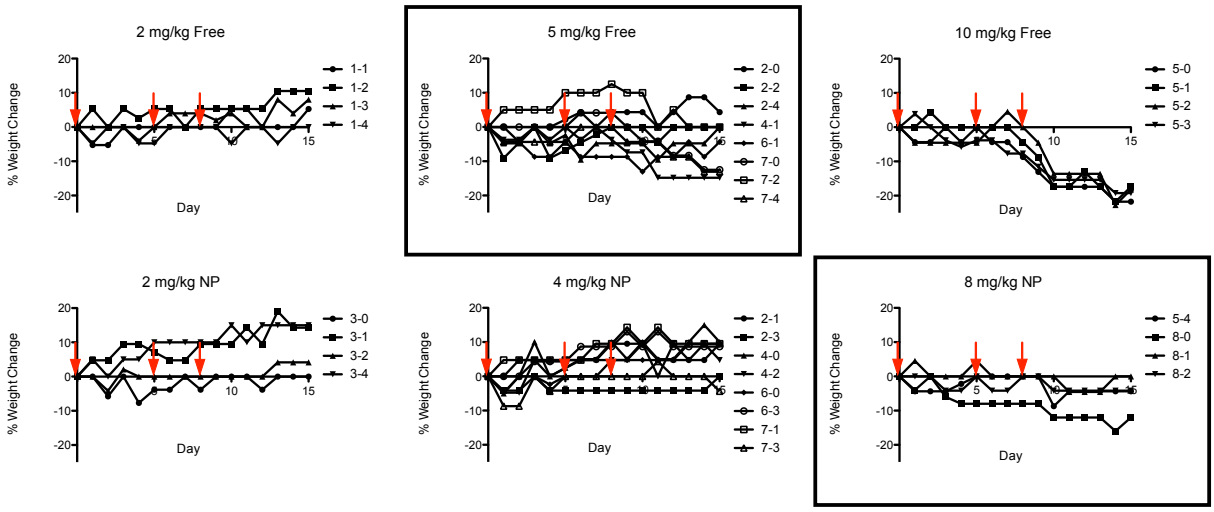

Figure 5.2: MTD study. Weight change for mice receiving dose escalation of either Free or NP-DTX formulations. Free DTX at 10 mg/kg induced significant weight loss (>20%) in all four mice. At 5 mg/kg, Free DTX caused weight loss >10% in 4/8 animals, and was determined as the MTD for this formulation, consistent with previous reports in NSG mice. The MTD of NP-DTX was not reached, but at the highest concentration of the formulation, 8 mg/kg, only 1/4 mice had weight loss >10%.

5.4.3 Pharmacokinetics and biodistribution

Pharmacokinetics and biodistribution of formulations were evaluated at the MTD of the free drug formulation (5 mg/kg), thereby allowing the two formulations to be compared at equivalent doses. Following a bolus intravenous injection, docetaxel quickly distributes through the body and is metabolized and eliminated. Consistent with previously reported pharmacokinetic profiles of this drug [131], [232], both the free and NP formulations show a significant drop in plasma concentration immediately following injection, with less than 10% of the initial dose remaining in the plasma after ten minutes (Figure 5.3). NP DTX showed a modest improvement in pharmacokinetic parameters over the 7 h time period. The lambda half-life ($t_{1/2,\lambda}$) of the drug in the plasma showed a 1.5-fold increase. The area-under-the-curve (AUC), a measure of drug exposure, had a 2-fold increase while the clearance (Cl), a measure of drug elimination, was reduced to half of that of the conventional formulation (Figure 5.3). Interestingly, these seemingly modest improvements are consistent with those seen with clinically used NP formulations of paclitaxel such as Genexol-PM [233] and Nanoxel-PM, a docetaxel formulation currently under evaluation [234]. Importantly, these parameters suggest greater drug exposure to

the tumour at equivalent doses, and the extended circulation time enables greater tumour accumulation.

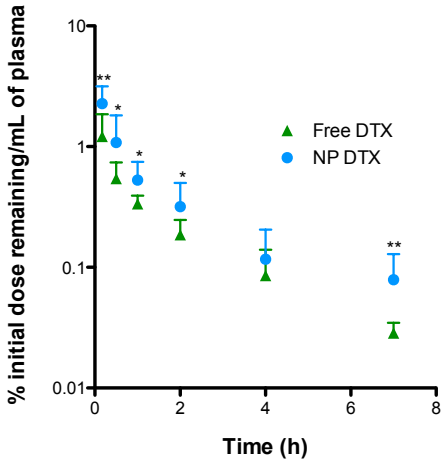

Parameter	Free DTX	NP DTX
$t_{1/2,\lambda}$	1.69 h	2.29 h
AUC (to t=7h)	1730 h $ng^{-1}mL^{-1}$	3100 h ng^{-1} mL^{-1}
Cl	1940 mL h^{-1} kg^{-1}	1060 mL h^{-1} kg^{-1}

Figure 5.3: Pharmacokinetic profiles of Free DTX and NP DTX in tumour bearing mice. Plasma concentration is significantly higher in the NP DTX formulation at all time points except for 4 h (where there is no statistical difference), and gives a higher half-life, $t_{1/2,\lambda}$ (1.5x), area under the curve, AUC (2x) and slower clearance, Cl (~½) (n=10, mean + SD, *p<0.05, **p<0.01)

To evaluate biodistribution, a panel of organs was harvested at sacrificial time points between 1 and 24 h. DTX was quantified after extraction from tissue by HPLC-MS/MS. While nanoparticles frequently accumulate in organs of the mononuclear phagocyte system, such as the liver or spleen, no significant differences were seen between the NP and conventional formulation. With the exception of the 1 h time point, the distribution was similar between the two formulations in the liver, spleen, kidney, heart and lungs (Figure 5.4). In the liver we see the drug is rapidly washed out or metabolized, with <0.1% of the initial dose present at the 24 h time point. The other organs show a sharp decline in DTX concentration over the 24 h, consistent with clearance from these organs. Interestingly, reduction in DTX content in the tumour tissue was more gradual, with NP DTX formulations maintaining approximately 1% of the initial dose at the 24 h time point. The tumour tissue showed increased accumulation (between 1.7 and 2.8-times) of DTX at early time points when delivered in the NP formulation vs. in the free form, suggesting passive targeting to the tumour site of NP DTX.

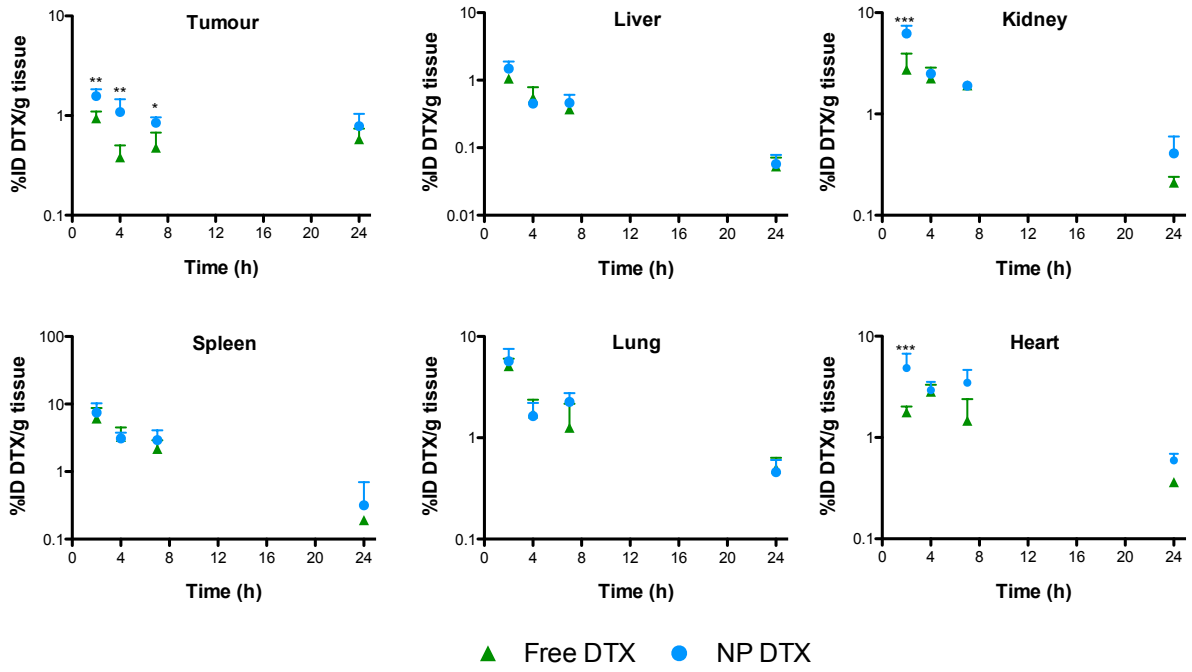

Figure 5.4: Biodistribution profiles of Free DTX and NP DTX in tumour, liver, kidney, spleen, lung and heart at 4 time points. Tumour shows increased accumulation of DTX when delivered in NP formulation at early time points (n=3, mean + SD, *p<0.05, **p<0.01, ***p<0.001).

5.4.4 Efficacy in MDA-MB-231/H2N tumour model

We used an orthotopic HER2+ breast cancer model in NSG mice to evaluate the anti-tumour efficacy of systemically administered NP DTX compared to both actively targeted Fab-NP DTX and Free DTX. When tumours were palpable, with an average volume of 10 mm^3, mice were administered three doses (at days 0, 5, and 8 after palpable tumours) of either NP alone, 5 mg/kg Free DTX, 5 mg/kg NP DTX, 8 mg/kg NP DTX or 8 mg/kg Fab-NP DTX. By comparing the maximum tolerated dose of Free DTX (5 mg/kg) to the same dose of NP DTX and to the maximum tolerated dose of NP DTX (8 mg/kg), we gained a better understanding of the benefit of encapsulation. Furthermore by comparing the NP DTX to the Fab-NP DTX, we gained a better understanding of the benefit of active targeting. On Day 39, both Free and NP DTX at 5 mg/kg significantly inhibited tumour growth by 50% compared to the NP alone group ($p<0.001$, Figure 5.5A and B). At 8 mg/kg, inhibition of growth was more pronounced than the lower dose, with both NP DTX and Fab-NP DTX formulations significantly inhibiting growth by 72%

compared to NP alone and 48% compared to the lower dose ($p<0.001$). Importantly, this difference was seen over a month after injection, suggesting that long-term tumour growth was reduced with early treatment. While in this immunocompromised NSG model, we did not expect additional toxicity associated with the 73JFab, we did expect enhanced efficacy at the tumour, associated with targeting to HER2. There was no difference in Fab-NP DTX and NP DTX, indicating that the 73JFab had minimal impact on DTX tumour targeting. Notably, no visible signs of distress were detected in mice treated with NP DTX at either dose and the limited weight loss observed (Figure 5.5C) showed good tolerability of these selected doses over the 60-day study period. The improved tolerability of the NP DTX formulation correlated with better survival due to higher dosing, with animals receiving 8 mg/kg NP DTX living an average of 30% longer than those receiving Free DTX drug at 5 mg/kg ($p<0.001$, Mantel-Cox test, Figure 5.5D).

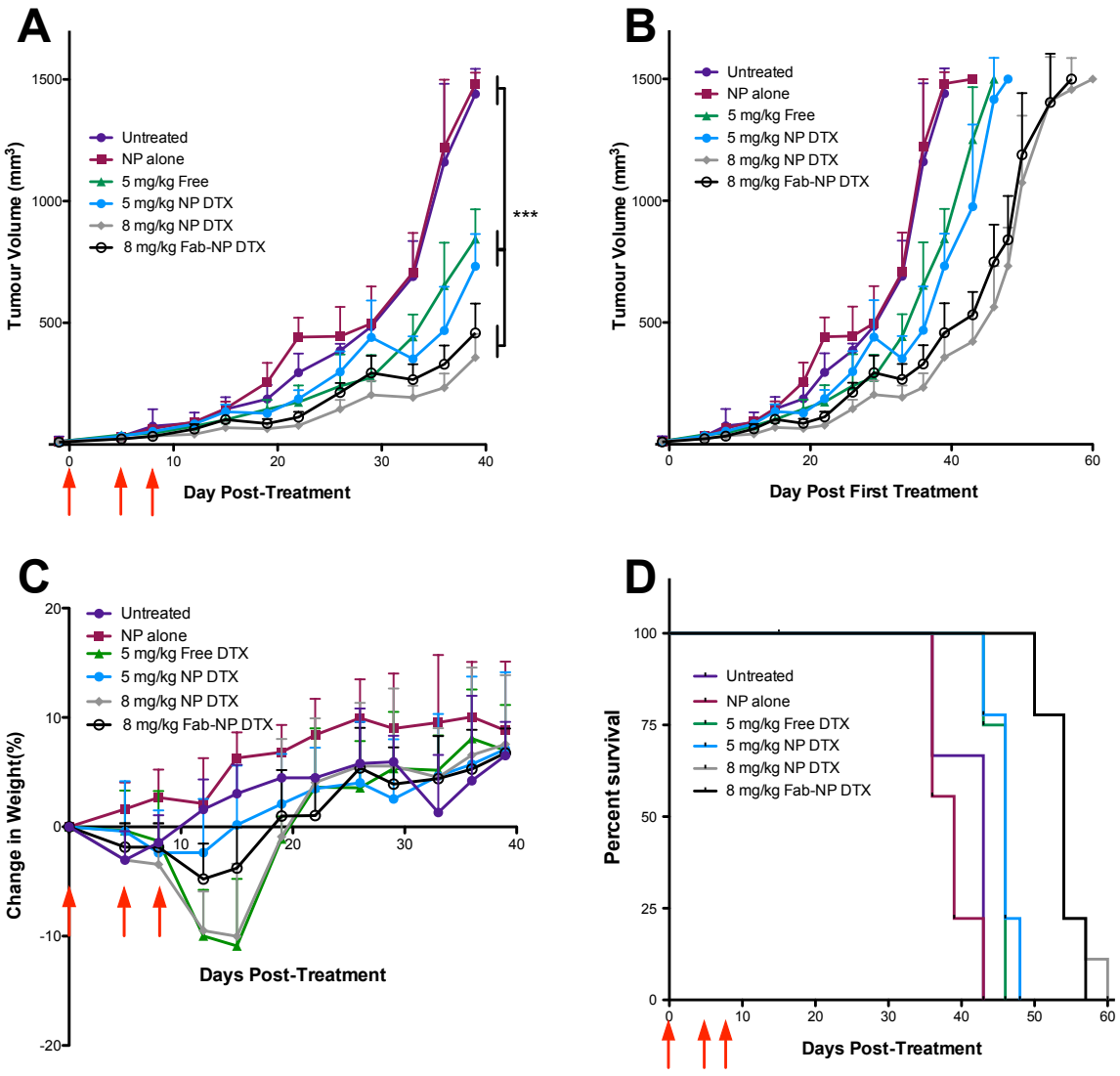

Figure 5.5: Efficacy of NP-DTX in MDA-MB-231/H2N bearing NSG mice. (A) Anti-tumour effect of NP DTX (with or without Fab73J, 5 mg/kg or 8 mg/kg) compared to Free DTX (5 mg/kg). Higher doses (8 mg/kg) of NP DTX resulted in significant inhibition of tumour growth compared to controls and Free DTX at 5 mg/kg ($p<0.001$). (n=9, except for untreated n=3, mean + SD) (B) Tumour growth curves to study completion at day 60. (C) Weight loss showed good tolerability of all formulations (maximum weight loss was ~10%) with recovery within 5 days. (n=9, mean + SD). Red arrows indicate injections of specified treatments. (D) Kaplan-Meier survival plots correlate to tumour growth plot, showing high doses of NP DTX allow survival up to 60 d post-initial injection.

5.5 Discussion

Polymeric micelles for chemotherapeutic delivery are frequently limited by their low loading and poor stability in vivo. By modifying the polymeric backbone with the taxol-binding peptide, high drug loading is achieved without loss of micelle stability. This high loading facilitates efficacious doses of docetaxel to be delivered in vivo with 2-fold lower polymer concentrations than typical NP systems. This NP formulation is tolerated better than the conventional surfactant based formulation, increasing the maximum tolerated dose from 5 mg/kg to 8 mg/kg; this increase of 1.6-times had a dramatic effect in vivo. While there are currently no FDA-approved nanoparticle formulations of docetaxel, formulations of other chemotherapeutics have been approved as first-line therapy for a range of cancers (e.g. Abraxane, Marqibo, Genexol-PM and Doxil) [38]. Enhanced tolerability has proven crucial to the clinical success of these nanoparticles [233], with all of the clinical formulations being given approval on the basis of improving the drug's toxicological profile in patients [49], [235]. Many of these nanoparticles have also improved clinical outcomes of drugs due to increased dosing and favorable pharmacokinetic profiles. Notably, the delivery of paclitaxel in a nanoparticle (Abraxane) allowed a 1.7-fold increase of the maximum tolerated dose over Taxol, and showed a significantly better response rate (33% versus 19%) in a Phase III trial in breast cancer patients [236].

The rationale behind many NP delivery strategies is based on tumour accumulation due to the enhanced permeability and retention (EPR) effect [34]. This has become a widely debated area, as the translation of NPs to humans has been hampered due to tumour heterogeneity between patients and cancers [237]. Clinical results suggest that the EPR effect is not consistent, and only a subset of patients may benefit from the use of vehicles on the nanoscale [40], [238]. Notwithstanding these observations, the value of NP platforms extends beyond the EPR effect. Successful solubilization of the hydrophobic drug in biocompatible carriers can improve the therapeutic index and enhance tumour accumulation [239]. Our novel taxol-binding peptide-conjugated particle platform showed improvements in pharmacokinetics compared to the free formulation, with an increase in parameters indicative of drug exposure, such as half-life and area-under-the-curve, and a decrease in parameters indicative of drug elimination, such as the clearance. Additionally, we see enhanced tumour accumulation at early time points up to 8 h, similar to improvements seen with other carriers of taxanes, such as Genexol-PM [233]. While other carriers show greater exposure and half-life [225], [232], since severe neutropenia and

thrombocytopenia are the main side effects of this drug [224], the modest enhancements in the plasma $t_{1/2}$ that we observe are likely more desirable for future translation. Remarkably, there was no significant enhancement of DTX levels in the organs of the mononuclear phagocyte system (MPS), the liver and spleen, suggesting that the highly PEGylated surface was able to successfully modulate the MPS response [197], [240].

Our novel NP DTX platform was efficacious against an orthotopic $HER2^+$ breast cancer tumour in NSG mice, showing a reduced tumour burden compared to NP alone. Importantly, the heightened tolerability of this formulation allowed higher doses than the surfactant based formulation, resulting in reduced tumour size and longer survival. It should be noted that while orthotopic models have been shown to be more clinically relevant [228], [229], they also require the use of severely immunocompromised mouse strains, such as the NSG, whose sensitivity reduces tolerability for chemotherapeutics. The challenge of these models is that we do not see the sought-after complete tumour regression, which has been achieved in other mouse strains; however, the significant reduction in tumour burden that we observed over the course of the study is promising [241]. Importantly, tumour response alone is not a good endpoint and does not always correlate with overall survival [237]. For this reason, we also show that high doses of NP DTX can extend survival of animals by over 30% compared to the maximum tolerated dose of Free DTX. At matched doses, there are no significant differences between NP DTX and Free DTX in terms of tumour size and survival, suggesting that the enhancements in PK and biodistribution of NP DTX do not correlate to an improvement in efficacy. While tumour sizes are smaller for dose-matched NP DTX at most time points, these differences are not significant. This result is similar to a recent study by Yan et al., where paclitaxel delivered in NPs showed improvement based on tolerability, but not in tumour burden at matched doses [192].

The utility of the Fab 73J targeting ligand is of particular interest. We chose the Fab vs. the full IgG to minimize the immune response to the Fc region, even though we recognize that this would have minimal (if any) impact in the NSG mouse model. While previous in vitro studies [29] showed that the incorporation of an active targeting ligand increases cell uptake, this did not result in improved efficacy in vivo. There were no significant differences between Fab-NP DTX and NP DTX at matched doses, suggesting that the incorporation of the Fab does not impact efficacy in this system. This is consistent with a number of previous reports, which suggest that, for the delivery of hydrophobic small molecules which freely penetrate cell membranes when

released from their vehicle, active targeting ligands provide no additional benefit [83], [242]-[244]. While ligands are able to efficiently get NPs into cancer cells in vitro, they neither change the in vivo biodistribution nor the tumour accumulation [64], [245]. It should be noted that active targeting ligands could have significant value for the delivery of hydrophilic therapeutics, such as siRNA, which cannot passively diffuse across membranes [246], [247]. They also have utility when the antibody has therapeutic efficacy, as in antibody-drug conjugates wherein both the antibody and drug act on tumours. While the 73JFab was designed to bind to the HER2+ breast cancer cells, the missing Fc region may prevent antibody dependent cell-mediated cytotoxicity (ADCC) [29], [59]; however, even a full IgG (73JIgG or the clinically used trastuzumab) would not be efficacious by this mechanism in our immunocompromised mouse model [21].

Achieving more efficacious formulations of docetaxel is critical for clinical use. Here we show that by using a high-load, serum-stable, TBP-modified NP system, we can deliver DTX more effectively and at higher doses compared to a free surfactant based formulation. We expect this strategy of TBP modification to be broadly applicable to other delivery vehicles and not limited to our polymeric nanoparticles. The surfactants used to solubilize these hydrophobic drugs for intravenous formulations are toxic, and associated with a number of adverse reactions in patients. By eliminating the surfactant and using a biocompatible nanoparticle, we are able to increase the dose in NSG mice bearing an orthotopic breast tumour, leading to enhanced survival and reduced tumour burden.

5.6 Acknowledgements

The authors wish to thank Peter Poon and Nikolaos Mitrousis for their assistance with animal experiments, and Drs. Robert Kerbel (Sunnybrook Health Science Centre) and Armand Keating (Princess Margaret Hospital) for help in establishing the mouse tumour model. Dr. Ying Fang Chen, Sohrab Zand, Sonja Inj and Dr. Mike Cooke assisted with histopathology staining. The authors would like to acknowledge the CMHD Pathology Core, especially Dr. Susan Newbigging, for their technical services (www.cmhd.ca). Prof. Sachdev Sidhu and Dr. Jarrett Adams (Toronto Recombinant Antibody Centre) provided the Fab-73J used in these experiments. Dr. Vianney Delplace kindly created the first schematic. We are grateful for partial funding from the Natural Sciences and Engineering Research Council of Canada (Discovery

grant to MSS, PGSD scholarships to JL and ANG) and the Canadian Institutes of Health Research (Foundation Grant to MSS).

6 Thesis Discussion

Despite the vast amount of research in the area, cancer remains a clinical challenge due to a lack of specific targets. Severe side effects limit the utility of currently available chemotherapeutics, which are often used in combination with radiation and surgical interventions. Polymeric micelles have been evaluated as biocompatible delivery vehicles that, with the right formulation, may mitigate many of the harmful side effects and provide a more effective treatment. Despite the initial promise of these nanoparticle carriers, few polymeric micelles reach the clinic due to poor stability, low drug loading and a lack of predictive pre-clinical models.

This thesis presents a rational approach to the design of polymeric micelle drug delivery systems in order to improve the efficacy of formulations. Sequential polymer modifications allowed us to design polymers that self-assemble with high kinetic stability and increased drug loading. We first investigated the role of PEG density on polymeric micelle stability, showing that by increasing PEG graft density we could achieve polymeric micelles stable through lyophilization and in serum. Next, we investigated mechanisms of enhancing drug loading. We showed that for colloid forming drugs, like PPD, we could form drug-laden particles by stabilizing a colloidal drug core within a polymer corona. For other drugs, like docetaxel, the affinity of the drug for the core was increased by facilitating intermolecular interactions with the polymer backbone. Specifically, by incorporating a peptide from the native binding site of docetaxel, we were able to form particles that reached effective doses of the drug without jeopardizing the particle stability. Finally, we demonstrated that these particles were efficacious against an orthotopic model of breast cancer and improved survival over free DTX due to an increased therapeutic index. In this study we also showed that active targeting ligands had no benefit on the efficacy of this system. In the following discussion we will explore the importance of these findings to the field of nanoparticle drug delivery.

6.1 Establishing the role of PEG in polymeric micelle stability

It is well established that upon injection, many proteins present in the physiological environment will adsorb to the surface of a micelle non-specifically, marking it for removal by phagocytes in a process known as opsonization [189], [248]. Opsonization has been shown to cause premature clearance of nanoparticles [52], [249], [250]. Protein adsorption may also induce premature

release of drugs due to a partitioning effect before they reach their target [85], [155]. PEG is frequently employed in nanoparticle formulations to decrease protein adsorption and reduce opsonization, conferring “stealth” properties to the nanoparticle [164]. This is usually achieved by incorporating PEG into the polymer, using either long linear PEG chains or branched PEGs onto the polymer backbone [166], [251]. Increasing PEG density is well established to reduce both total protein adsorption and change the profile of those proteins that adsorb [73], [77], [79], [80].

Despite the role of PEG in mediating nteractions with the components of the serum, few publications address the stability of polymeric micelles in serum or proteins. Several groups [252], [253] have studied the effect of single protein components, such as albumin, on the size of particles overtime, however, this does not accurately represent the full complement of proteins in blood [155]. In serum, the stability of micelles has been measured by methods using the quantification of conjugated fluorogenic probes or encapsulated FRET pairs [156]-[159]. While these methods provide valuable information, the incorporation of an external probe may alter the stability of the formulation. The use of a probe-free strategy, such as the size exclusion chromatography method developed by Hammond et al., allows for the assessment of the inherent kinetic stability of micelles [105]. To validate the role of PEG density on the kinetic stability of our polymeric micelles, in Chapter 2.3.10 we investigated the stability of micelles in serum containing conditions at 37°C to better reflect physiological conditions. Limitations of available analytical methods prevent testing stability in full serum, but provide a good indication of the effect of serum proteins (20% serum conditions) on the particle stability. This study demonstrated that increasing PEG density has the additional benefit of increased serum half-life of particles, going from 24 h (low PEG density) to greater than 72 h (high PEG density). This observation was important, as the presence of serum proteins is well-known to destabilize micelles upon injection, and provides a rationale for using a more heavily PEGylated formulation for future studies. Importantly, the shift in the hydrophobic-hydrophilic balance did not negatively impact the drug loading, which was maintained relative to the backbone polymer concentration. While the role of PEG in preventing protein opsonization has been well studied, the influence of PEG density on the kinetic stability of the particle had not previously been established.

The surface chemistry of a polymeric micelle dictates its resistance towards aggregation, and it has been observed that without certain surface characteristics, aggregation due to van der Waals interactions between particles will occur in solution [254]. PEG-like surfactants (e.g. Pluronic F68, Pluronic F127, PS80) are frequently added as cryoprotectants when drying particles for powder formulations in order to eliminate nanoparticle fusion and interparticle bridging that occurs with inadequate surface protection [255]. The ability to lyophilize particles is crucial for the scalability and long-term storage of products. We hypothesized that increasing the PEG density on the surface of polymeric micelles may simplify lyophilization, removing the need for additional surfactants. To test this hypothesis, in Chapter 2.3 we synthesized micelles with varying PEG densities by controlling the PEG graft chemistry on the backbone. We concluded that micelles of polymers with at least 1.5 PEG/backbone could be lyophilized without using additional excipients or changing the CMC, indicative of the thermodynamic stability of the system. Importantly, the unique graft architecture of our polymer, P(LA-co-TMCC)-g-PEG, allows for the conjugation of multiple PEG chains by tightly controlling the carbodiimide coupling chemistry. If a linear block co-polymer was used, which in general can only be modified at the end group, this strategy could be amended with the use of branched PEGs [166]. Alternatively, incorporation of other monomers with functional handles into the polymer backbone could be used, such as derivatives of peptides [256], methacrylamides [110] or methacrylates [257]

6.2 Mechanisms for high drug loading

One of the main limitations to translation of polymeric micelles is low drug loading. The conventional route of drug encapsulation is based upon hydrophobic interactions within the core [258]. This approach suggests that if a small molecule drug is hydrophobic, it will be entropically driven to the hydrophobic core of micelles during self-assembly. The success of this approach is limited by the self-aggregation and precipitation of many of these small molecules, as well as partial solubilization within the corona of the micelle, which leads to premature burst release [167]. To circumvent this limitation, a variety of non-covalent and covalent chemistries have been applied to introduce drug-polymer interactions within the core of micelles, increasing the loading of desired cargo [212].

The general principle for non-covalent interactions is “like attracts like”, so for example, the incorporation of aromatic groups increases the loading of a drug with aromatic groups through pi-pi interactions [110]. This strategy has evolved to incorporate other interactions including ionic [126], crystalline [108] and hydrogen bond donor-acceptor pairs [128]. Collectively, the incorporation of alternative intermolecular interactions has shifted the loadings of polymeric micelles from ~5 to ~15-20 wt%, representing a significant advancement for the field and enabling efficacious doses in a variety of cancer models [211]. Notably, this increased loading frequently comes at the cost of the stability of micelles, especially in the protein milieu encountered in vivo [167], [212]. To address this, covalent strategies have been applied, such as cross-linking of the core [259], [260] and chemical conjugation of the drug [182], [261], [262]. While these strategies overcome the thermodynamic and kinetic instability of many of these systems, the robustness of this chemistry can make the controlled release of cargo challenging [127], [212]. There are some noteworthy exceptions, such as the paclitaxel-recombinant polypeptide nanoparticle developed by Chilkoti et al., which outperforms Abraxane in multiple cancer models [263] and CRLX101, a camptothecin conjugated nanoparticle in clinical trials for the treatment of a number of solid tumours [264], [265].

In this thesis, we integrated more specific non-covalent interactions within the core to increase drug loading without reducing the particle stability or preventing drug release. The mechanism of these interactions is discussed in subsequent sections. Importantly, we confirm in our work that there is no “one-size-fits-all” approach, and each drug candidate requires a unique polymer solution that exploits distinct intermolecular interactions for core solubilization [76], [206].

6.2.1 Colloidal aggregation to enhance drug loading

The aggregation of a subset of hydrophobic drugs into colloidal structures in aqueous media has largely been thought to be a nuisance in biochemical and drug screening assays [112], [193]. These drugs have low critical aggregation concentrations (CACs), analogous to the CMCs of polymers, above which they self-assemble in solution [117]. While many of these colloids are nano-sized initially, the high energy state of the amorphous phase means that these aggregates are unstable over long periods of time [121]. Interestingly, the use of additives such as surfactants or dye molecules in these colloids has increased the stability for utility in enzyme sequestration [121] as well as for oral [116], [120], [195], [266] and parenteral [154], [267] drug

delivery. Furthermore, several groups have sought to modify small molecules with hydrophobic tails, such as squalene, in order to enable colloidal particle formation [122], [268].

Taking these observations one step further, in Chapter 3 we devised an approach in which we take advantage of the intrinsic physicochemical properties of certain drugs within the core of our particles, and incorporate polymers for surface stabilization. The polymers serve not only to prevent further aggregation through steric repulsion [177], but also to prevent protein adsorption in serum containing media [79]. We were particularly interested in two colloidal aggregators, PPD and fulvestrant, which are both poorly soluble, efficacious chemotherapeutics that present a significant formulation challenge [15], [196]. We were able to optimize polymer-stabilized colloidal formulations of these drugs by screening a number of polymeric excipients used in pharmaceuticals (e.g. UP80, Pluronics) and in polymeric micelles (e.g. P(LA-co-TMCC)-g-PEG, Vitamin-E-PEG). As expected, the optimum polymer for the two drugs was different, due to differences in intermolecular interactions at the colloidal surface. PPD-P(LA-co-TMCC)-g-PEG showed exceptional stability in salt and serum-containing solutions due to shielding at the particle surface and had an exceptionally high loading of 50%. Notably, we validated the mechanism of stability in serum containing solutions using a gel-electrophoresis assay, which confirmed reduced adsorption of the major protein components of serum albumin, fibrinogen and globulin when polymers were present. Current efforts to assess the in vivo efficacy of these formulations are ongoing. In addition, more thorough examination of small molecule aggregation behavior and polymeric excipients will be key to understanding this type of formulation strategy and its utility with delivery of other therapeutics.

6.2.2 Specific taxol binding peptide polymer modification

Unlike PPD and fulvestrant, the taxanes (docetaxel and paclitaxel) do not form well-defined colloidal aggregates in aqueous solution and instead self-associate into long fibers that cannot be readily controlled by this type of formulation [269]. In order to increase drug loading beyond the 20wt% that could be achieved with previously established modifications (e.g. aromatic group incorporation [110], direct drug conjugation [107], [109]), we sought to conjugate a moiety for which docetaxel would have a greater affinity. We looked at the binding site of docetaxel on β-tubulin, which has been well characterized using biochemical techniques such as photoaffinity labelling [13] and electron crystallography [14].

As described in Chapter 4, we incorporated a peptide sequence from the binding site of docetaxel on β-tubulin into our polymer backbone. The taxol binding peptide was synthesized by microwave peptide synthesis and modified with a maleimide, allowing conjugation to the thiolated backbone via a Michael addition. This orthogonal reaction was selected to prevent peptide self-oligomerization that could happen with the carbodiimide amide-carboxylic acid couplings used for previous backbone grafting. The conjugation proved to be facile (Scheme 4.3) and afforded polymers with a 1:1 molar ratio of backbone to peptide. Drug loading of 50 wt% relative to the backbone was achieved suggesting a specific interaction between the TBP and DTX. This loading is significantly higher than loadings achieved with less specific modifications, that range from 5 to 20 wt% [109], [225]. Interestingly, this is also significantly higher than many DTX conjugate systems, which are limited to 40 wt% [107], [270].

To validate the specificity of the taxol binding peptide, we also synthesized and quantified the loading of a scrambled peptide, which showed a more modest increase in loading due to hydrophobic interactions of around 20 wt%. Further characterizing the interaction was an analytical challenge. Techniques such as isothermal calorimetry require aqueous experimental conditions and high concentrations that cannot be achieved with DTX and the peptides. Techniques that use organic solvents, such as NMR, do not reflect the native environment within the micelle core and can cause conformational changes of the molecules [220], [221]. This work suggests the need for computer simulations or analytical techniques that can better characterize complex interactions within the micelle, in order to better understand their structure-activity relationship.

The assessment of drug release in physiologically relevant media is rare, but can provide crucial information about their in vivo behaviour [105], [155], [190]. The majority of release assays done in the literature use aqueous buffer conditions, which limits our understanding and can lead to confounding results in biological environments [41], [167], [271]. Specifically, the presence of proteins can lead to premature drug release due to a partitioning effect between the hydrophobic core of the micelle and the hydrophobic pockets of the proteins [85]. This effect is augmented in systems with high loading, where there is lower polymer content and thus increased protein adsorption [154], [167]. In our system, we are able to prevent protein adsorption using the heavily PEGylated brush structure discussed in Chapter 2 and combining it with the increased loading described in Chapter 4. We were able to validate that the increased loading in our system

was not at the cost of the kinetic serum stability by showing an equivalent DTX release profile to an unmodified polymer control. Thus, we have investigated the role of TBP modification on both drug loading and serum stability to ensure these properties will be translated effectively in the in vivo setting, described in the next section.

6.3 Increasing the therapeutic index of docetaxel

There are several nanoparticle formulations of small molecule drugs currently on the market for their improved tolerability over conventional surfactant based formulations. Although the initial excitement of nanoparticle drug delivery focused on the potential of improved efficacy due to specificity, this has not been translated into the clinic. Instead, nanoparticle strategies have proven beneficial for increasing the therapeutic index of these drugs. In fact, all of the clinical nanoparticles were given approval on the basis of improving the drug's toxicological profile in patients [38]. Notable successes include Abraxane [236] and Genexol-PM [272], nanoparticle formulations of paclitaxel; Marqibo [273], a liposomal formulation of vincristine; and Doxil [274], the benchmark liposomal formulation of doxorubicin. Significant research has led to clinical trials of several docetaxel nanoparticles trials including BIND-014 [275], however, there are currently no clinically approved docetaxel nano-formulations. The increased toxicity of docetaxel over paclitaxel provides a potential benefit for using a more tolerable formulation [276].

In Chapter 5, we investigated our novel NP DTX platform in an orthotopic mouse model of breast cancer. Our system had improved pharmacokinetics (increased half-life and area-under-the-curve) over free DTX comparable to previous observations [131], that were expected based on the low CMC, good kinetic stability and high PEG density of the formulation [190], [197]. Notably, the main side effects of DTX are neutropenia and thrombocytopenia [224], thus dramatic increases in plasma residence time may not be desirable. Instead, the modest improvements in serum half-life give way to increased tumour accumulation at all early time points. A parallel increase in non-target organs was not observed except for transient cases at early time points. More importantly, no changes in accumulation in the organs of the mononuclear phagocyte system were observed, suggesting that the PEG effectively prevented premature clearance. Similar to clinical formulations, the pharmacokinetic improvements did not translate to better efficacy, where dose-matched NP DTX showed similar tumour reduction and

survival to Free DTX. The main benefit of this system was the improved tolerability, with an increased maximum tolerated dose when DTX was delivered in our NP, allowing higher dosing regimens and increased survival (over 30%) compared to the maximum tolerated dose of Free DTX. The preclinical behaviour of our system is similar to what was seen with clinically approved formulations of other drugs, providing evidence for its potential applications moving forward.

6.4 Utility of active targeting ligands in nanoparticle drug delivery

Active drug targeting has received a great deal of research attention including a significant number of preclinical studies. In contrast to passive targeting, which is based on the passive extravasation of the tumour, active targeting incorporates ligands that are designed to bind to receptors overexpressed on the cancer cell surface. These targeting ligands range from small molecules to sugars to antibodies [277] and are used to increase particle cell uptake. Despite the research focus, very few actively targeted nanoparticles have reached clinical trials and none have been approved for clinical use [278]. Several explanations have emerged, however it is generally well accepted that the incorporation of ligands does not change the in vivo biodistribution nor the tumour accumulation [64], [245] and thus may not provide benefit for molecules that freely penetrate cell membranes [83], [242]-[244]. In fact, targeting ligands may be a hindrance to the therapeutic effect of the cargo if they prevent tumour penetration due to binding of receptors close to the surface of the tumour [41]. Importantly, active targeting may be advantageous for formulations that rely on cell uptake for efficacy such as CALAA-01, a cyclodextrin based nanoparticle delivering siRNA [279]. This particle requires cell internalization in order for the siRNA to be effective and shows substantial improvements with the incorporation of transferrin. Other hydrophilic therapeutics may also benefit from the inclusion of targeting ligands [246], [247]. Notwithstanding this surmounting evidence against the use of an active targeting strategy, we sought to verify the utility of a novel targeting ligand in our nanoparticle to see if trends observed hold true for systems with enhanced stability.

Antibodies have been beneficial as stand-alone therapies [21], [226] and conjugated in other systems, such as in the case of antibody-drug conjugates [280]. The efficacy relies on the mechanism of antibody dependent cell-mediated cytotoxicity [21], [59], which is not available in immunocompromised mouse models or without the Fc region. Coating nanoparticles with

antibodies can lead to premature clearance due to an enhanced immune response to the Fc region, therefore investigations in immune competent animals are crucial to establish accurate nanoparticle behaviour [226]. In order to investigate the effect of the antibody as a targeting ligand without concerns of premature clearance in future studies, we incorporated the fragment antigen binding (Fab) of a novel HER2 antibody, 73J. In vitro, Fab 73J-NP show improved cell uptake, suggesting a potential benefit in drug delivery to HER2+ cells [29]. However, in Chapter 5.4, we showed that Fab 73J had no impact on the efficacy of the NP DTX, showing similar tumour growth and survival to the untargeted formulation. This corroborated previous reports and suggests that active targeting is not beneficial for the delivery of DTX in nanoparticles. Further exploration on the use of conjugated antibodies should be geared towards the delivery of hydrophilic cargo, such as siRNA, or in combination therapies, such as a therapeutic antibody with the small molecule drug. In addition, studies in immunocompetent models would be important to analyze both the immune response to ligand coated particles, and the therapeutic benefit of certain targeting ligands (i.e. antibodies), whose mechanism of action relies on complement activation.

6.5 Conclusions

Over the course of this thesis, an efficacious nanoparticle drug delivery system was designed for increased stability and drug loading over conventional polymeric micelles. This validated the primary hypothesis that “chemically designed P(LA-co-TMCC)-g-PEG will self-assemble to form stable micelles and effectively deliver drug to tumours”. Using the carboxylic acid functionality and the unique graft architecture of our polymer system, the PEG density was tuned to improve the stability of the micelles through both lyophilization and in serum conditions. It was found that shifting the PEG density to greater than 1 PEG/backbone enabled lyophilization without the use of toxic excipients, such as Pluronics. The increasing PEG density also correlated with enhanced serum stability, shifting the half-life from around 24 h (for low PEG density systems) to greater than 72 h (for high PEG density systems). Importantly, this was not at the cost of drug loading and instead contributed to denser PEG brush architecture at the corona of the particle.

In order to increase the drug loading and thus the usability of our micelles therapeutically, we pursued two different strategies. For drugs that had self-assembling colloidal properties, such as

fulvestrant and PPD, we developed a novel method of stabilizing the colloidal core using polymers. We showed that the incorporation of polymers prevents aggregation of the colloids, and enhances the stability in serum by reducing adsorption of serum protein components, including globulin, albumin and fibrinogen. In contrast, for DTX, a drug that does not self-assemble into colloids and instead aggregates and precipitates out of solution, we presented a strategy to facilitate intermolecular interactions within the core in order to increase loading. A peptide from the binding site of docetaxel on the microtubule, termed taxol binding peptide, was conjugated to the polymer backbone using a maleimide-thiol Michael addition. Drug loading was found to be five times higher than unmodified polymeric micelles, and more than two times higher than less-specific conventional modifications. Release studies showed that the stability of the micelles was retained, with no release of DTX before 24 h in serum conditions. Collectively, these studies highlight that drug delivery vehicles are not a "one-size-fits-all" approach and rational design is necessary to formulate drugs stably for use in vivo.

Finally, we sought to test the efficacy of our NP DTX in a relevant orthotopic mouse model of breast cancer. We demonstrated that the NP DTX improved blood circulation and tumour distribution over the conventional surfactant-based Free DTX formulation. Importantly, we found that the more tolerable NP DTX formulation allowed higher dosing regimens over the Free DTX, which led to reduced tumour size and longer survival in the mice. These properties validated the P(LA-co-TMCC)-g-PEG, TBP as an alternative to surfactant-based formulations with improved tolerability in animals.

6.6 Achievement of objectives

This research was motivated by the following hypothesis:

Chemically designed P(LA-co-TMCC)-g-PEG will self-assemble to form stable nanoparticles with high drug loading and effectively deliver drug to tumours.

Herein, we describe chemical modifications to produce serum-stable P(LA-co-TMCC)-g-PEG micelles with high loading which effectively deliver drug to tumours. Achievement of the objectives originally laid out in Chapter 1 are summarized below:

1. To increase polymeric nanoparticle stability.

- P(LA-co-TMCC) was functionalized with between 0.5 to 6 PEG/backbone by controlling carbodiimide graft conditions.
- Increasing PEG density had no impact on the thermodynamic stability (CMC) or drug loading of micelles.
- Lyophilization studies revealed that polymers with greater than 1.5 PEG/backbone served as a self-cryoprotectant and enabled surfactant-free freeze drying and resuspension.
- Higher PEG densities increased serum stability of polymer micelles, increasing the half-life to over 72 h with 6 PEG/backbone.

These data were presented in Chapter 2 and published in *Chemistry of Materials*[197].

2. To encapsulate pentyl PABC-doxaz in a polymeric nanoparticle.
    - Fulvestrant and Pentyl PABC-Doxaz (PPD) were formulated as salt-stable colloids using UP80 and P(LA-co-TMCC)-g-PEG, respectfully.
    - PPD-P(LA-co-TMCC)-g-PEG colloids, with a loading of 50%, were monitored by the drug's absorbance at 280 nm, and were stable in serum for over 48 h.
    - The mechanism of serum stabilization was confirmed to be a reduction in protein adsorption, specifically albumin, globulin and fibrinogen, to the surface of particles.

These data were presented in Chapter 3 and have been submitted to *Molecular Pharmaceutics*.

3. To increase docetaxel loading in polymeric nanoparticles.
    - P(LA-co-TMCC)-g-PEG was functionalized with thiol moieties, which could be selectively reacted with maleimide-taxol binding peptide to form P_{TBP}.
    - P_{TBP} formed micelles with DTX loading five times higher than unmodified polymer, or 50 wt% relative to the backbone.
    - The specificity of the TBP modification was confirmed using a scrambled peptide control that showed only 20 wt% loading relative to the backbone.
    - P_{TBP} showed similar DTX release profiles to unmodified polymer in serum, with no significant drug release before 24 h.

- Cytotoxicity of DTX was maintained when delivered in P_{TBP} micelles, and polymers alone were cytocompatible.

These data were presented in Chapter 4 and published in *Chemical Communications*[190].

4. To assess the in vivo efficacy of DTX loaded Fab 73J conjugated-micelles in an orthotopic human xenograft tumour model in mice.
    - NP DTX increases the therapeutic index of DTX over the conventional ethanolic polysorbate 80 formulation, with a maximum tolerated dose 1.6-times higher.
    - Pharmacokinetic and biodistribution studies established improved blood circulation and tumour distribution of NP DTX over the Free DTX formulation.
    - The reduced toxicity of the NP DTX allowed higher dosing regimens in an orthotopic breast cancer mouse model, in which we showed better efficacy and survival than the Free DTX formulation.
    - The incorporation of an active targeting ligand, Fab 73J, did not impact the efficacy of the NP DTX, corroborating previous reports that targeting ligands provide no additional benefit for the delivery of hydrophobic small molecules.

These data were presented in Chapter 5 and submitted to *Biomaterials***.**

7 Recommendations for future work

In this thesis, polymeric nanoparticles were developed for the delivery of two different chemotherapeutics using a rational design strategy. Chemical modification of the polymer backbone enabled the production of polymeric nanoparticles that were serum stable, exhibited high drug loading, and were efficacious against an orthotopic breast cancer mouse model. Future work stemming from this thesis falls under three categories: tracking nanoparticles to better understand the biological fate of the polymeric micelle, expanding the system for the delivery of novel and combination therapeutics and using metastatic and more clinically relevant models of cancer to better predict translation of this system into patients.

7.1 Tracking nanoparticles

In Chapter 4, we compared the pharmacokinetics and biodistribution of NP DTX to Free DTX using a sensitive HPLC-MS/MS method that can quantify DTX down to nM levels [197]. While this method provides important information about the pharmacokinetics and biodistribution of the drug, it is not indicative of the elimination or the distribution of the polymer components, intact particles, or the DTX metabolites. Tracking the polymers and thus the particle, could provide a better an understanding of the micelle's biological fate, and allow correlations between the tumour morphology and the efficacy. Several established imaging and labelling techniques could be applied to our novel micelle formulation to provide a deeper understanding of the micelle's biological interactions. In vitro labelling of the micelle could inform particle design based on the micelle-cell interaction. In vivo micelle tracking would allow a more accurate measure of biodistribution over time [47], [281], [282] and establish the degradation and elimination of the polymer chains [283].

There are several methods to label the polymeric micelles for tracking both in vitro and in vivo. Conjugation of a fluorophore can be achieved by chemically modifying either the PEG end-group or modifying the backbone directly. Direct conjugation allows tracking of the polymer within the cell, which, in combination with other cell compartment staining, could reveal the particle's uptake mechanism and fate within the cell [284], [285]. This is of particular importance when delivering hydrophilic cargo, such as siRNA, where the mechanism of action requires penetrating membranes of the endo-lysosomal pathway [138]. In vivo, this strategy

could be used to evaluate the biodistribution of the particles overtime by investigating co-localization of the particles with fluorescently tagged tumours (e.g. GFP-overexpressing cancer cells) [286]. Whole body imaging [287] and intravital microscopy [288], [289] would allow for real time analysis of the circulation, adsorption and elimination of particles, enabling a better understanding of the biological fate of the particle and its accumulation at target sites, such as the solid tumour. Importantly, these techniques could also be used to investigate the morphology and vasculature of tumours to preselect patients that may benefit from nanoparticle treatments [238], [290] and to correlate response with degree of tumour penetration [289] .

An alternative method to direct conjugation of a fluorophore is encapsulation. Hydrophobic fluorophores, such as the FRET pair DiO and DiI, can be encapsulated within the core of the micelle to establish the in vivo stability overtime as disassembly of micelles will shift the emission profile of the cargo [291]. This would allow correlations between the in vitro assessments of micelle stability, such as those described in Chapters 2.3.10, 3.4.2 and 4.4.4, with the stability upon injection in vivo. In order to better understand the degradation and elimination of the P(LA-co-TMCC)-g-PEG, radio-labelled polymers (such as ^{14}C) can be used [283] in combination with an imaging technique like positron emission tomography (PET) [292]. This would clarify the mechanisms of elimination of the polymers and highlight potential organ toxicities associated with the materials, which are important for approval by governing agencies. Notably, in vivo assessments could be combined with mechanistic in vitro degradation studies using proton NMR and GPC [293], in order to establish the stability of polymers over long time periods, relevant to the storage of pharmaceuticals.

Together, the labelling and imaging techniques discussed in this section would clarify the biological fate of our novel polymeric micelle delivery system and provide mechanistic insight into the efficacy and pharmacokinetics that have been observed. These results can both guide the design of future iterations of the polymeric micelle to improve its targeting and present a personalized medicine approach, guiding the selection of patients who can benefit from nanoparticle drug delivery.

7.2 Delivery of novel and combination therapeutics

In Chapters 3 and 4, we demonstrated the optimization of our polymeric micelle system for the delivery of two chemotherapeutics, PPD and DTX, based on their innate physicochemical properties. There is substantial opportunity to use our novel polymeric micelle as a platform for the delivery of alternative small molecule therapeutics, owing to the heightened serum stability and simple functionalization of the polymer system. As previously stressed, nanoparticles have made significant progress in improving the tolerability and increasing the specificity of hydrophobic small molecules, which normally require harsh excipients for their solubilization [37], [213], [290]. This property could be extended beyond clinically established drugs and be used for compounds which, although highly potent, fall short in preclinical studies due to poor pharmacokinetics and narrow therapeutic indices [294]. These compounds have been used successfully in antibody-drug conjugates, in which toxicity as a monotherapy is circumvented with conjugation to an antibody. Specifically, the antibody enables discrimination between healthy and diseased tissues, reducing off-target effects that usually limit the use of potent cytotoxic agents. Examples of antibody-drug conjugates include Kadcyla (trastuzumab emtansine) and Adcetris (brentuximab vedontin), which are both clinically approved and well tolerated [295].

The majority of cancer patients are treated with combinations of chemotherapeutics that address multiple targets, providing the opportunity to design elegant drug delivery vehicles encapsulating more than one cargo. Our polymeric micelle platform could be adapted for the delivery of combination therapeutics, enabling dosing regimens and synergistic effects not possible with conventional surfactant systems. This strategy has been used in several nanoparticle formulations currently in clinical trials. VYXEOS (CPX-351, Celator), is a liposomal carrier which co-encapsulates two drugs, cytarabine and daunorubicin, at a fixed synergistic ratio for the treatment of high-risk acute myeloid leukemia. In a recent Phase III study, VYXEOS improved the survival in these patients by over 30% [296]. Alternative combination nanotherapies have been used to augment the effect of immunotherapy. Fahmy and colleagues recently developed a nanoscale polymeric particle, which co-encapsulated transforming growth factor beta and interleukin-2, in order to activate the innate and adaptive immune response and significantly increase the activity of natural killer and T-cells, improving survival and delaying tumour growth in a mouse model [297]. Both of these examples suggest the potential of combination therapies

for cancer therapy, providing the basis for the encapsulation of synergistic drug combinations in our polymeric micelle system.

Taking advantage of the chemical flexibility of our polymer, unique solutions (such as those discussed in Chapters 3 and 4) can be used to increase drug loading of a wide variety of hydrophobic drugs. These include modifying the polymer to facilitate intermolecular interactions with specific functional groups on the drug (such as aromatic groups [225], or hydrogen bond donors and acceptors [128]), conjugating the drug directly to the polymer [55], or using the polymer to stabilize colloidal aggregates of a drug itself [192]. To allow for serum stability and desired release kinetics, the PEG density of the system can be tuned using the chemistry established in Chapter 2. If targeting is beneficial, the delivery system can be expanded with the conjugation of a variety of ligands using bio-orthogonal click chemistry with terminal PEG end-groups [135]. To this end, our novel polymeric micelle system should be expanded for the delivery of numerous therapeutics.

7.3 Metastatic and predictive models of disease

In order to predict the efficacy of nanoparticles on human cancers, the majority of models use immunocompromised mouse strains bearing human tumour xenografts from single clonal cell lines[229]. While these models provide valuable insights, translation of nanoparticles to the clinic has been limited and results collected from mouse models are rarely validated in patients [40], [44]. The use of orthotopic models, such as the MDA-MB-231/H2N model employed in Chapter 5, better reflects the vascular capacity and metastatic potential of human cancers [61], [62], [227], improving upon the predictability of subcutaneous models in the back or flank of the animal [228]. Notwithstanding these improvements, cell-line derived tumour models show accelerated growth rates that reduce the neovascularization and blood vessel remodeling observed in human samples [298]. Moreover, single cell lines do not adequately recapitulate the complexity of treating human tumours with multiple cell types and varying phenotypes [299]. For example, recent evidence has suggested that cancer stem cells are responsible for the recurrence of aggressive forms of cancer such as glioblastoma [300]-[302]. Cell line xenograft models do not exhibit the recurrence of these cancers due to cancer stem cells, which is the main cause of mortality in patients [303].

Current efforts in the field on the establishment of a well-defined and predictive panel of animal models for cancer research are ongoing [278]. Using a mixed cell population from primary tumour biopsy provides a more clinically relevant response [304]. While these patient derived xenograft models better represent the broad molecular diversity of the disease, they still do not recapitulate the human cancer stroma or the growth rate of patient tumours [305]. Reliance on xenograft analyses has been slowly shifting with the development of genetic mouse models, balancing the needs for short latency and adequate modelling of human disease. Genetic spontaneous tumour models better mimic the biological evolution of human cancers and more accurately predict clinical outcomes [298], [306]. Importantly, genetic models allow the use of immune competent animal strains, providing a more predictive MPS response [307]. Although not perfect, a solid understanding of the human target can aid in the development of more accurate models that mimic tumour progression and response. In the future, accurate mouse models of human cancer could predict therapeutic resistance in advance of the clinical presentation, facilitating better response with therapeutics in the clinic [298], [308]. To this end, further evaluation of our novel docetaxel loaded NP system should be done in more relevant models of disease, such as genetic spontaneous models, which better predict translation into patients.

Appendix A: Abbreviations

ADCC	Antibody Dependent Cellular Cytotoxicity
CMC	Critical Micelle Concentration
DLS	Dynamic Light Scattering
DMF	Dimethylformamide
DTX	Docetaxel
EPR	Enhanced Permeability and Retention
Fab	Fragment, antibody binding region
Free DTX	Ethanolic polysorbate 80 formulation of docetaxel
FPLC	Fast Protein Liquid Chromatography
GPC	Gel Permeation Chromatography
HER2	Human Epidermal Growth Factor Receptor 2
HPLC-MS/MS	High Performance Liquid Chromatography coupled to Tandem Mass Spectrometry
IgG	Immunoglobulin G
IV	Intravenous
LA	Lactide
MPS	Mononuclear Phagocyte System
NMR	Nuclear Magnetic Resonance
NP	Nanoparticle

NP DTX	Nanoparticle containing encapsulated docetaxel
P(LA-co-TMCC)-g-PEG-furan	Poly (D,L-lactide –co- 2-methyl-2-carboxytrimethylene carbonate)-graft-poly(ethylene glycol)-furan
P_{TBP}	P(LA-co-TMCC)-g-PEG_3,TBP
P_{Bn}	P(LA-co-TMCC)-g-PEG_3,Bn
P_{DTX}	P(LA-co-TMCC)-g-PEG_3, DTX
P68	Pluronic® F68
PBS	Phosphate Buffered Saline
PDI	Polydispersity Index
PEG	Polyethylene Glycol
PK	Pharmacokinetics
PS80	Polysorbate (Tween) 80
SEC	Size Exclusion Chromatography
TMCC	2-methyl-2-carboxy trimethylene carbonate

Copyright Acknowledgements

Portions of Chapter 1 are reprinted with permission from Wiley from the following publication:

McLaughlin CK, Logie J and Shoichet, MS (2013) Core and corona modifications for the design of polymeric micelle drug-delivery systems. *Isreal Journal of Chemistry.* 53: 670-679.

Chapter 2 is reprinted with permission from American Chemical Society publications from the following publication:

Logie J, Owen SC, McLaughlin CK and Shoichet MS (2014) PEG-graft density controls polymeric nanoparticle micelle stability. *Chemistry of Materials.* 26: 2847-2855.

Chapter 4 is reprinted with permission from the Royal Society of Chemistry from the following publication:

Logie J, McLaughlin CK, Tam, RY and Shoichet MS (2015) Innovative use of the taxol binding peptide overcomes key challenges of stable and high drug loading in polymeric nanomicelles. *Chemical Communications*. 51: 12000-12003.

References

[1] V. P. Torchilin, “Drug targeting.,” *Eur J Pharm Sci*, vol. 11, pp. S81–91, Oct. 2000.

[2] D. N. Nguyen, J. J. Green, J. M. Chan, R. Langer, and D. G. Anderson, “Polymeric Materials for Gene Delivery and DNA Vaccination,” *Adv Mater*, vol. 21, no. 8, pp. 847–867, Feb. 2009.

[3] S. M. Moghimi, D. Peer, and R. Langer, “Reshaping the Future of Nanopharmaceuticals: Ad Iudicium,” *ACS Nano*, vol. 5, no. 11, pp. 8454–8458, Nov. 2011.

[4] K. E. Sapsford, W. R. Algar, L. Berti, K. B. Gemmill, B. J. Casey, E. Oh, M. H. Stewart, and I. L. Medintz, “Functionalizing Nanoparticles with Biological Molecules: Developing Chemistries that Facilitate Nanotechnology,” *Chem. Rev.*, vol. 113, no. 3, pp. 1904–2074, Mar. 2013.

[5] Statistics Canada, *Canadian Cancer Statistics 2012*. 2012.

[6] H. Gelderblom, J. Verweij, K. Nooter, and A. Sparreboom, “Cremophor EL,” *European Journal of Cancer*, vol. 37, no. 13, pp. 1590–1598, Sep. 2001.

[7] A. J. ten Tije, J. Verweij, W. J. Loos, and A. Sparreboom, “Pharmacological Effects of Formulation Vehicles,” *Clinical Pharmacokinetics*, vol. 42, no. 7, pp. 665–685, 2003.

[8] R. S. Herbst and F. R. Khuri, “Mode of action of docetaxel – a basis for combination with novel anticancer agents,” *Cancer Treatment Reviews*, vol. 29, no. 5, pp. 407–415, Oct. 2003.

[9] P. Zhao and D. Astruc, “Docetaxel Nanotechnology in Anticancer Therapy,” *ChemMedChem*, vol. 7, no. 6, pp. 952–972, Apr. 2012.

[10] B. Fulton and C. M. Spencer, “Docetaxel,” *Drugs*, vol. 51, no. 6, pp. 1075–1092, Jun. 1996.

[11] K. A. Lyseng-Williamson and C. Fenton, “Docetaxel,” *Drugs*, vol. 65, no. 17, pp. 2513–2531, 2005.

[12] N. J. Mackler and K. J. Pienta, “Drug Insight: use of docetaxel in prostate and urothelial cancers,” *Nat Clin Pract Urol*, vol. 2, no. 2, pp. 92–100, Feb. 2005.

[13] S. Rao, L. He, S. Chakravarty, I. Ojima, G. A. Orr, and S. B. Horwitz, “Characterization of the Taxol Binding Site on the Microtubule: Identification of Arg282 in tubulin as the site of photoincorporation of a 7-benzophenone analogue of taxol,” *Journal of Biological Chemistry*, vol. 274, no. 53, pp. 37990–37994, Dec. 1999.

[14] J. P. Snyder, J. H. Nettles, B. Cornett, K. H. Downing, and E. Nogales, “The binding conformation of Taxol in -tubulin: A model based on electron crystallographic density,” *Proc. Natl. Acad. Sci. U.S.A.*, vol. 98, no. 9, pp. 5312–5316, Apr. 2001.

[15] B. L. Barthel, Z. Zhang, D. L. Rudnicki, C. D. Coldren, M. Polinkovsky, H. Sun, G. G. Koch, D. C. F. Chan, and T. H. Koch, “Preclinical Efficacy of a Carboxylesterase 2-Activated

Prodrug of Doxazolidine," *J Med Chem*, vol. 52, no. 23, pp. 7678–7688, Dec. 2009.

[16] B. L. Barthel, R. C. Torres, J. L. Hyatt, C. C. Edwards, M. J. Hatfield, P. M. Potter, and T. H. Koch, "Identification of Human Intestinal Carboxylesterase as the Primary Enzyme for Activation of a Doxazolidine Carbamate Prodrug," *J Med Chem*, vol. 51, no. 2, pp. 298–304, Jan. 2008.

[17] B. T. Kalet, M. B. McBryde, J. M. Espinosa, and T. H. Koch, "Doxazolidine Induction of Apoptosis by a Topoisomerase II Independent Mechanism," *J Med Chem*, vol. 50, no. 18, pp. 4493–4500, Sep. 2007.

[18] P. J. Carter, "Potent antibody therapeutics by design," *Nat Rev Immunol*, vol. 6, no. 5, pp. 343–357, Apr. 2006.

[19] M. Colombo, F. Corsi, D. Foschi, E. Mazzantini, S. Mazzucchelli, C. Morasso, E. Occhipinti, L. Polito, D. Prosperi, S. Ronchi, and P. Verderio, "HER2 targeting as a two-sided strategy for breast cancer diagnosis and treatment: Outlook and recent implications in nanomedical approaches," *Pharmacological Research*, vol. 62, no. 2, pp. 150–165, Aug. 2010.

[20] P. Dinh, E. de Azambuja, F. Cardoso, and M. J. Piccart-Gebhart, "Facts and controversies in the use of trastuzumab in the adjuvant setting," *Nat Clin Prac Oncol*, vol. 5, no. 11, pp. 645–654, Sep. 2008.

[21] C. A. Hudis, "Trastuzumab — Mechanism of Action and Use in Clinical Practice," *N Engl J Med*, vol. 357, no. 1, pp. 39–51, Jul. 2007.

[22] I. E. Krop, M. Beeram, S. Modi, S. F. Jones, S. N. Holden, W. Yu, S. Girish, J. Tibbitts, J. H. Yi, M. X. Sliwkowski, F. Jacobson, S. G. Lutzker, and H. A. Burris, "Phase I Study of Trastuzumab-DM1, an HER2 Antibody-Drug Conjugate, Given Every 3 Weeks to Patients With HER2-Positive Metastatic Breast Cancer," *J. Clin. Oncol.*, vol. 28, no. 16, pp. 2698–2704, May 2010.

[23] H. A. Burris, H. S. Rugo, S. J. Vukelja, C. L. Vogel, R. A. Borson, S. Limentani, E. Tan-Chiu, I. E. Krop, R. A. Michaelson, S. Girish, L. Amler, M. Zheng, Y. W. Chu, B. Klencke, and J. A. O'Shaughnessy, "Phase II Study of the Antibody Drug Conjugate Trastuzumab-DM1 for the Treatment of Human Epidermal Growth Factor Receptor 2 (HER2) -Positive Breast Cancer After Prior HER2-Directed Therapy," *J. Clin. Oncol.*, vol. 29, no. 4, pp. 398–405, Jan. 2011.

[24] L. Amiri-Kordestani, G. M. Blumenthal, Q. C. Xu, L. Zhang, S. W. Tang, L. Ha, W. C. Weinberg, B. Chi, R. Candau-Chacon, P. Hughes, A. M. Russell, S. P. Miksinski, X. H. Chen, W. D. McGuinn, T. Palmby, S. J. Schrieber, Q. Liu, J. Wang, P. Song, N. Mehrotra, L. Skarupa, K. Clouse, A. Al-Hakim, R. Sridhara, A. Ibrahim, R. Justice, R. Pazdur, and P. Cortazar, "FDA Approval: Ado-Trastuzumab Emtansine for the Treatment of Patients with HER2-Positive Metastatic Breast Cancer," *Clin. Cancer Res.*, vol. 20, no. 17, pp. 4436–4441, Sep. 2014.

[25] G. Valabrega, F. Montemurro, and M. Aglietta, "Trastuzumab: mechanism of action, resistance and future perspectives in HER2-overexpressing breast cancer," *Annals of Oncology*, vol. 18, no. 6, pp. 977–984, Apr. 2007.

[26] J. Albanell, J. Codony, A. Rovira, B. Mellado, and P. Gascón, "Mechanism of Action

of Anti-Her2 Monoclonal Antibodies: Scientific Update on Trastuzumab and 2c4," in *New Trends in Cancer for the 21stCentury*, vol. 532, no. 21, Boston, MA: Springer US, 2003, pp. 253–268.

[27] S. Cooley, L. J. Burns, T. Repka, and J. S. Miller, "Natural killer cell cytotoxicity of breast cancer targets is enhanced by two distinct mechanisms of antibody-dependent cellular cytotoxicity against LFA-3 and HER2/neu," *Experimental Hematology*, vol. 27, no. 10, pp. 1533–1541, Oct. 1999.

[28] G. Hudelist, W. J. Köstler, J. Attems, K. Czerwenka, R. Müller, M. Manavi, G. G. Steger, E. Kubista, C. C. Zielinski, and C. F. Singer, "Her-2/neu-triggered intracellular tyrosine kinase activation: in vivo relevance of ligand-independent activation mechanisms and impact upon the efficacy of trastuzumab-based treatment," *Br J Cancer*, vol. 89, no. 6, pp. 983–991, Sep. 2003.

[29] S. C. Owen, N. Patel, J. Logie, G. Pan, H. Persson, J. Moffat, S. S. Sidhu, and M. S. Shoichet, "Targeting HER2+ breast cancer cells: Lysosomal accumulation of anti-HER2 antibodies is influenced by antibody binding site and conjugation to polymeric nanoparticles," *Journal of Controlled Release*, vol. 172, no. 2, pp. 395–404, Dec. 2013.

[30] L. Zhang, F. X. Gu, J. M. Chan, A. Z. Wang, R. S. Langer, and O. C. Farokhzad, "Nanoparticles in Medicine: Therapeutic Applications and Developments," *Clinical Pharmacology & Therapeutics*, vol. 83, no. 5, pp. 761–769, Oct. 2007.

[31] P. Kocbek, N. Obermajer, M. Cegnar, J. Kos, and J. Kristl, "Targeting cancer cells using PLGA nanoparticles surface modified with monoclonal antibody," *Journal of Controlled Release*, vol. 120, no. 1, pp. 18–26, Jul. 2007.

[32] S. Kumar, J. Aaron, and K. Sokolov, "Directional conjugation of antibodies to nanoparticles for synthesis of multiplexed optical contrast agents with both delivery and targeting moieties," *Nat Protoc*, vol. 3, no. 2, pp. 314–320, Feb. 2008.

[33] N. Dinauer, S. Balthasar, C. Weber, J. Kreuter, K. Langer, and H. von Briesen, "Selective targeting of antibody-conjugated nanoparticles to leukemic cells and primary T-lymphocytes," *Biomaterials*, vol. 26, no. 29, pp. 5898–5906, Oct. 2005.

[34] H. Maeda, L. W. Seymour, and Y. Miyamoto, "Conjugates of anticancer agents and polymers: advantages of macromolecular therapeutics in vivo," *Bioconjugate Chem*, vol. 3, no. 5, pp. 351–362, Sep. 1992.

[35] S. Mitra, U. Gaur, P. C. Ghosh, and A. N. Maitra, "Tumour targeted delivery of encapsulated dextran–doxorubicin conjugate using chitosan nanoparticles as carrier," *Journal of Controlled Release*, vol. 74, no. 1, pp. 317–323, Jul. 2001.

[36] H. Maeda, J. Wu, T. Sawa, Y. Matsumura, and K. Hori, "Tumor vascular permeability and the EPR effect in macromolecular therapeutics: a review," *Journal of Controlled Release*, vol. 65, no. 1, pp. 271–284, Mar. 2000.

[37] A. Z. Wang, R. Langer, and O. C. Farokhzad, "Nanoparticle Delivery of Cancer Drugs," *Annu. Rev. Med.*, vol. 63, no. 1, pp. 185–198, Feb. 2012.

[38] A. Wicki, D. Witzigmann, V. Balasubramanian, and J. Huwyler, “Nanomedicine in cancer therapy: Challenges, opportunities, and clinical applications,” *Journal of Controlled Release*, vol. 200, pp. 138–157, Feb. 2015.

[39] K. Cho, X. Wang, S. Nie, Z. Chen, and D. M. Shin, “Therapeutic Nanoparticles for Drug Delivery in Cancer,” *Clin. Cancer Res.*, vol. 14, no. 5, pp. 1310–1316, Mar. 2008.

[40] J. W. Nichols and Y. H. Bae, “EPR: Evidence and fallacy,” *Journal of Controlled Release*, vol. 190, pp. 451–464, Sep. 2014.

[41] S. Eetezadi, S. N. Ekdawi, and C. Allen, “The challenges facing block copolymer micelles for cancer therapy: In vivo barriers and clinical translation,” *Adv Drug Deliver Rev*, vol. 91, pp. 7–22, Aug. 2015.

[42] S. N. Ekdawi, D. A. Jaffray, and C. Allen, “Nanomedicine and tumor heterogeneity: Concept and complex reality,” *Nano Today*, vol. 11, no. 4, pp. 402–414, Aug. 2016.

[43] K. Park, “Facing the Truth about Nanotechnology in Drug Delivery,” *ACS Nano*, vol. 7, no. 9, pp. 7442–7447, Sep. 2013.

[44] G. H. Petersen, S. K. Alzghari, W. Chee, S. S. Sankari, and N. M. La-Beck, “Meta-analysis of clinical and preclinical studies comparing the anticancer efficacy of liposomal versus conventional non-liposomal doxorubicin,” *Journal of Controlled Release*, vol. 232, pp. 255–264, Jun. 2016.

[45] L. NIPPON KAYAKU Co, “Results of Phase III study of NK105, a novel macromolecular micelle encapsulating an anticancer drug.” Tokyo. Jul. 2016.

[46] M. R. Kano, Y. Bae, C. Iwata, Y. Morishita, M. Yashiro, M. Oka, T. Fujii, A. Komuro, K. Kiyono, M. Kaminishi, K. Hirakawa, Y. Ouchi, N. Nishiyama, K. Kataoka, and K. Miyazono, “Improvement of cancer-targeting therapy, using nanocarriers for intractable solid tumors by inhibition of TGF-beta signaling,” *Proc. Natl. Acad. Sci. U.S.A.*, vol. 104, no. 9, pp. 3460–3465, Feb. 2007.

[47] H. Cabral, Y. Matsumoto, K. Mizuno, Q. Chen, M. Murakami, M. Kimura, Y. Terada, M. R. Kano, K. Miyazono, M. Uesaka, N. Nishiyama, and K. Kataoka, “Accumulation of sub-100 nm polymeric micelles in poorly permeable tumours depends on size,” *Nat Nanotechnol*, vol. 6, no. 12, pp. 815–823, Oct. 2011.

[48] L. Eikenes, M. Tari, I. Tufto, Ø. S. Bruland, and C. de Lange Davies, “Hyaluronidase induces a transcapillary pressure gradient and improves the distribution and uptake of liposomal doxorubicin (Caelyx™) in human osteosarcoma xenografts,” *Br J Cancer*, vol. 93, no. 1, pp. 81–88, Jun. 2005.

[49] S. Wilhelm, A. J. Tavares, Q. Dai, S. Ohta, J. Audet, H. F. Dvorak, and W. C. W. Chan, “Analysis of nanoparticle delivery to tumours,” *Nature Publishing Group*, vol. 1, no. 5, p. 16014, Apr. 2016.

[50] E. Blanco, H. Shen, and M. Ferrari, “Principles of nanoparticle design for overcoming biological barriers to drug delivery,” *Nat Biotechnol*, vol. 33, no. 9, pp. 941–951, Sep. 2015.

[51] K. S. Ho and M. S. Shoichet, “Design considerations of polymeric nanoparticle micelles for chemotherapeutic delivery,” *Current Opinion in Chemical Engineering*, vol. 2, no. 1, pp. 53–59, Feb. 2013.

[52] M. Elsabahy and K. L. Wooley, “Design of polymeric nanoparticles for biomedical delivery applications,” *Chem Soc Rev*, vol. 41, no. 7, p. 2545, 2012.

[53] N. K. Mehra, V. Mishra, and N. K. Jain, “Receptor-based targeting of therapeutics,” *Therapeutic Delivery*, vol. 4, no. 3, pp. 369–394, Mar. 2013.

[54] D. Peer, J. M. Karp, S. Hong, O. C. Farokhzad, R. Margalit, and R. Langer, “Nanocarriers as an emerging platform for cancer therapy,” *Nat Nanotechnol*, vol. 2, no. 12, pp. 751–760, Dec. 2007.

[55] M. Shi, K. Ho, A. Keating, and M. S. Shoichet, “Doxorubicin-Conjugated Immuno-Nanoparticles for Intracellular Anticancer Drug Delivery,” *Adv. Funct. Mater.*, vol. 19, no. 11, pp. 1689–1696, Jun. 2009.

[56] S. Inoue, H. Ding, J. Portilla-Arias, J. Hu, B. Konda, M. Fujita, A. Espinoza, S. Suhane, M. Riley, M. Gates, R. Patil, M. L. Penichet, A. V. Ljubimov, K. L. Black, E. Holler, and J. Y. Ljubimova, “Polymalic Acid-Based Nanobiopolymer Provides Efficient Systemic Breast Cancer Treatment by Inhibiting both HER2/neu Receptor Synthesis and Activity,” *Cancer Research*, vol. 71, no. 4, pp. 1454–1464, Feb. 2011.

[57] S. C. Abeylath, S. Ganta, A. K. Iyer, and M. Amiji, “Combinatorial-Designed Multifunctional Polymeric Nanosystems for Tumor-Targeted Therapeutic Delivery,” *Accounts Chem Res*, vol. 44, no. 10, pp. 1009–1017, Oct. 2011.

[58] A. Accardo, D. Tesauro, and G. Morelli, “Peptide-based targeting strategies for simultaneous imaging and therapy with nanovectors,” *Polym J*, vol. 45, no. 5, pp. 481–493, Feb. 2013.

[59] R. Nahta and F. J. Esteva, “Herceptin: mechanisms of action and resistance,” *Cancer Letters*, vol. 232, no. 2, pp. 123–138, Feb. 2006.

[60] S. Miura, H. Suzuki, and Y. H. Bae, “A multilayered cell culture model for transport study in solid tumors: Evaluation of tissue penetration of polyethyleneimine based cationic micelles,” *Nano Today*, vol. 9, no. 6, pp. 695–704, Dec. 2014.

[61] J. J. Killion, R. Radinsky, and I. J. Fidler, *Cancer and Metastasis Reviews*, vol. 17, no. 3, pp. 279–284, 1998.

[62] M. C. Bibby, “Orthotopic models of cancer for preclinical drug evaluation,” *European Journal of Cancer*, vol. 40, no. 6, pp. 852–857, Apr. 2004.

[63] M. Lacroix and G. Leclercq, “Relevance of Breast Cancer Cell Lines as Models for Breast Tumours: An Update,” *Breast Cancer Res Treat*, vol. 83, no. 3, pp. 249–289, Feb. 2004.

[64] N. Kamaly, Z. Xiao, P. M. Valencia, A. F. Radovic-Moreno, and O. C. Farokhzad, “Targeted polymeric therapeutic nanoparticles: design, development and clinical translation,” *Chem Soc Rev*, vol. 41, no. 7, p. 2971, 2012.

[65] J. Nicolas, S. Mura, D. Brambilla, N. Mackiewicz, and P. Couvreur, “Design, functionalization strategies and biomedical applications of targeted biodegradable/biocompatible polymer-based nanocarriers for drug delivery,” *Chem Soc Rev*, vol. 42, no. 3, pp. 1147–1235, 2013.

[66] C. Allen, D. Maysinger, and A. Eisenberg, “Nano-engineering block copolymer aggregates for drug delivery,” *Colloids and Surfaces B: Biointerfaces*, vol. 16, no. 1, pp. 3–27, Nov. 1999.

[67] J. Du and R. K. O'Reilly, “Advances and challenges in smart and functional polymer vesicles,” *Soft Matter*, vol. 5, no. 19, p. 3544, 2009.

[68] R. K. Iha, K. L. Wooley, A. M. Nyström, D. J. Burke, M. J. Kade, and C. J. Hawker, “Applications of Orthogonal ‘Click’ Chemistries in the Synthesis of Functional Soft Materials,” *Chem. Rev.*, vol. 109, no. 11, pp. 5620–5686, Nov. 2009.

[69] S. C. Owen, D. P. Y. Chan, and M. S. Shoichet, “Polymeric micelle stability,” *Nano Today*, vol. 7, no. 1, pp. 53–65, Feb. 2012.

[70] B. Yu, H. C. Tai, W. Xue, L. J. Lee, and R. J. Lee, “Receptor-targeted nanocarriers for therapeutic delivery to cancer,” *Molecular Membrane Biology*, vol. 27, no. 7, pp. 286–298, Oct. 2010.

[71] Z. Xiao and O. C. Farokhzad, “Aptamer-Functionalized Nanoparticles for Medical Applications: Challenges and Opportunities,” *ACS Nano*, vol. 6, no. 5, pp. 3670–3676, May 2012.

[72] V. P. Torchilin, “Multifunctional nanocarriers,” *Adv Drug Deliver Rev*, vol. 64, pp. 302–315, Dec. 2012.

[73] F. M. Veronese and G. Pasut, “PEGylation, successful approach to drug delivery,” *Drug Discovery Today*, vol. 10, no. 21, pp. 1451–1458, Nov. 2005.

[74] M. Elsabahy, M. Dufresne, and J. Leroux, “Polymeric Micelles as Versatile Carriers for Drugs and Nucleic Acids Delivery,” in *Handbook of materials for nanomedicine*, no. 4, 2011.

[75] V. Kumar and R. K. Prud'homme, “Thermodynamic limits on drug loading in nanoparticle cores,” *J Pharm Sci-Us*, vol. 97, no. 11, pp. 4904–4914, Nov. 2008.

[76] J. Liu, Y. Xiao, and C. Allen, “Polymer–drug compatibility: A guide to the development of delivery systems for the anticancer agent, ellipticine,” *J Pharm Sci-Us*, vol. 93, no. 1, pp. 132–143, Jan. 2004.

[77] C. D. Walkey, J. B. Olsen, H. Guo, A. Emili, and W. C. W. Chan, “Nanoparticle Size and Surface Chemistry Determine Serum Protein Adsorption and Macrophage Uptake,” *J Am Chem Soc*, vol. 134, no. 4, pp. 2139–2147, Feb. 2012.

[78] A. L. Klibanov, K. Maruyama, V. P. Torchilin, and L. Huang, “Amphipathic polyethyleneglycols effectively prolong the circulation time of liposomes,” *FEBS Letters*, vol. 268, no. 1, pp. 235–237, Oct. 2001.

[79] R. Gref, M. Lück, P. Quellec, M. Marchand, E. Dellacherie, S. Harnisch, T. Blunk, and

R. H. Müller, "'Stealth' corona-core nanoparticles surface modified by polyethylene glycol (PEG): influences of the corona (PEG chain length and surface density) and of the core composition on phagocytic uptake and plasma protein adsorption," *Colloids and Surfaces B: Biointerfaces*, vol. 18, no. 3, pp. 301–313, Oct. 2000.

[80] C. D. Walkey, J. B. Olsen, F. Song, R. Liu, H. Guo, D. W. H. Olsen, Y. Cohen, A. Emili, and W. C. W. Chan, "Protein Corona Fingerprinting Predicts the Cellular Interaction of Gold and Silver Nanoparticles," *ACS Nano*, vol. 8, no. 3, pp. 2439–2455, Mar. 2014.

[81] Q. Xu, L. M. Ensign, N. J. Boylan, A. Schön, X. Gong, J.-C. Yang, N. W. Lamb, S. Cai, T. Yu, E. Freire, and J. Hanes, "Impact of Surface Polyethylene Glycol (PEG) Density on Biodegradable Nanoparticle Transport in Mucus ex Vivoand Distribution in Vivo," *ACS Nano*, vol. 9, no. 9, pp. 9217–9227, Sep. 2015.

[82] E. A. Nance, G. F. Woodworth, K. A. Sailor, T. Y. Shih, Q. Xu, G. Swaminathan, D. Xiang, C. Eberhart, and J. Hanes, "A Dense Poly(Ethylene Glycol) Coating Improves Penetration of Large Polymeric Nanoparticles Within Brain Tissue," *Science Translational Medicine*, vol. 4, no. 149, pp. 149ra119–149ra119, Aug. 2012.

[83] H. Lee, H. Fonge, B. Hoang, R. M. Reilly, and C. Allen, "The Effects of Particle Size and Molecular Targeting on the Intratumoral and Subcellular Distribution of Polymeric Nanoparticles," *Mol Pharmaceut*, vol. 7, no. 4, pp. 1195–1208, Aug. 2010.

[84] J. Wang, W. Mao, L. L. Lock, J. Tang, M. Sui, W. Sun, H. Cui, D. Xu, and Y. Shen, "The Role of Micelle Size in Tumor Accumulation, Penetration, and Treatment," *ACS Nano*, vol. 9, no. 7, pp. 7195–7206, Jul. 2015.

[85] J. Liu, F. Zeng, and C. Allen, "Influence of serum protein on polycarbonate-based copolymer micelles as a delivery system for a hydrophobic anti-cancer agent," *Journal of Controlled Release*, vol. 103, no. 2, pp. 481–497, Mar. 2005.

[86] M. Shi, J. Lu, and M. S. Shoichet, "Organic nanoscale drug carriers coupled with ligands for targeted drug delivery in cancer," *J. Mater. Chem.*, vol. 19, no. 31, p. 5485, 2009.

[87] W. R. Algar, D. E. Prasuhn, M. H. Stewart, T. L. Jennings, J. B. Blanco-Canosa, P. E. Dawson, and I. L. Medintz, "The Controlled Display of Biomolecules on Nanoparticles: A Challenge Suited to Bioorthogonal Chemistry," *Bioconjugate Chem*, vol. 22, no. 5, pp. 825–858, May 2011.

[88] H. C. Kolb, M. G. Finn, and K. B. Sharpless, "Click Chemistry: Diverse Chemical Function from a Few Good Reactions," *Angew Chem Int Ed Engl*, vol. 40, no. 11, pp. 2004–2021, Jun. 2001.

[89] C. E. Hoyle, A. B. Lowe, and C. N. Bowman, "Thiol-click chemistry: a multifaceted toolbox for small molecule and polymer synthesis," *Chem Soc Rev*, vol. 39, no. 4, p. 1355, 2010.

[90] N. Li and W. H. Binder, "Click-chemistry for nanoparticle-modification," *J. Mater. Chem.*, vol. 21, no. 42, p. 16717, 2011.

[91] E. Lallana, A. Sousa-Herves, F. Fernandez-Trillo, R. Riguera, and E. Fernandez-Megia, "Click Chemistry for Drug Delivery Nanosystems," *Pharm Res*, vol. 29, no. 1, pp. 1–34,

Sep. 2011.

[92] G. K. Such, A. P. R. Johnston, K. Liang, and F. Caruso, “Synthesis and functionalization of nanoengineered materials using click chemistry,” *Prog Polym Sci*, vol. 37, no. 7, pp. 985–1003, Jul. 2012.

[93] P. Ostrovskis, C. M R Volla, M. Turks, and D. Markovic, “Application of Metal Free Click Chemistry in Biological Studies,” *COC*, vol. 17, no. 6, pp. 610–640, Apr. 2013.

[94] M. A. Tasdelen, “Diels–Alder ‘click’ reactions: recent applications in polymer and material science,” *Polym. Chem.*, vol. 2, no. 10, p. 2133, 2011.

[95] A. Gandini, “The furan/maleimide Diels–Alder reaction: A versatile click–unclick tool in macromolecular synthesis,” *Prog Polym Sci*, vol. 38, no. 1, pp. 1–29, Jan. 2013.

[96] M. Shi, J. H. Wosnick, K. Ho, A. Keating, and M. S. Shoichet, “Immuno-Polymeric Nanoparticles by Diels–Alder Chemistry,” *Angew. Chem. Int. Ed.*, vol. 46, no. 32, pp. 6126–6131, Aug. 2007.

[97] D. P. Nair, M. Podgórski, S. Chatani, T. Gong, W. Xi, C. R. Fenoli, and C. N. Bowman, “The Thiol-Michael Addition Click Reaction: A Powerful and Widely Used Tool in Materials Chemistry,” *Chem. Mater.*, vol. 26, no. 1, pp. 724–744, Jan. 2014.

[98] S. D. Fontaine, R. Reid, L. Robinson, G. W. Ashley, and D. V. Santi, “Long-Term Stabilization of Maleimide–Thiol Conjugates,” *Bioconjugate Chem*, vol. 26, no. 1, pp. 145–152, Jan. 2015.

[99] R. A. Petros and J. M. DeSimone, “Strategies in the design of nanoparticles for therapeutic applications,” *Nat Rev Drug Discov*, vol. 9, no. 8, pp. 615–627, Jul. 2010.

[100] Z. L. Tyrrell, Y. Shen, and M. Radosz, “Fabrication of micellar nanoparticles for drug delivery through the self-assembly of block copolymers,” *Prog Polym Sci*, vol. 35, no. 9, pp. 1128–1143, Sep. 2010.

[101] M. G. Carstens, C. J. F. Rijcken, C. F. van Nostrum, and W. E. Hennink, “Pharmaceutical Micelles: Combining Longevity, Stability, and Stimuli Sensitivity,” in *Multifunctional Pharmaceutical Nanocarriers*, vol. 4, no. 9, New York, NY: Springer New York, 2008, pp. 263–308.

[102] D. Sutton, S. Wang, N. Nasongkla, J. Gao, and E. E. Dormidontova, “Doxorubicin and -Lapachone Release and Interaction with Micellar Core Materials: Experiment and Modeling,” *Experimental Biology and Medicine*, vol. 232, no. 8, pp. 1090–1099, Sep. 2007.

[103] X. Yang, B. Zhu, T. Dong, P. Pan, X. Shuai, and Y. Inoue, “Interactions between an Anticancer Drug and Polymeric Micelles Based on Biodegradable Polyesters,” *Macromol Biosci*, vol. 8, no. 12, pp. 1116–1125, Dec. 2008.

[104] A. L. Z. Lee, S. Venkataraman, S. B. M. Sirat, S. Gao, J. L. Hedrick, and Y. Y. Yang, “The use of cholesterol-containing biodegradable block copolymers to exploit hydrophobic interactions for the delivery of anticancer drugs,” *Biomaterials*, vol. 33, no. 6, pp. 1921–1928, Feb. 2012.

[105] X. Zhao, Z. Poon, A. C. Engler, D. K. Bonner, and P. T. Hammond, "Enhanced Stability of Polymeric Micelles Based on Postfunctionalized Poly(ethylene glycol)- b-poly(γ-propargyl l-glutamate): The Substituent Effect," *Biomacromolecules*, vol. 13, no. 5, pp. 1315–1322, May 2012.

[106] T. Nakanishi, S. Fukushima, K. Okamoto, M. Suzuki, Y. Matsumura, M. Yokoyama, T. Okano, Y. Sakurai, and K. Kataoka, "Development of the polymer micelle carrier system for doxorubicin," *Journal of Controlled Release*, vol. 74, no. 1, pp. 295–302, Jul. 2001.

[107] J. Liu, P. Zahedi, F. Zeng, and C. Allen, "Nano-Sized Assemblies of a PEG-Docetaxel Conjugate as a Formulation Strategy for Docetaxel," *J Pharm Sci-Us*, vol. 97, no. 8, pp. 3274–3290, Aug. 2008.

[108] A. S. Mikhail and C. Allen, "Poly(ethylene glycol)- b-poly(ε-caprolactone) Micelles Containing Chemically Conjugated and Physically Entrapped Docetaxel: Synthesis, Characterization, and the Influence of the Drug on Micelle Morphology," *Biomacromolecules*, vol. 11, no. 5, pp. 1273–1280, May 2010.

[109] M. Shahin and A. Lavasanifar, "Novel self-associating poly(ethylene oxide)-b-poly(ε-caprolactone) based drug conjugates and nano-containers for paclitaxel delivery," *International Journal of Pharmaceutics*, vol. 389, no. 1, pp. 213–222, Apr. 2010.

[110] Y. Shi, M. J. van Steenbergen, E. A. Teunissen, L. Novo, S. Gradmann, M. Baldus, C. F. van Nostrum, and W. E. Hennink, "Π–Π Stacking Increases the Stability and Loading Capacity of Thermosensitive Polymeric Micelles for Chemotherapeutic Drugs," *Biomacromolecules*, vol. 14, no. 6, pp. 1826–1837, Jun. 2013.

[111] T. Ishida, X. Wang, T. Shimizu, K. Nawata, and H. Kiwada, "PEGylated liposomes elicit an anti-PEG IgM response in a T cell-independent manner," *Journal of Controlled Release*, vol. 122, no. 3, pp. 349–355, Oct. 2007.

[112] S. C. Owen, A. K. Doak, P. Wassam, M. S. Shoichet, and B. K. Shoichet, "Colloidal Aggregation Affects the Efficacy of Anticancer Drugs in Cell Culture," *Acs Chem Biol*, vol. 7, no. 8, pp. 1429–1435, Aug. 2012.

[113] S. C. Owen, A. K. Doak, A. N. Ganesh, L. Nedyalkova, C. K. McLaughlin, B. K. Shoichet, and M. S. Shoichet, "Colloidal Drug Formulations Can Explain 'Bell-Shaped' Concentration–Response Curves," *Acs Chem Biol*, vol. 9, no. 3, pp. 777–784, Mar. 2014.

[114] K. E. D. Coan, D. A. Maltby, A. L. Burlingame, and B. K. Shoichet, "Promiscuous Aggregate-Based Inhibitors Promote Enzyme Unfolding," *J Med Chem*, vol. 52, no. 7, pp. 2067–2075, Apr. 2009.

[115] K. E. D. Coan and B. K. Shoichet, "Stoichiometry and Physical Chemistry of Promiscuous Aggregate-Based Inhibitors," *J Am Chem Soc*, vol. 130, no. 29, pp. 9606–9612, Jul. 2008.

[116] G. A. Ilevbare and L. S. Taylor, "Liquid–Liquid Phase Separation in Highly Supersaturated Aqueous Solutions of Poorly Water-Soluble Drugs: Implications for Solubility Enhancing Formulations," *Crystal Growth & Design*, vol. 13, no. 4, pp. 1497–1509, Apr. 2013.

[117] S. L. McGovern, E. Caselli, N. Grigorieff, and B. K. Shoichet, “A Common Mechanism Underlying Promiscuous Inhibitors from Virtual and High-Throughput Screening,” *J Med Chem*, vol. 45, no. 8, pp. 1712–1722, Apr. 2002.

[118] S. L. McGovern, B. T. Helfand, B. Feng, and B. K. Shoichet, “A Specific Mechanism of Nonspecific Inhibition,” *J Med Chem*, vol. 46, no. 20, pp. 4265–4272, Sep. 2003.

[119] S. Harrisson, J. Nicolas, A. Maksimenko, D. T. Bui, J. Mougin, and P. Couvreur, “Nanoparticles with In Vivo Anticancer Activity from Polymer Prodrug Amphiphiles Prepared by Living Radical Polymerization,” *Angew. Chem. Int. Ed.*, vol. 52, no. 6, pp. 1678–1682, Dec. 2012.

[120] G. A. Ilevbare, H. Liu, J. Pereira, K. J. Edgar, and L. S. Taylor, “Influence of Additives on the Properties of Nanodroplets Formed in Highly Supersaturated Aqueous Solutions of Ritonavir,” *Mol Pharmaceut*, vol. 10, no. 9, pp. 3392–3403, Sep. 2013.

[121] C. K. McLaughlin, D. Duan, A. N. Ganesh, H. Torosyan, B. K. Shoichet, and M. S. Shoichet, “Stable Colloidal Drug Aggregates Catch and Release Active Enzymes,” *Acs Chem Biol*, vol. 11, no. 4, pp. 992–1000, Apr. 2016.

[122] A. Maksimenko, F. Dosio, J. Mougin, A. Ferrero, S. Wack, L. H. Reddy, A. A. Weyn, E. Lepeltier, C. Bourgaux, B. Stella, L. Cattel, and P. Couvreur, “A unique squalenoylated and nonpegylated doxorubicin nanomedicine with systemic long-circulating properties and anticancer activity,” *Proc. Natl. Acad. Sci. U.S.A.*, vol. 111, no. 2, pp. E217–E226, Jan. 2014.

[123] P. Huang, D. Wang, Y. Su, W. Huang, Y. Zhou, D. Cui, X. Zhu, and D. Yan, “Combination of Small Molecule Prodrug and Nanodrug Delivery: Amphiphilic Drug–Drug Conjugate for Cancer Therapy,” *J Am Chem Soc*, vol. 136, no. 33, pp. 11748–11756, Aug. 2014.

[124] E.-J. Cha, J. E. Kim, and C.-H. Ahn, “Stabilized polymeric micelles by electrostatic interactions for drug delivery system,” *European Journal of Pharmaceutical Sciences*, vol. 38, no. 4, pp. 341–346, Nov. 2009.

[125] C. Giacomelli, V. Schmidt, and R. Borsali, “Specific Interactions Improve the Loading Capacity of Block Copolymer Micelles in Aqueous Media,” *Langmuir*, vol. 23, no. 13, pp. 6947–6955, Jun. 2007.

[126] C. Yang, J. P. K. Tan, W. Cheng, A. B. E. Attia, C. T. Y. Ting, A. Nelson, J. L. Hedrick, and Y. Y. Yang, “Supramolecular nanostructures designed for high cargo loading capacity and kinetic stability,” *Nano Today*, vol. 5, no. 6, pp. 515–523, Dec. 2010.

[127] A. B. Ebrahim Attia, Z. Y. Ong, J. L. Hedrick, P. P. Lee, P. L. R. Ee, P. T. Hammond, and Y. Y. Yang, “Mixed micelles self-assembled from block copolymers for drug delivery,” *Current Opinion in Colloid & Interface Science*, vol. 16, no. 3, pp. 182–194, Jun. 2011.

[128] C. Yang, A. B. Ebrahim Attia, J. P. K. Tan, X. Ke, S. Gao, J. L. Hedrick, and Y. Y. Yang, “The role of non-covalent interactions in anticancer drug loading and kinetic stability of polymeric micelles,” *Biomaterials*, vol. 33, no. 10, pp. 2971–2979, Apr. 2012.

[129] S. K. Patel, A. Lavasanifar, and P. Choi, “Molecular dynamics study of the encapsulation capability of a PCL–PEO based block copolymer for hydrophobic drugs with

different spatial distributions of hydrogen bond donors and acceptors," *Biomaterials*, vol. 31, no. 7, pp. 1780–1786, Mar. 2010.

[130] J. C. Middleton and A. J. Tipton, "Synthetic biodegradable polymers as orthopedic devices," *Biomaterials*, vol. 21, no. 23, pp. 2335–2346, Dec. 2000.

[131] K. S. Ho, A. M. Aman, R. S. Al-awar, and M. S. Shoichet, "Amphiphilic micelles of poly(2-methyl-2-carboxytrimethylene carbonate-co-d,l-lactide)-graft-poly(ethylene glycol) for anti-cancer drug delivery to solid tumours," *Biomaterials*, vol. 33, no. 7, pp. 2223–2229, Mar. 2012.

[132] J. Lu and M. S. Shoichet, "Self-Assembled Polymeric Nanoparticles of Organocatalytic Copolymerizated d, l-Lactide and 2-Methyl 2-Carboxytrimethylene Carbonate," *Macromolecules*, vol. 43, no. 11, pp. 4943–4953, Jun. 2010.

[133] R. C. Pratt, B. G. G. Lohmeijer, D. A. Long, P. N. P. Lundberg, A. P. Dove, H. Li, C. G. Wade, R. M. Waymouth, and J. L. Hedrick, "Exploration, Optimization, and Application of Supramolecular Thiourea−Amine Catalysts for the Synthesis of Lactide (Co)polymers," *Macromolecules*, vol. 39, no. 23, pp. 7863–7871, Nov. 2006.

[134] D. P. Y. Chan, G. F. Deleavey, S. C. Owen, M. J. Damha, and M. S. Shoichet, "Click conjugated polymeric immuno-nanoparticles for targeted siRNA and antisense oligonucleotide delivery," *Biomaterials*, vol. 34, no. 33, pp. 8408–8415, Nov. 2013.

[135] D. P. Y. Chan, S. C. Owen, and M. S. Shoichet, "Double Click: Dual Functionalized Polymeric Micelles with Antibodies and Peptides," *Bioconjugate Chem*, vol. 24, no. 1, pp. 105–113, Jan. 2013.

[136] X.-L. Sun, C. L. Stabler, C. S. Cazalis, and E. L. Chaikof, "Carbohydrate and Protein Immobilization onto Solid Surfaces by Sequential Diels−Alder and Azide−Alkyne Cycloadditions," *Bioconjugate Chem*, vol. 17, no. 1, pp. 52–57, Jan. 2006.

[137] K. Kataoka, A. Harada, and Y. Nagasaki, "Block copolymer micelles for drug delivery: Design, characterization and biological significance," *Adv Drug Deliver Rev*, vol. 64, pp. 37–48, Dec. 2012.

[138] M. E. Davis, Z. G. Chen, and D. M. Shin, "Nanoparticle therapeutics: an emerging treatment modality for cancer," *Nat Rev Drug Discov*, vol. 7, no. 9, pp. 771–782, Sep. 2008.

[139] R. Duncan and R. Gaspar, "Nanomedicine(s) under the Microscope," *Mol Pharmaceut*, vol. 8, no. 6, pp. 2101–2141, Dec. 2011.

[140] V. P. Torchilin, "Targeted polymeric micelles for delivery of poorly soluble drugs," *CMLS, Cell. Mol. Life Sci.*, vol. 61, no. 19, pp. 2549–2559, Oct. 2004.

[141] G. Gaucher, M.-H. Dufresne, V. P. Sant, N. Kang, D. Maysinger, and J.-C. Leroux, "Block copolymer micelles: preparation, characterization and application in drug delivery," *Journal of Controlled Release*, vol. 109, no. 1, pp. 169–188, Dec. 2005.

[142] A. Abuchowski, T. van Es, N. C. Palczuk, and F. F. Davis, "Alteration of immunological properties of bovine serum albumin by covalent attachment of polyethylene

glycol.," *Journal of Biological Chemistry*, vol. 252, pp. 3578–3581, 1977.

[143] K. Park, "To PEGylate or not to PEGylate, that is not the question," *Journal of Controlled Release*, vol. 142, no. 2, pp. 147–148, Mar. 2010.

[144] G. Pasut and F. M. Veronese, "PEG conjugates in clinical development or use as anticancer agents: An overview," *Adv Drug Deliver Rev*, vol. 61, no. 13, pp. 1177–1188, Nov. 2009.

[145] S. M. Ryan, G. Mantovani, X. Wang, D. M. Haddleton, and D. J. Brayden, "Advances in PEGylation of important biotech molecules: delivery aspects," *Expert Opin. Drug Deliv.*, vol. 5, no. 4, pp. 371–383, Apr. 2008.

[146] J. L. Perry, K. G. Reuter, M. P. Kai, K. P. Herlihy, S. W. Jones, J. C. Luft, M. Napier, J. E. Bear, and J. M. DeSimone, "PEGylated PRINT Nanoparticles: The Impact of PEG Density on Protein Binding, Macrophage Association, Biodistribution, and Pharmacokinetics," *Nano Lett.*, vol. 12, no. 10, pp. 5304–5310, Oct. 2012.

[147] R. Gref, Y. Minamitake, M. Peracchia, V. Trubetskoy, V. Torchilin, and R. Langer, "Biodegradable long-circulating polymeric nanospheres," *Science*, vol. 263, no. 5153, pp. 1600–1603, Mar. 1994.

[148] P. Aggarwal, J. B. Hall, C. B. McLeland, M. A. Dobrovolskaia, and S. E. McNeil, "Nanoparticle interaction with plasma proteins as it relates to particle biodistribution, biocompatibility and therapeutic efficacy," *Adv Drug Deliver Rev*, vol. 61, no. 6, pp. 428–437, Jun. 2009.

[149] S. Y. Kim and C. F. Zukoski, "Molecular Weight Effects on Particle and Polymer Microstructure in Concentrated Polymer Solutions," *Macromolecules*, vol. 46, no. 16, pp. 6634–6643, Aug. 2013.

[150] P. Kingshott, H. Thissen, and H. J. Griesser, "Effects of cloud-point grafting, chain length, and density of PEG layers on competitive adsorption of ocular proteins," *Biomaterials*, vol. 23, no. 9, pp. 2043–2056, May 2002.

[151] M. Shi and M. S. Shoichet, "Furan-functionalized co-polymers for targeted drug delivery: caracterization, self-assembly and drug encapsulation," *J Biomat Sci-Polym E*, vol. 19, no. 9, pp. 1143–1157, Jan. 2008.

[152] J. Lu, M. Shi, and M. S. Shoichet, "Click Chemistry Functionalized Polymeric Nanoparticles Target Corneal Epithelial Cells through RGD-Cell Surface Receptors," *Bioconjugate Chem*, vol. 20, no. 1, pp. 87–94, Jan. 2009.

[153] A. M. Layre, P. Couvreur, J. Richard, D. Requier, N. Eddine Ghermani, and R. Gref, "Freeze-Drying of Composite Core-Shell Nanoparticles," *Drug Development and Industrial Pharmacy*, vol. 32, no. 7, pp. 839–846, Sep. 2008.

[154] S. M. D'Addio and R. K. Prud'homme, "Controlling drug nanoparticle formation by rapid precipitation," *Adv Drug Deliver Rev*, vol. 63, no. 6, pp. 417–426, May 2011.

[155] J. Lu, S. C. Owen, and M. S. Shoichet, "Stability of Self-Assembled Polymeric

Micelles in Serum," *Macromolecules*, vol. 44, no. 15, pp. 6002–6008, Aug. 2011.

[156] T. A. Diezi, Y. Bae, and G. S. Kwon, "Enhanced Stability of PEG- block-poly(N-hexyl stearate l-aspartamide) Micelles in the Presence of Serum Proteins," *Mol Pharmaceut*, vol. 7, no. 4, pp. 1355–1360, Aug. 2010.

[157] H. Chen, S. Kim, W. He, H. Wang, P. S. Low, K. Park, and J.-X. Cheng, "Fast Release of Lipophilic Agents from Circulating PEG-PDLLA Micelles Revealed by in VivoFörster Resonance Energy Transfer Imaging," *Langmuir*, vol. 24, no. 10, pp. 5213–5217, May 2008.

[158] R. Savić, T. Azzam, A. Eisenberg, and D. Maysinger, "Assessment of the Integrity of Poly(caprolactone)- b-poly(ethylene oxide) Micelles under Biological Conditions: A Fluorogenic-Based Approach," *Langmuir*, vol. 22, no. 8, pp. 3570–3578, Apr. 2006.

[159] M. Murakami, H. Cabral, Y. Matsumoto, S. Wu, M. R. Kano, T. Yamori, N. Nishiyama, and K. Kataoka, "Improving Drug Potency and Efficacy by Nanocarrier-Mediated Subcellular Targeting," *Science Translational Medicine*, vol. 3, no. 64, pp. 64ra2–64ra2, Jan. 2011.

[160] Y. Sun, W. Zou, S. Bian, Y. Huang, Y. Tan, J. Liang, Y. Fan, and X. Zhang, "Bioreducible PAA-g-PEG graft micelles with high doxorubicin loading for targeted antitumor effect against mouse breast carcinoma," *Biomaterials*, vol. 34, no. 28, pp. 6818–6828, Sep. 2013.

[161] R. R. Sawant and V. P. Torchilin, "Polymeric Micelles: Polyethylene Glycol-Phosphatidylethanolamine (PEG-PE)-Based Micelles as an Example," in *Cancer Nanotechnology*, vol. 624, no. 9, Totowa, NJ: Humana Press, 2010, pp. 131–149.

[162] S. Flanary, A. S. Hoffman, and P. S. Stayton, "Antigen Delivery with Poly(Propylacrylic Acid) Conjugation Enhances MHC-1 Presentation and T-Cell Activation," *Bioconjugate Chem*, vol. 20, no. 2, pp. 241–248, Feb. 2009.

[163] C. Donini, D. N. Robinson, P. Colombo, F. Giordano, and N. A. Peppas, "Preparation of poly(methacrylic acid-g-poly(ethylene glycol)) nanospheres from methacrylic monomers for pharmaceutical applications," *International Journal of Pharmaceutics*, vol. 245, no. 1, pp. 83–91, Oct. 2002.

[164] H. Otsuka, Y. Nagasaki, and K. Kataoka, "PEGylated nanoparticles for biological and pharmaceutical applications," *Adv Drug Deliver Rev*, vol. 64, pp. 246–255, Dec. 2012.

[165] H.-M. Ding and Y.-Q. Ma, "Role of physicochemical properties of coating ligands in receptor-mediated endocytosis of nanoparticles," *Biomaterials*, vol. 33, no. 23, pp. 5798–5802, Aug. 2012.

[166] G. Prencipe, S. M. Tabakman, K. Welsher, Z. Liu, A. P. Goodwin, L. Zhang, J. Henry, and H. Dai, "PEG Branched Polymer for Functionalization of Nanomaterials with Ultralong Blood Circulation," *J Am Chem Soc*, vol. 131, no. 13, pp. 4783–4787, Apr. 2009.

[167] S. Kim, Y. Shi, J. Y. Kim, K. Park, and J.-X. Cheng, "Overcoming the barriers in micellar drug delivery: loading efficiency, in vivostability, and micelle–cell interaction," *Expert Opin. Drug Deliv.*, vol. 7, no. 1, pp. 49–62, Dec. 2009.

[168] A. K. Singla, A. Garg, and D. Aggarwal, “Paclitaxel and its formulations,” *International Journal of Pharmaceutics*, vol. 235, no. 1, pp. 179–192, Mar. 2002.

[169] M. Cegnar, J. Kristl, and J. Kos, “Nanoscale polymer carriers to deliver chemotherapeutic agents to tumours,” *Expert Opin. Biol. Ther.*, vol. 5, no. 12, pp. 1557–1569, Nov. 2005.

[170] R. C. Bravo González, J. Huwyler, F. Boess, I. Walter, and B. Bittner, “In vitro investigation on the impact of the surface-active excipients Cremophor EL, Tween 80 and Solutol HS 15 on the metabolism of midazolam,” *Biopharm. Drug Dispos.*, vol. 25, no. 1, pp. 37–49, Jan. 2004.

[171] K. Izutsu, S. Yoshioka, S. Kojima, and T. W. Randolph, “Effects of Sugars and Polymers on Crystallization of Poly(ethylene glycol) in Frozen Solutions: Phase Separation Between Incompatible Polymers - Springer,” *Pharm Res*, vol. 13, pp. 1393–1400, 1996.

[172] F. De Jaeghere, E. Allémann, J.-C. Leroux, W. Stevels, J. Feijen, E. Doelker, and R. Gurny, “Formulation and lyoprotection of poly(lactic acid-co-ethylene oxide) nanoparticles: influence on physical stability and in vitro cell uptake,” *Pharm Res*, vol. 16, no. 6, pp. 859–866, 1999.

[173] J.-T. Li, K. D. Caldwell, and N. Rapoport, “Surface Properties of Pluronic-Coated Polymeric Colloids,” *Langmuir*, vol. 10, no. 12, pp. 4475–4482, Dec. 1994.

[174] M. J. Santander-Ortega, A. B. Jodar-Reyes, N. Csaba, D. Bastos-Gonzalez, and J. L. Ortega-Vinuesa, “Colloidal stability of Pluronic F68-coated PLGA nanoparticles: A variety of stabilisation mechanisms,” *J Colloid Interf Sci*, vol. 302, no. 2, pp. 522–529, Oct. 2006.

[175] M. L. Adams and G. S. Kwon, “The effects of acyl chain length on the micelle properties of poly(ethylene oxide)-block-poly(N-hexylL-aspartamide)-acyl conjugates,” *J Biomat Sci-Polym E*, vol. 13, no. 9, pp. 991–1006, Jan. 2002.

[176] J. T. G. Overbeek, “Recent developments in the understanding of colloid stability,” *J Colloid Interf Sci*, vol. 58, no. 2, pp. 408–422, Feb. 1977.

[177] D. Owens III and N. Peppas, “Opsonization, biodistribution, and pharmacokinetics of polymeric nanoparticles,” *International Journal of Pharmaceutics*, vol. 307, no. 1, pp. 93–102, Jan. 2006.

[178] D. V. Devine, K. Wong, K. Serrano, A. Chonn, and P. R. Cullis, “Liposome—complement interactions in rat serum: implications for liposome survival studies,” *Biochimica et Biophysica Acta (BBA) - Biomembranes*, vol. 1191, no. 1, pp. 43–51, Apr. 1994.

[179] C. Foged, B. Brodin, S. Frokjaer, and A. Sundblad, “Particle size and surface charge affect particle uptake by human dendritic cells in an in vitro model,” *International Journal of Pharmaceutics*, vol. 298, no. 2, pp. 315–322, Jul. 2005.

[180] M. A. Dobrovolskaia, P. Aggarwal, J. B. Hall, and S. E. McNeil, “Preclinical Studies To Understand Nanoparticle Interaction with the Immune System and Its Potential Effects on Nanoparticle Biodistribution,” *Mol Pharmaceut*, vol. 5, no. 4, pp. 487–495, Aug. 2008.

[181] H.-J. Cho, H. Y. Yoon, H. Koo, S.-H. Ko, J.-S. Shim, J.-H. Lee, K. Kim, I. Chan Kwon, and D.-D. Kim, "Self-assembled nanoparticles based on hyaluronic acid-ceramide (HA-CE) and Pluronic® for tumor-targeted delivery of docetaxel," *Biomaterials*, vol. 32, no. 29, pp. 7181–7190, Oct. 2011.

[182] Y. Li, H. He, X. Jia, W.-L. Lu, J. Lou, and Y. Wei, "A dual-targeting nanocarrier based on poly(amidoamine) dendrimers conjugated with transferrin and tamoxifen for treating brain gliomas," *Biomaterials*, vol. 33, no. 15, pp. 3899–3908, May 2012.

[183] P. L. Rodriguez, T. Harada, D. A. Christian, D. A. Pantano, R. K. Tsai, and D. E. Discher, "Minimal 'Self' Peptides That Inhibit Phagocytic Clearance and Enhance Delivery of Nanoparticles," *Science*, vol. 339, no. 6122, pp. 971–975, Feb. 2013.

[184] R. H. Fang, C.-M. J. Hu, and L. Zhang, "Nanoparticles disguised as red blood cells to evade the immune system," *Expert Opin. Biol. Ther.*, vol. 12, no. 4, pp. 385–389, Mar. 2012.

[185] R. G. Strickley, "Solubilizing Excipients in Oral and Injectable Formulations," *Pharm Res*, vol. 21, no. 2, pp. 201–230.

[186] L. Kiss, F. R. Walter, A. Bocsik, S. Veszelka, B. Ózsvári, L. G. Puskás, P. Szabó-Révész, and M. A. Deli, "Kinetic Analysis of the Toxicity of Pharmaceutical Excipients Cremophor EL and RH40 on Endothelial and Epithelial Cells," *J Pharm Sci-Us*, vol. 102, no. 4, pp. 1173–1181, Apr. 2013.

[187] H. Cabral and K. Kataoka, "Progress of drug-loaded polymeric micelles into clinical studies," *Journal of Controlled Release*, vol. 190, pp. 465–476, Sep. 2014.

[188] E. Luque-Michel, E. Imbuluzqueta, V. Sebastián, and M. J. Blanco-Prieto, "Clinical advances of nanocarrier-based cancer therapy and diagnostics," *Expert Opin. Drug Deliv.*, pp. 1–18, Jul. 2016.

[189] F. Alexis, E. Pridgen, L. K. Molnar, and O. C. Farokhzad, "Factors Affecting the Clearance and Biodistribution of Polymeric Nanoparticles," *Mol Pharmaceut*, vol. 5, no. 4, pp. 505–515, Aug. 2008.

[190] J. Logie, C. K. McLaughlin, R. Y. Tam, and M. S. Shoichet, "Innovative use of the taxol binding peptide overcomes key challenges of stable and high drug loading in polymeric nanomicelles," *Chem. Commun.*, vol. 51, no. 60, pp. 12000–12003, 2015.

[191] W. Ma, A. G. Cheetham, and H. Cui, "Building nanostructures with drugs," *Nano Today*, vol. 11, no. 1, pp. 13–30, Feb. 2016.

[192] G. Shen, R. Xing, N. Zhang, C. Chen, G. Ma, and X. Yan, "Interfacial Cohesion and Assembly of Bioadhesive Molecules for Design of Long-Term Stable Hydrophobic Nanodrugs toward Effective Anticancer Therapy," *ACS Nano*, vol. 10, no. 6, pp. 5720–5729, Jun. 2016.

[193] M. F. Sassano, A. K. Doak, B. L. Roth, and B. K. Shoichet, "Colloidal Aggregation Causes Inhibition of G Protein-Coupled Receptors," *J Med Chem*, vol. 56, no. 6, pp. 2406–2414, Mar. 2013.

[194] J. J. Irwin, D. Duan, H. Torosyan, A. K. Doak, K. T. Ziebart, T. Sterling, G. Tumanian,

and B. K. Shoichet, “An Aggregation Advisor for Ligand Discovery,” *J Med Chem*, vol. 58, no. 17, pp. 7076–7087, Sep. 2015.

[195] M. J. Jackson, S. J. Toth, U. S. Kestur, J. Huang, F. Qian, M. A. Hussain, G. J. Simpson, and L. S. Taylor, “Impact of Polymers on the Precipitation Behavior of Highly Supersaturated Aqueous Danazol Solutions,” *Mol Pharmaceut*, vol. 11, no. 9, pp. 3027–3038, Sep. 2014.

[196] A. E. Wakeling, M. Dukes, and J. Bowler, “A potent specific pure antiestrogen with clinical potential.,” *Cancer Research*, vol. 51, no. 15, pp. 3867–3873, Aug. 1991.

[197] J. Logie, S. C. Owen, C. K. McLaughlin, and M. S. Shoichet, “PEG-Graft Density Controls Polymeric Nanoparticle Micelle Stability,” *Chem. Mater.*, vol. 26, no. 9, pp. 2847–2855, May 2014.

[198] S. Kalepu and V. Nekkanti, “Insoluble drug delivery strategies: review of recent advances and business prospects,” *Acta Pharmaceutica Sinica B*, vol. 5, no. 5, pp. 442–453, Sep. 2015.

[199] Y. Liu, Y. Hu, and L. Huang, “Influence of polyethylene glycol density and surface lipid on pharmacokinetics and biodistribution of lipid-calcium-phosphate nanoparticles,” *Biomaterials*, vol. 35, no. 9, pp. 3027–3034, Mar. 2014.

[200] J. P. Latere Dwan'Isa, L. Rouxhet, V. Préat, M. E. Brewster, and A. Ariën, “Prediction of drug solubility in amphiphilic di-block copolymer micelles: the role of polymer-drug compatibility,” *Die Pharmazie-An …*, 2007.

[201] P. J. Marsac, S. L. Shamblin, and L. S. Taylor, “Theoretical and Practical Approaches for Prediction of Drug–Polymer Miscibility and Solubility,” *Pharm Res*, vol. 23, no. 10, pp. 2417–2426, Aug. 2006.

[202] A. Zaccone, H. Wu, M. Lattuada, and M. Morbidelli, “Correlation between Colloidal Stability and Surfactant Adsorption/Association Phenomena Studied by Light Scattering,” *J. Phys. Chem. B*, vol. 112, no. 7, pp. 1976–1986, Feb. 2008.

[203] A. Gaudin, O. Tagit, D. Sobot, S. Lepetre-Mouelhi, J. Mougin, T. F. Martens, K. Braeckmans, V. Nicolas, D. Desmaële, S. C. De Smedt, N. Hildebrandt, P. Couvreur, and K. Andrieux, “Transport Mechanisms of Squalenoyl-Adenosine Nanoparticles Across the Blood–Brain Barrier,” *Chem. Mater.*, vol. 27, no. 10, pp. 3636–3647, May 2015.

[204] B. Yameen, W. I. Choi, C. Vilos, A. Swami, J. Shi, and O. C. Farokhzad, “Insight into nanoparticle cellular uptake and intracellular targeting,” *Journal of Controlled Release*, vol. 190, pp. 485–499, Sep. 2014.

[205] O. Tacar, P. Sriamornsak, and C. R. Dass, “Doxorubicin: an update on anticancer molecular action, toxicity and novel drug delivery systems,” *J Pharm Pharmacol*, vol. 65, no. 2, pp. 157–170, Aug. 2012.

[206] K. Letchford, R. Liggins, and H. Burt, “Solubilization of hydrophobic drugs by methoxy poly(ethylene glycol)-block-polycaprolactone diblock copolymer micelles: Theoretical and experimental data and correlations,” *J Pharm Sci-Us*, vol. 97, no. 3, pp. 1179–1190, Mar.

2008.

[207] J. Gou, S. Feng, H. Xu, G. Fang, Y. Chao, Y. Zhang, H. Xu, and X. Tang, “Decreased Core Crystallinity Facilitated Drug Loading in Polymeric Micelles without Affecting Their Biological Performances,” *Biomacromolecules*, vol. 16, no. 9, pp. 2920–2929, Sep. 2015.

[208] Y. Zhao, F. Fay, S. Hak, J. Manuel Perez-Aguilar, B. L. Sanchez-Gaytan, B. Goode, R. Duivenvoorden, C. de Lange Davies, A. Bjørkøy, H. Weinstein, Z. A. Fayad, C. Pérez-Medina, and W. J. M. Mulder, “Augmenting drug–carrier compatibility improves tumour nanotherapy efficacy,” *Nature Communications*, vol. 7, p. 11221, Apr. 2016.

[209] Sanofi, “Sanofi Returns to Growth in Q4 2013.” Paris, pp. 1–24, 06-Feb-2014.

[210] R. R. Sawant and V. P. Torchilin, “Enhanced cytotoxicity of TATp-bearing paclitaxel-loaded micelles in vitro and in vivo,” *International Journal of Pharmaceutics*, vol. 374, no. 1, pp. 114–118, Jun. 2009.

[211] C. K. McLaughlin, J. Logie and M.S. Shoichet, “Core and Corona Modifications for the Design of Polymeric Micelle Drug-Delivery Systems,” *Israel Journal of Chemistry*, vol. 53, pp. 670–679, 2013.

[212] X. Ke, V. W. L. Ng, R. J. Ono, J. M. W. Chan, S. Krishnamurthy, Y. Wang, J. L. Hedrick, and Y. Y. Yang, “Role of non-covalent and covalent interactions in cargo loading capacity and stability of polymeric micelles,” *Journal of Controlled Release*, vol. 193, pp. 9–26, Nov. 2014.

[213] P. Couvreur, “Nanoparticles in drug delivery: Past, present and future,” *Adv Drug Deliver Rev*, vol. 65, no. 1, pp. 21–23, Jan. 2013.

[214] X. Z. Shu, Y. Liu, Y. Luo, M. C. Roberts, and G. D. Prestwich, “Disulfide Cross-Linked Hyaluronan Hydrogels,” *Biomacromolecules*, vol. 3, no. 6, pp. 1304–1311, Nov. 2002.

[215] M. Boncler, M. Różalski, U. Krajewska, A. Podsędek, and C. Watala, “Comparison of PrestoBlue and MTT assays of cellular viability in the assessment of anti-proliferative effects of plant extracts on human endothelial cells,” *Journal of Pharmacological and Toxicological Methods*, vol. 69, no. 1, pp. 9–16, Jan. 2014.

[216] Y. T. Zheng, W. L. Chan, P. Chan, H. Huang, and S. C. Tam, “Enhancement of the anti-herpetic effect of trichosanthin by acyclovir and interferon,” *FEBS Letters*, vol. 496, no. 2, pp. 139–142, May 2001.

[217] K. Vulic and M. S. Shoichet, “Tunable Growth Factor Delivery from Injectable Hydrogels for Tissue Engineering,” *J Am Chem Soc*, vol. 134, no. 2, pp. 882–885, Jan. 2012.

[218] J. J. Field, J. F. Díaz, and J. H. Miller, “The Binding Sites of Microtubule-Stabilizing Agents,” *Chemistry & Biology*, vol. 20, no. 3, pp. 301–315, Mar. 2013.

[219] T. Hara, K. Ushio, M. Nishiwaki, J. Kouno, H. Araki, Y. Hikichi, M. Hattori, Y. Imai, and M. Yamaoka, “A mutation in β-tubulin and a sustained dependence on androgen receptor signalling in a newly established docetaxel-resistant prostate cancer cell line,” *Cell. Biol. Int.*, vol. 34, no. 2, pp. 177–184, Jan. 2010.

[220] H. J. Williams, A. I. Scott, R. A. Dieden, C. S. Swindell, L. E. Chirlian, M. M. Francl, J. M. Heerding, and N. E. Krauss, "NMR and molecular modeling study of active and inactive taxol analogues in aqueous and nonaqueous solution," *Can. J. Chem.*, vol. 72, no. 1, pp. 252–260, Jan. 1994.

[221] P. E. Wright, H. J. Dyson, and R. A. Lerner, "Conformation of peptide fragments of proteins in aqueous solution: implications for initiation of protein folding," *Biochemistry*, vol. 27, no. 19, pp. 7167–7175, Sep. 1988.

[222] K. M. Huh, S. C. Lee, Y. W. Cho, J. Lee, J. H. Jeong, and K. Park, "Hydrotropic polymer micelle system for delivery of paclitaxel," *Journal of Controlled Release*, vol. 101, no. 1, pp. 59–68, Jan. 2005.

[223] H. M. Burt, X. Zhang, P. Toleikis, L. Embree, and W. L. Hunter, "Development of copolymers of poly(d,l-lactide) and methoxypolyethylene glycol as micellar carriers of paclitaxel," *Colloids and Surfaces B: Biointerfaces*, vol. 16, no. 1, pp. 161–171, Nov. 1999.

[224] J. E. Cortes and R. Pazdur, "Docetaxel.," *J. Clin. Oncol.*, vol. 13, no. 10, pp. 2643–2655, Oct. 1995.

[225] Y. Shi, R. van der Meel, B. Theek, E. Oude Blenke, E. H. E. Pieters, M. H. A. M. Fens, J. Ehling, R. M. Schiffelers, G. Storm, C. F. van Nostrum, T. Lammers, and W. E. Hennink, "Complete Regression of Xenograft Tumors upon Targeted Delivery of Paclitaxel viaΠ–Π Stacking Stabilized Polymeric Micelles," *ACS Nano*, vol. 9, no. 4, pp. 3740–3752, Apr. 2015.

[226] M. X. Sliwkowski and I. Mellman, "Antibody Therapeutics in Cancer," *Science*, vol. 341, no. 6151, pp. 1192–1198, Sep. 2013.

[227] M. Schneider, A. Ny, C. R. de Almodovar, and P. Carmeliet, "A New Mouse Model to Study Acquired Lymphedema," *PLoS Med*, vol. 3, no. 7, p. e264, Jul. 2006.

[228] B. A. Ruggeri, F. Camp, and S. Miknyoczki, "Animal models of disease: Pre-clinical animal models of cancer and their applications and utility in drug discovery," *Biochemical Pharmacology*, vol. 87, no. 1, pp. 150–161, Jan. 2014.

[229] M. Das Thakur, N. K. Pryer, and M. Singh, "Mouse tumour models to guide drug development and identify resistance mechanisms," *J. Pathol.*, vol. 232, no. 2, pp. 103–111, Dec. 2013.

[230] K. Ho, Y. Lapitsky, M. Shi, and M. S. Shoichet, "Tunable immunonanoparticle binding to cancer cells: thermodynamic analysis of targeted drug delivery vehicles," *Soft Matter*, vol. 5, no. 5, p. 1074, 2009.

[231] J. Hrkach, D. Von Hoff, M. M. Ali, E. Andrianova, J. Auer, T. Campbell, D. De Witt, M. Figa, M. Figueiredo, A. Horhota, S. Low, K. McDonnell, E. Peeke, B. Retnarajan, A. Sabnis, E. Schnipper, J. J. Song, Y. H. Song, J. Summa, D. Tompsett, G. Troiano, T. Van Geen Hoven, J. Wright, P. LoRusso, P. W. Kantoff, N. H. Bander, C. Sweeney, O. C. Farokhzad, R. Langer, and S. Zale, "Preclinical Development and Clinical Translation of a PSMA-Targeted Docetaxel Nanoparticle with a Differentiated Pharmacological Profile," *Science Translational Medicine*, vol. 4, no. 128, pp. 128ra39–128ra39, Apr. 2012.

[232] M. J. Ernsting, W.-L. Tang, N. W. Maccallum, and S.-D. Li, “Preclinical pharmacokinetic, biodistribution, and anti-cancer efficacy studies of a docetaxel-carboxymethylcellulose nanoparticle in mouse models,” *Biomaterials*, vol. 33, no. 5, pp. 1445–1454, Feb. 2012.

[233] S. C. Kim, D. W. Kim, Y. H. Shim, J. S. Bang, H. S. Oh, S. W. Kim, and M. H. Seo, “In vivo evaluation of polymeric micellar paclitaxel formulation: toxicity and efficacy,” *Journal of Controlled Release*, vol. 72, no. 1, pp. 191–202, May 2001.

[234] S.-W. Lee, M.-H. Yun, S. W. Jeong, C.-H. In, J. Y. Kim, M. H. Seo, C.-M. Pai, and S.-O. Kim, “Development of docetaxel-loaded intravenous formulation, Nanoxel-PM™ using polymer-based delivery system,” *Journal of Controlled Release*, vol. 155, no. 2, pp. 262–271, Oct. 2011.

[235] C. M. Dawidczyk, C. Kim, J. H. Park, L. M. Russell, K. H. Lee, M. G. Pomper, and P. C. Searson, “State-of-the-art in design rules for drug delivery platforms: Lessons learned from FDA-approved nanomedicines,” *Journal of Controlled Release*, vol. 187, pp. 133–144, Aug. 2014.

[236] W. J. Gradishar, “Phase III Trial of Nanoparticle Albumin-Bound Paclitaxel Compared With Polyethylated Castor Oil-Based Paclitaxel in Women With Breast Cancer,” *J. Clin. Oncol.*, vol. 23, no. 31, pp. 7794–7803, Nov. 2005.

[237] U. Prabhakar, H. Maeda, R. K. Jain, E. M. Sevick-Muraca, W. Zamboni, O. C. Farokhzad, S. T. Barry, A. Gabizon, P. Grodzinski, and D. C. Blakey, “Challenges and Key Considerations of the Enhanced Permeability and Retention Effect for Nanomedicine Drug Delivery in Oncology,” *Cancer Research*, vol. 73, no. 8, pp. 2412–2417, Apr. 2013.

[238] T. Lammers, L. Y. Rizzo, G. Storm, and F. Kiessling, “Personalized Nanomedicine,” *Clin. Cancer Res.*, vol. 18, no. 18, pp. 4889–4894, Sep. 2012.

[239] T. Miller, S. Breyer, G. van Colen, W. Mier, U. Haberkorn, S. Geissler, S. Voss, M. Weigandt, and A. Goepferich, “Premature drug release of polymeric micelles and its effects on tumor targeting,” *International Journal of Pharmaceutics*, vol. 445, no. 1, pp. 117–124, Mar. 2013.

[240] M. N. Khalid, P. Simard, D. Hoarau, A. Dragomir, and J.-C. Leroux, “Long Circulating Poly(Ethylene Glycol)-Decorated Lipid Nanocapsules Deliver Docetaxel to Solid Tumors,” *Pharm Res*, vol. 23, no. 4, pp. 752–758, Mar. 2006.

[241] C. C. Milsom, C. R. Lee, C. Hackl, S. Man, and R. S. Kerbel, “Differential Post-Surgical Metastasis and Survival in SCID, NOD-SCID and NOD-SCID-IL-2Rγnull Mice with Parental and Subline Variants of Human Breast Cancer: Implications for Host Defense Mechanisms Regulating Metastasis,” *PLoS ONE*, vol. 8, no. 8, p. e71270, Aug. 2013.

[242] K. F. Pirollo and E. H. Chang, “Does a targeting ligand influence nanoparticle tumor localization or uptake?,” *Trends in Biotechnology*, vol. 26, no. 10, pp. 552–558, Oct. 2008.

[243] A. T. Florence, “‘Targeting’ nanoparticles: The constraints of physical laws and physical barriers,” *Journal of Controlled Release*, vol. 164, no. 2, pp. 115–124, Dec. 2012.

[244] M. Ahmed, D. W. Pan, and M. E. Davis, “Lack of in Vivo Antibody Dependent Cellular Cytotoxicity with Antibody Containing Gold Nanoparticles,” *Bioconjugate Chem*, vol. 26, no. 5, pp. 812–816, May 2015.

[245] D. B. Kirpotin, “Antibody Targeting of Long-Circulating Lipidic Nanoparticles Does Not Increase Tumor Localization but Does Increase Internalization in Animal Models,” *Cancer Research*, vol. 66, no. 13, pp. 6732–6740, Jul. 2006.

[246] J. D. Heidel and M. E. Davis, “Clinical Developments in Nanotechnology for Cancer Therapy,” *Pharm Res*, vol. 28, no. 2, pp. 187–199, Jun. 2010.

[247] Y. Chen, X. Zhu, X. Zhang, B. Liu, and L. Huang, “Nanoparticles Modified With Tumor-targeting scFv Deliver siRNA and miRNA for Cancer Therapy,” *Mol Ther*, vol. 18, no. 9, pp. 1650–1656, Jul. 2010.

[248] T. Cedervall, I. Lynch, S. Lindman, T. Berggård, E. Thulin, H. Nilsson, K. A. Dawson, and S. Linse, “Understanding the nanoparticle-protein corona using methods to quantify exchange rates and affinities of proteins for nanoparticles,” *Proc. Natl. Acad. Sci. U.S.A.*, vol. 104, no. 7, pp. 2050–2055, Feb. 2007.

[249] M. Beck-Broichsitter, J. Nicolas, and P. Couvreur, “Design attributes of long-circulating polymeric drug delivery vehicles,” *European Journal of Pharmaceutics and Biopharmaceutics*, vol. 97, pp. 304–317, Nov. 2015.

[250] Y. Li, M. Kröger, and W. K. Liu, “Endocytosis of PEGylated nanoparticles accompanied by structural and free energy changes of the grafted polyethylene glycol,” *Biomaterials*, vol. 35, no. 30, pp. 8467–8478, Oct. 2014.

[251] L. D. Unsworth, H. Sheardown, and J. L. Brash, “Protein-Resistant Poly(ethylene oxide)-Grafted Surfaces: Chain Density-Dependent Multiple Mechanisms of Action,” *Langmuir*, vol. 24, no. 5, pp. 1924–1929, Mar. 2008.

[252] C.-L. Lo, C.-K. Huang, K.-M. Lin, and G.-H. Hsiue, “Mixed micelles formed from graft and diblock copolymers for application in intracellular drug delivery,” *Biomaterials*, vol. 28, no. 6, pp. 1225–1235, Feb. 2007.

[253] Y. Li, S. Pan, W. Zhang, and Z. Du, “Novel thermo-sensitive core–shell nanoparticles for targeted paclitaxel delivery,” *Nanotechnology*, vol. 20, no. 6, p. 065104, Jan. 2009.

[254] S. M. D'Addio, C. Kafka, M. Akbulut, P. Beattie, W. Saad, M. Herrera, M. T. Kennedy, and R. K. Prud'homme, “Novel Method for Concentrating and Drying Polymeric Nanoparticles: Hydrogen Bonding Coacervate Precipitation,” *Mol Pharmaceut*, vol. 7, no. 2, pp. 557–564, Apr. 2010.

[255] W. Abdelwahed, G. Degobert, S. Stainmesse, and H. Fessi, “Freeze-drying of nanoparticles: Formulation, process and storage considerations□ ,” *Adv Drug Deliver Rev*, vol. 58, no. 15, pp. 1688–1713, Dec. 2006.

[256] M. Liu, G. Huang, Y. Cong, G. Tong, Z. Lin, Y. Yin, and C. Zhang, “The preparation and characterization of micelles from poly(γ-glutamic acid)-graft-poly(l-lactide) and the cellular uptake thereof,” *J Mater Sci: Mater Med*, vol. 26, no. 5, p. 187, Apr. 2015.

[257] M. Dübner, T. N. Gevrek, A. Sanyal, N. D. Spencer, and C. Padeste, “Fabrication of Thiol–Ene ‘Clickable’ Copolymer-Brush Nanostructures on Polymeric Substrates via Extreme Ultraviolet Interference Lithography,” *ACS Appl. Mater. Interfaces*, vol. 7, no. 21, pp. 11337–11345, Jun. 2015.

[258] F. Alexis, E. M. Pridgen, R. Langer, and O. C. Farokhzad, “Nanoparticle Technologies for Cancer Therapy,” in *Drug Delivery*, vol. 197, no. 2, Berlin, Heidelberg: Springer Berlin Heidelberg, 2009, pp. 55–86.

[259] Y. Kim, M. H. Pourgholami, D. L. Morris, and M. H. Stenzel, “Effect of Cross-Linking on the Performance of Micelles As Drug Delivery Carriers: A Cell Uptake Study,” *Biomacromolecules*, vol. 13, no. 3, pp. 814–825, Mar. 2012.

[260] A. N. Koo, K. H. Min, H. J. Lee, S.-U. Lee, K. Kim, I. Chan Kwon, S. H. Cho, S. Y. Jeong, and S. C. Lee, “Tumor accumulation and antitumor efficacy of docetaxel-loaded core-shell-corona micelles with shell-specific redox-responsive cross-links,” *Biomaterials*, vol. 33, no. 5, pp. 1489–1499, Feb. 2012.

[261] S. M. Garg, M. R. Vakili, and A. Lavasanifar, “Polymeric micelles based on poly(ethylene oxide) and α-carbon substituted poly(ε-caprolactone): An in vitro study on the effect of core forming block on polymeric micellar stability, biocompatibility, and immunogenicity,” *Colloids and Surfaces B: Biointerfaces*, vol. 132, pp. 161–170, Aug. 2015.

[262] S. Aryal, C.-M. J. Hu, and L. Zhang, “Polymer−Cisplatin Conjugate Nanoparticles for Acid-Responsive Drug Delivery,” *ACS Nano*, vol. 4, no. 1, pp. 251–258, Jan. 2010.

[263] J. Bhattacharyya, J. J. Bellucci, I. Weitzhandler, J. R. McDaniel, I. Spasojevic, X. Li, C.-C. Lin, J.-T. A. Chi, and A. Chilkoti, “A paclitaxel-loaded recombinant polypeptide nanoparticle outperforms Abraxane in multiple murine cancer models,” *Nature Communications*, vol. 6, p. 7939, Aug. 2015.

[264] C.-J. Lin, Y.-L. Lin, F. Luh, Y. Yen, and R.-M. Chen, “Preclinical effects of CRLX101, an investigational camptothecin-containing nanoparticle drug conjugate, on treating glioblastoma multiforme via apoptosis and antiangiogenesis,” *Oncotarget*, Jul. 2016.

[265] A. J. Clark, D. T. Wiley, J. E. Zuckerman, P. Webster, J. Chao, J. Lin, Y. Yen, and M. E. Davis, “CRLX101 nanoparticles localize in human tumors and not in adjacent, nonneoplastic tissue after intravenous dosing,” *Proc. Natl. Acad. Sci. U.S.A.*, vol. 113, no. 14, pp. 3850–3854, Apr. 2016.

[266] H. Grohganz, P. A. Priemel, K. Löbmann, L. H. Nielsen, R. Laitinen, A. Mullertz, G. Van den Mooter, and T. Rades, “Refining stability and dissolution rate of amorphous drug formulations,” *Expert Opin. Drug Deliv.*, vol. 11, no. 6, pp. 977–989, Mar. 2014.

[267] K. Fuhrmann, M. A. Gauthier, and J.-C. Leroux, “Targeting of Injectable Drug Nanocrystals,” *Mol Pharmaceut*, vol. 11, no. 6, pp. 1762–1771, Jun. 2014.

[268] D. Trung Bui, A. Maksimenko, D. Desmaële, S. Harrisson, C. Vauthier, P. Couvreur, and J. Nicolas, “Polymer Prodrug Nanoparticles Based on Naturally Occurring Isoprenoid for Anticancer Therapy,” *Biomacromolecules*, vol. 14, no. 8, pp. 2837–2847, Aug. 2013.

[269] D. Guénard, F. Gueritte-Voegelein, and P. Potier, “Taxol and taxotere: discovery, chemistry, and structure-activity relationships,” *Accounts Chem Res*, vol. 26, no. 4, pp. 160–167, Apr. 1993.

[270] B. Hoang, M. J. Ernsting, A. Roy, M. Murakami, E. Undzys, and S.-D. Li, “Docetaxel-carboxymethylcellulose nanoparticles target cells via a SPARC and albumin dependent mechanism,” *Biomaterials*, vol. 59, pp. 66–76, Aug. 2015.

[271] Y. H. Bae and H. Yin, “Stability issues of polymeric micelles,” *Journal of Controlled Release*, vol. 131, no. 1, pp. 2–4, Oct. 2008.

[272] D. W. Kim, S. Y. Kim, H. K. Kim, S. W. Kim, S. W. Shin, J. S. Kim, K. Park, M. Y. Lee, and D. S. Heo, “Multicenter phase II trial of Genexol-PM, a novel Cremophor-free, polymeric micelle formulation of paclitaxel, with cisplatin in patients with advanced non-small-cell lung cancer,” *Annals of Oncology*, vol. 18, no. 12, pp. 2009–2014, Dec. 2007.

[273] D. Douer, “Efficacy and Safety of Vincristine Sulfate Liposome Injection in the Treatment of Adult Acute Lymphocytic Leukemia,” *The Oncologist*, vol. 21, no. 7, pp. 840–847, Jul. 2016.

[274] F. Muggia and A. Hamilton, “Phase III data on Caelyx® in ovarian cancer,” *European Journal of Cancer*, vol. 37, pp. 15–18, Dec. 2001.

[275] D. D. Von Hoff, M. M. Mita, R. K. Ramanathan, G. J. Weiss, A. C. Mita, P. M. LoRusso, H. A. Burris, L. L. Hart, S. C. Low, D. M. Parsons, S. E. Zale, J. M. Summa, H. Youssoufian, and J. C. Sachdev, “Phase I Study of PSMA-Targeted Docetaxel-Containing Nanoparticle BIND-014 in Patients with Advanced Solid Tumors,” *Clin. Cancer Res.*, vol. 22, no. 13, pp. 3157–3163, Jun. 2016.

[276] A. L. Chen and A. Pavlick, “Docetaxel more active than paclitaxel as second-line therapy for metastatic breast cancer,” *The Women's Oncology Review*, vol. 6, no. 1, pp. 99–100, Dec. 2011.

[277] Y. Zhong, F. Meng, C. Deng, and Z. Zhong, “Ligand-Directed Active Tumor-Targeting Polymeric Nanoparticles for Cancer Chemotherapy,” *Biomacromolecules*, vol. 15, no. 6, pp. 1955–1969, Jun. 2014.

[278] T. Lammers, F. Kiessling, W. E. Hennink, and G. Storm, “Drug targeting to tumors: Principles, pitfalls and (pre-) clinical progress,” *Journal of Controlled Release*, vol. 161, no. 2, pp. 175–187, Jul. 2012.

[279] J. E. Zuckerman, I. Gritli, A. Tolcher, J. D. Heidel, D. Lim, R. Morgan, B. Chmielowski, A. Ribas, M. E. Davis, and Y. Yen, “Correlating animal and human phase Ia/Ib clinical data with CALAA-01, a targeted, polymer-based nanoparticle containing siRNA,” *Proc. Natl. Acad. Sci. U.S.A.*, vol. 111, no. 31, pp. 11449–11454, Aug. 2014.

[280] T. T. Junttila, G. Li, K. Parsons, G. L. Phillips, and M. X. Sliwkowski, “Trastuzumab-DM1 (T-DM1) retains all the mechanisms of action of trastuzumab and efficiently inhibits growth of lapatinib insensitive breast cancer,” *Breast Cancer Res Treat*, vol. 128, no. 2, pp. 347–356, Aug. 2010.

[281] H. Cabral, J. Makino, Y. Matsumoto, P. Mi, H. Wu, T. Nomoto, K. Toh, N. Yamada, Y. Higuchi, S. Konishi, M. R. Kano, H. Nishihara, Y. Miura, N. Nishiyama, and K. Kataoka, "Systemic Targeting of Lymph Node Metastasis through the Blood Vascular System by Using Size-Controlled Nanocarriers," *ACS Nano*, vol. 9, no. 5, pp. 4957–4967, May 2015.

[282] F. Zhang, S. Zhang, S. F. Pollack, R. Li, A. M. Gonzalez, J. Fan, J. Zou, S. E. Leininger, A. Pavía-Sanders, R. Johnson, L. D. Nelson, J. E. Raymond, M. Elsabahy, D. M. P. Hughes, M. W. Lenox, T. P. Gustafson, and K. L. Wooley, "Improving Paclitaxel Delivery: In Vitroand In VivoCharacterization of PEGylated Polyphosphoester-Based Nanocarriers," *J Am Chem Soc*, vol. 137, no. 5, pp. 2056–2066, Feb. 2015.

[283] J. M. Anderson and M. S. Shive, "Biodegradation and biocompatibility of PLA and PLGA microspheres," *Adv Drug Deliver Rev*, vol. 64, pp. 72–82, Dec. 2012.

[284] H. Y. Nam, S. M. Kwon, H. Chung, S.-Y. Lee, S.-H. Kwon, H. Jeon, Y. Kim, J. H. Park, J. Kim, S. Her, Y.-K. Oh, I. C. Kwon, K. Kim, and S. Y. Jeong, "Cellular uptake mechanism and intracellular fate of hydrophobically modified glycol chitosan nanoparticles," *Journal of Controlled Release*, vol. 135, no. 3, pp. 259–267, May 2009.

[285] S. LAI, K. Hida, S. MAN, C. Chen, C. Machamer, T. SCHROER, and J. Hanes, "Privileged delivery of polymer nanoparticles to the perinuclear region of live cells via a non-clathrin, non-degradative pathway," *Biomaterials*, vol. 28, no. 18, pp. 2876–2884, 2007.

[286] H. Maeda, H. Nakamura, and J. Fang, "The EPR effect for macromolecular drug delivery to solid tumors: Improvement of tumor uptake, lowering of systemic toxicity, and distinct tumor imaging in vivo," *Adv Drug Deliver Rev*, vol. 65, no. 1, pp. 71–79, Jan. 2013.

[287] D.-E. Lee, H. Koo, I.-C. Sun, J. H. Ryu, K. Kim, and I. C. Kwon, "Multifunctional nanoparticles for multimodal imaging and theragnosis," *Chem Soc Rev*, vol. 41, no. 7, pp. 2656–2672, 2012.

[288] Y. Matsumoto, J. W. Nichols, K. Toh, T. Nomoto, H. Cabral, Y. Miura, R. J. Christie, N. Yamada, T. Ogura, M. R. Kano, Y. Matsumura, N. Nishiyama, T. Yamasoba, Y. H. Bae, and K. Kataoka, "Vascular bursts enhance permeability of tumour blood vessels and improve nanoparticle delivery," *Nat Nanotechnol*, vol. 11, no. 6, pp. 533–538, Feb. 2016.

[289] A. S. Mikhail, S. Eetezadi, S. N. Ekdawi, J. Stewart, and C. Allen, "Image-based analysis of the size- and time-dependent penetration of polymeric micelles in multicellular tumor spheroids and tumor xenografts," *International Journal of Pharmaceutics*, vol. 464, no. 1, pp. 168–177, Apr. 2014.

[290] C. Allen, "Why I'm Holding onto Hope for Nano in Oncology," *Mol Pharmaceut*, vol. 13, no. 8, pp. 2603–2604, Aug. 2016.

[291] A. Wagh, S. Y. Qian, and B. Law, "Development of Biocompatible Polymeric Nanoparticles for in Vivo NIR and FRET Imaging," *Bioconjugate Chem*, vol. 23, no. 5, pp. 981–992, May 2012.

[292] K. Stockhofe, J. Postema, H. Schieferstein, and T. Ross, "Radiolabeling of Nanoparticles and Polymers for PET Imaging," *Pharmaceuticals*, vol. 7, no. 4, pp. 392–418, Apr. 2014.

[293] S. H. Lee, S. Hyun Kim, Y. K. Han, and Y. H. Kim, “Synthesis and degradation of end-group-functionalized polylactide,” *J. Polym. Sci. A Polym. Chem.*, vol. 39, no. 7, pp. 973–985, Apr. 2001.

[294] T. Lammers, F. Kiessling, M. Ashford, W. Hennink, D. Crommelin, and G. Strom, “Cancer nanomedicine: is targeting our target?,” *Nature Publishing Group*, vol. 1, no. 9, p. 16069, Sep. 2016.

[295] S. K. Singh, D. L. Luisi, and R. H. Pak, “Antibody-Drug Conjugates: Design, Formulation and Physicochemical Stability,” *Pharm Res*, vol. 32, no. 11, pp. 3541–3571, May 2015.

[296] M. Gordon, P. Tardi, L. D. Mayer, and J. Tyner, “Abstract 287: CPX-351 cytotoxicity against fresh AML blasts is increased for FLT3-ITD+ cells and correlates with drug uptake and clinical outcomes,” *Cancer Research*, vol. 76, no. 14, pp. 287–287, Jul. 2016.

[297] J. Park, S. H. Wrzesinski, E. Stern, M. Look, J. Criscione, R. Ragheb, S. M. Jay, S. L. Demento, A. Agawu, P. Licona Limon, A. F. Ferrandino, D. Gonzalez, A. Habermann, R. A. Flavell, and T. M. Fahmy, “Combination delivery of TGF-β inhibitor and IL-2 by nanoscale liposomal polymeric gels enhances tumour immunotherapy,” *Nat Mater*, vol. 11, no. 10, pp. 895–905, Jul. 2012.

[298] N. E. Sharpless and R. A. DePinho, “The mighty mouse: genetically engineered mouse models in cancer drug development,” *Nat Rev Drug Discov*, vol. 5, no. 9, pp. 741–754, Aug. 2006.

[299] G. I. Evan and K. H. Vousden, "Proliferation, cell cycle and apoptosis in cancer," *Nature*, vol. 411, no. 6835, pp. 342–348, May 2001.

[300] J. E. Visvader and G. J. Lindeman, “Cancer stem cells in solid tumours: accumulating evidence and unresolved questions,” *Nat Rev Cancer*, vol. 8, no. 10, pp. 755–768, Sep. 2008.

[301] D. Beier, J. B. Schulz, and C. P. Beier, “Chemoresistance of glioblastoma cancer stem cells - much more complex than expected,” *Mol Cancer*, vol. 10, no. 1, p. 128, 2011.

[302] J. E. Dick, “Breast cancer stem cells revealed,” *Proc. Natl. Acad. Sci. U.S.A.*, vol. 100, no. 7, pp. 3547–3549, Mar. 2003.

[303] A. M. Stark, A. Nabavi, H. M. Mehdorn, and U. Blömer, “Glioblastoma multiforme—report of 267 cases treated at a single institution,” *Surgical Neurology*, vol. 63, no. 2, pp. 162–169, Feb. 2005.

[304] C. G. Marsden, M. J. Wright, L. Carrier, K. Moroz, R. Pochampally, and B. G. Rowan, “‘A novel in vivo model for the study of human breast cancer metastasis using primary breast tumor-initiating cells from patient biopsies’,” *BMC Cancer*, vol. 12, no. 1, p. 1315, Jan. 2012.

[305] S. Aparicio, M. Hidalgo, and A. L. Kung, “Examining the utility of patient-derived xenograft mouse models,” *Nat Rev Cancer*, vol. 15, no. 5, pp. 311–316, Apr. 2015.

[306] J. I. Herschkowitz, K. Simin, V. J. Weigman, I. Mikaelian, J. Usary, Z. Hu, K. E. Rasmussen, L. P. Jones, S. Assefnia, S. Chandrasekharan, M. G. Backlund, Y. Yin, A. I.

Khramtsov, R. Bastein, J. Quackenbush, R. I. Glazer, P. H. Brown, J. E. Green, L. Kopelovich, P. A. Furth, J. P. Palazzo, O. I. Olopade, P. S. Bernard, G. A. Churchill, T. Van Dyke, and C. M. Perou, "Identification of conserved gene expression features between murine mammary carcinoma models and human breast tumors," *Genome Biol*, vol. 8, no. 5, p. R76, 2007.

[307] A. T. Lucas, A. J. Madden, and W. C. Zamboni, "Challenges in preclinical to clinical translation for anticancer carrier-mediated agents," *WIREs Nanomed Nanobiotechnol*, vol. 8, no. 5, pp. 642–653, Feb. 2016.

[308] G. Francia, W. Cruz-Munoz, S. Man, P. Xu, and R. S. Kerbel, "Mouse models of advanced spontaneous metastasis for experimental therapeutics," *Nat Rev Cancer*, vol. 11, no. 2, pp. 135–141, Feb. 2011.